

From meson-baryon scattering to meson photoproduction

Dissertation

zur

Erlangung des Doktorgrades (Dr. rer. nat.)

der

Mathematisch-Naturwissenschaftlichen Fakultät

der

Rheinischen Friedrich-Wilhelms-Universität Bonn

vorgelegt von

Maxim Mai

aus

Pawlodar, Kasachstan

Bonn 2012

Angefertigt mit Genehmigung der Mathematisch-Naturwissenschaftlichen Fakultät
der Rheinischen Friedrich-Wilhelms-Universität Bonn.

1. Gutachter: Prof. Dr. Ulf-G. Meißner
 2. Gutachter: PD Dr. A. Rusetsky
- Tag der Promotion: 19.12.2012
Erscheinungsjahr: 2013

“Die Welt ist die Gesamtheit der Tatsachen, nicht der Dinge.”

Ludwig Wittgenstein [1].

From meson-baryon scattering to meson photoproduction

In the present work we investigate the properties of the lowest baryon resonances. The starting point of our analyses is the low-energy effective theory of quantum chromodynamics, called chiral perturbation theory. As such it describes the long-range observables in terms of the low-energy effects, while the high-energy effects are subsumed in the so-called low-energy constants. In the region of the aforesaid lowest baryon resonances any strict perturbative expansion fails and some resummation scheme is required. For this we will employ the Bethe-Salpeter equation (BSE) which guarantees the exact unitarity of the S-matrix and allows to generate resonances dynamically, however, abandoning some other basic principles of quantum field theory as described in chapter 2. Restricting the driving term of this equation to local terms of the second chiral order, we will derive an exact solution of the BSE for meson-baryon scattering in chapter 2. Without putting the interaction kernel on shell we preserve the exact correspondence of this solution to an infinite chain of Feynman diagrams.

In chapter 4 we will apply this ansatz for antikaon-nucleon scattering, trying to get a new insight into the nature of the subthreshold resonance, i.e. $\Lambda(1405)$. The properties of this resonance have been debated for decades and in recent years it has again attracted a lot of attention by theoreticians since this resonance can be dynamically generated from the so-called chiral unitary approaches. Moreover, the recent measurement of the energy shift and width of kaonic hydrogen in the SIDDHARTA experiment at DAΦNE has provided a very tight constraint on K^-p scattering length. Typically, these approaches predict a two pole structure of $\Lambda(1405)$, but the question is how precise one can determine the position of these poles relying on data at and above the $\bar{K}N$ threshold.

Moreover, we will apply our framework for the analysis of pion-nucleon scattering in chapter 3. There we will show that the iteration of local terms of second chiral order allows to reproduce the s-wave resonances $N^*(1535)S_{11}$ and $N^*(1650)S_{11}$. Then in chapter 5 we will adopt this hadronic amplitude as a part of a gauge invariant framework to address pion and eta photoproduction in a combined analysis. There all terms of the next-to-leading chiral order will be included reproducing the scattering data very well in both channels. After that we calculate the photoproduction multipoles in a parameter-free prediction which will then be compared with more phenomenological analyses by the MAID, ETAMAID, SAID and Bonn-Gatchina groups.

Contents

1	Introduction	1
1.1	Quantum chromodynamics	1
1.2	Chiral perturbation theory	4
1.3	Baryon ChPT	11
1.4	Chiral unitary approach to hadron physics	15
2	Solution of the Bethe-Salpeter equation	22
2.1	Framework	22
2.2	Regularization	25
2.3	Solution	27
3	πN scattering and properties of the $N^*(1535)$ and $N^*(1650)$ resonances¹	30
3.1	Introduction	30
3.2	Formalism	31
3.3	Numerics	33
3.4	Results	34
3.5	Summary and outlook	40
4	\bar{K}N scattering and properties of the $\Lambda(1405)$ resonance²	41
4.1	Introduction	41
4.2	Framework	42
4.3	Fit strategy	45
4.4	Results	46
4.5	Summary and outlook	53

¹Most of the contents of this chapter have been published in Ref. [2].

²Most of the contents of this chapter can be found in Ref. [3].

5	Pion photoproduction off the proton in a gauge-invariant chiral unitary framework³	54
5.1	Introduction	54
5.2	Hadronic scattering	55
5.2.1	Formalism	55
5.2.2	Fit	58
5.2.3	Results	59
5.3	Pion photoproduction off the proton	68
5.3.1	Formalism	69
5.3.2	Results	71
5.4	Summary and outlook	77
6	Outlook	79
	Appendix	81
A	Loop integrals	81
B	Reduction of the loop integrals	83
C	Channel space structures	90
D	Partial wave analysis of $\pi N \rightarrow \eta N$ scattering	92
E	One-photon vertices	96
F	Multipoles	97

³Most of the contents of this chapter can be found in Ref. [4] which has been accepted for publication in Physical Review D.

Chapter 1

Introduction

1.1 Quantum chromodynamics

The world manifests itself via forces, and to our present knowledge nature exhibits four fundamental forces: gravitation, the weak, electromagnetic and the strong force. In that order the strengths of these cover of about 39 orders of magnitude starting from the weakest one, gravity, which is responsible for the largest observed structures in the universe. The dynamics of the smallest structures in the universe on the other hand are caused by the three other fundamental interactions, which together build a theory nowadays called *The Standard Model* of particle physics. As such it has to take both quantum effects as well as special relativity¹ into account and the only way to reconcile both is quantum field theory.

In several groundbreaking and Nobel Prize awarded steps over the last century each part of the Standard Model was identified by the underlying gauge symmetry group which can be written very compactly as follows

$$\underbrace{SU(3)}_{\text{strong}} \times \underbrace{SU(2) \times U(1)}_{\text{electroweak}}.$$

The electroweak part has been found by Glashow, Weinberg and Salam to unify quantum electrodynamics (QED) and the weak interaction. The remaining part is the symmetry group of a non-Abelian gauge theory called quantum chromodynamics (QCD) which exhibits a completely different behaviour of the corresponding coupling compared to the electroweak sector. Whilst the electroweak sector can essentially be analyzed perturbatively, the strong coupling is antiscreened by the self-interacting gauge bosons, gluons, due to the non-Abelian character of QCD. Thus the QCD coupling is large for low energies (large distances) and small for high energies (small distances). The latter fact is usually referred to as *asymptotic freedom*. As a matter of fact it has been shown in Ref. [5] that asymptotic freedom of a renormalizable field theory in four dimensions requires the incorporation of non-Abelian gauge fields. On the other hand the increase of the strong coupling at low energies gives rise to the *confinement hypothesis* which states that no matter- or gauge-fields of QCD can be observed directly. Thus albeit there is no

¹A comprehensive description of General Relativity (gravity) and quantum effects remains an unsolved question.

reason to doubt about QCD as the correct theory of strong interactions, its non-perturbative character calls for more elaborative techniques to understand its implications.

The matter fields of QCD are quarks, q , which appear in three different colours denoted in the following by the indices a and b . The strong force is mediated by the gluon gauge-field G which by itself carries a colour quantum number. Additionally six different 'flavours' of quarks have been observed, $f \in \{u, d, s, c, b, t\}$, where each one of them carries a different mass. Thus we have to sum over all flavours to end up with

$$\mathcal{L}_{\text{QCD}} = \sum_f \bar{q}_f^a (i\gamma_\mu D_{ab}^\mu - m_f \delta_{ab}) q_f^b - \frac{1}{4} G_{\mu\nu}^a G_{\mu\nu}^a - g^2 \frac{\theta}{64\pi^2} G_{\mu\nu}^a \epsilon^{\mu\nu\mu'\nu'} G_{\mu'\nu'}^a, \quad (1.1)$$

where g is the strong coupling. The last term of the above Lagrangian allows for a CP-violation which has never been observed. Experimentally, the coefficient of this term is constrained to $|\theta| < 10^{-10}$, see Ref. [6], and we will neglect it in the following. Assuming invariance under local $SU(3)$ gauge transformations, generated by the 8 Gell-Mann matrices t , one has to replace simple derivatives by covariant ones which are given in the minimal form by

$$D_{ab}^\mu = \partial^\mu \delta_{ab} + ig \sum_{i=1}^8 t_{ab}^i G^{i, \mu}.$$

With the Lie bracket $[t^i, t^j] = if^{ijk}t^k$ the Gell-Mann matrices build a Lie algebra, where f^{ijk} are called structure constants. The gluon field-strength tensor reads

$$G_{\mu\nu}^a = \partial_\mu G_\nu^a - \partial_\nu G_\mu^a + gf^{abc} G_\mu^b G_\nu^c,$$

where the last term is due to the non-Abelian character of QCD and has extraordinary consequences as it induces three- and four-gluon interaction. One typical feature of all gauge field theories is that mass as well as coupling constants are renormalized by effects involving virtual particles. As a matter of fact without the self-interaction of gluons the strong coupling would behave exactly as the QED coupling, i.e. it is small for low energies and large for high energies. This would allow for a perturbative treatment of QCD in the low energy region. It turns out that the self-interaction of gluons reverses this pattern ($N_f \leq 16$ is assumed) and low-energy QCD becomes a truly non-perturbative theory.

In recent years two different approaches have crystallized to be promising describing the low energy sector of QCD, effective field theories (EFTs) and lattice QCD (LQCD). The latter is an attempt for a direct evaluation of QCD on discretized space-time lattices. Quarks are defined on the lattice points and gluons are supposed to be situated on the links between those. This implies directly that Lorentz invariance is broken and that the system to study can only have discrete values of momentum with the natural UV cutoff of order $1/a$, where a is the lattice spacing. The real-world QCD is assumed to be reproduced on the lattice in the limit $a \rightarrow 0$. Albeit the basic ideas of lattice regularized QCD are quite old, see Refs. [7,8], their applications are computationally very expensive and became available only with the rise of supercomputers in the last decade. Nowadays there are numerous groups around the globe working in this field and the results are now approaching the level of precision of modern experimental physics, see Ref. [9] for a recent determination of light hadron masses on the lattice.

We will follow a different path analyzing the low energy sector of QCD provided in the framework of effective field theories. Generally speaking, whenever a physical system exhibits

a scale separation one can describe the long-range (low-energy) observables in terms of the low-energy effects, i.e. integrating out the short-range effects. This gives rise to the so-called effective degrees of freedom in which this theory is defined, unlike in those of the underlying theory. There are several areas of physics where this philosophy has found a successful application and it is even thinkable that the Standard Model and general relativity itself is an EFT of some underlying theory. However, no successful candidates are found yet, see the discussion in Ref. [10]. Let us return to QCD. Its matter fields show a clear scale separation as three of them (u,d,s) can be considered as light and three others (c,b,t) as heavy compared to the 'typical' hadron mass scale given by the mass of the proton (938 MeV) or the ρ meson (776 MeV). It is therefore only natural to consider in the first approximation the light quarks as massless, usually referred to as the so-called SU(3) chiral limit. Obviously in this limit the QCD Lagrangian (1.1) is not the most general one, i.e. the right- and left-handed quark fields defined via

$$q_R := \frac{1}{2}(1 + \gamma_5)q \quad \text{and} \quad q_L := \frac{1}{2}(1 - \gamma_5)q$$

decouple from each other and fulfill the massless part of Eq. (1.1) separately as follows

$$\mathcal{L}_0 = \sum_{f=u,d,s} (\bar{q}_L^f i\gamma_\mu D^\mu q_L^f) + \sum_{f=u,d,s} (\bar{q}_R^f i\gamma_\mu D^\mu q_R^f) - \frac{1}{4} G_{\mu\nu} G^{\mu\nu}, \quad (1.2)$$

where we have suppressed the colour indices for convenience. Clearly the above Lagrangian is invariant under the replacement $q_R \mapsto Rq_R$ as well as $q_L \mapsto Lq_L$ for $R/L \in U(3)$ separately. Thus massless QCD is invariant under

$$U_L(3) \times U_R(3) = SU_V(3) \times SU_A(3) \times U_V(1) \times U_A(1),$$

where the subscript V denotes the vector ($L + R$) and A the axial-vector ($L - R$) symmetry groups. At the 'classical' level, using the Noether theorem, we would expect $(8 + 8 + 1 + 1)$ conserved currents, respectively to the above decomposition. The inclusion of loops, i.e. quantum effects, leads to the observation that the axial-vector current is not conserved if one imposes the Ward identities as it has been shown in Ref. [11]. On the other hand the $U_V(1)$ symmetry corresponds to the baryon number conservation which we expect to be fulfilled exactly². It remains to clarify whether the remaining part of the symmetry group is realized in nature. First, vector like theories, such as QCD, cannot spontaneously break down vector symmetries as it was shown (modulo some assumptions) by Vafa and Witten in Ref. [12]. Consequently $SU_V(3)$ annihilates the ground state and thus is realized in the so-called Wigner-Weyl mode. Now let us assume that the generators of $SU_A(3)$ also annihilate the QCD vacuum, then by Coleman's theorem [13] it will be observed as a symmetry of the hadronic spectrum. On the other hand applying a generator of the axial group to any state of the hadronic spectrum will produce a degenerate state with the opposite parity. Because such 'parity doublers' have not been observed in nature, the symmetry group of massless QCD, $SU_V(3) \times SU_A(3)$, must be broken spontaneously to the $SU_V(3)$. Consequently by the Goldstone theorem each generator of the broken/hidden symmetry ($SU_A(3)$) is associated with a massless Goldstone boson. Indeed the lightest particles of the hadronic spectrum appear to be the pseudoscalar mesons (π, K, η). The finite masses of these are caused by the explicit symmetry breaking, i.e. finite masses of u, d and s quarks.

²The issue of Baryogenesis lies outside of the scope of this thesis.

In principle those symmetry considerations were known since the sixties. Back then they led to rather protracted calculations of low energy dynamics of hadrons in the framework of “current algebra“ and “partially conserved axial-vector currents” (PCAC). The most popular results of that era are the Gell-Mann-Okubo [14], Gell-Mann-Oakes-Renner [15] relations as well as Weinberg’s prediction [16] for the isovector and isoscalar s-wave pion-nucleon scattering lengths

$$a^- = \frac{1}{8\pi F_\pi^2} \frac{M_\pi m_p}{m_p + M_\pi} \quad \text{and} \quad a^+ = 0, \quad (1.3)$$

where m_p and M_π denote the proton and pion masses, respectively, and F_π is the pion decay constant. In 1979 Weinberg [17] formulated a conjecture (also known as a folk theorem) which revealed a path of systematical calculations of the “current algebra“ results as well as corrections to it. The theorem states that to any given order of perturbation theory the matrix elements calculated from a most general effective Lagrangian which contains all terms consistent with all fundamental principles and the assumed symmetry yield a most general S-matrix consistent with all fundamental principles of quantum field theory, i.e. analyticity, (perturbative) unitarity and cluster decomposition as well as the assumed symmetries. There are two crucial observations to be made: First, one has to include every term allowed by the symmetries into the effective Lagrangian. These terms are accompanied by coupling constants which will be renormalized absorbing all possible UV loop divergences. Thus one can go beyond the tree level calculations which brings us to the second point. For practical calculations one has to organize the infinite number of terms of the most general effective Lagrangian to ensure some kind of perturbative expansion. In other words one has to decide which terms are more important and which are less. Chiral perturbation theory (ChPT) is an effective low energy theory organized in powers of small momenta and light quark masses as we will demonstrate in detail in the next section.

To conclude the present section we wish to note that LQCD and ChPT have different histories and, more importantly, different underlying philosophies. Nevertheless both methods must be seen as complementary taking benefit from each other. As already mentioned new coupling constants appear in the effective Lagrangian, in particular the chiral Lagrangian - called low-energy constants (LECs). These cannot be calculated from the chiral approach but only from the underlying theory (QCD) directly. Thus, in principle, LQCD should be a perfect method to pinpoint these constants. On the other hand, typically, calculations on the lattice are carried out at larger ($\sim 200..400$ MeV) than the physical pion mass ($M_\pi = 135$ MeV) to reduce the computational costs. To extract the real world quantities one inevitably has to extrapolate these results to the ‘physical point’ which requires the knowledge of their pion mass dependence. An almost perfect tool for this is ChPT as it is organized in powers of small external momenta and light quark masses, where $m_q \sim M_\pi^2$. We will show a particular example of the so-called chiral extrapolations relying on our results later.

1.2 Chiral perturbation theory

The dynamics of the hadronic systems which we will describe in the main part of this thesis are given by chiral perturbation theory. Numerous very precise calculations of different observables

have rendered ChPT a powerful tool and in many cases as a benchmark in the threshold and subthreshold energy region, see [18–21] and references therein. In the present section we wish to demonstrate the construction principles of the effective Lagrangian according to the symmetry considerations presented before. We will follow the general procedure of Gasser and Leutwyler [22, 23] but wish also to refer the reader to more recent introductions [20, 24, 25] for more details.

Our quantum field theoretical objects of study are the S-matrix elements which relate the initial and final state of a physical system. Now the Lehmann, Symanzik, Zimmermann reduction formula connects these to the time ordered correlation functions which themselves can be computed from the generating functional $Z[J]$ via functional derivatives with respect to the external field J . The generating functional is defined as follows

$$Z[J] = \langle 0 | T e^{i \int d^4x \bar{q} J(x) q} | 0 \rangle . \quad (1.4)$$

The external fields, coupling to QCD, can be written in terms of 8 vector (v_μ), 8 axial-vector (a_μ), one scalar (s) and one pseudoscalar (p) fields, i.e. $J(x) = \gamma_\mu v^\mu(x) + \gamma_\mu \gamma_5 a^\mu(x) - s(x) + i\gamma_5 p(x)$. The QCD Lagrangian (1.1) can then be obtained from the following generalized Lagrangian

$$\mathcal{L} = \mathcal{L}_0 + \bar{q} J q ,$$

taking the limit $v(x) = a(x) = p(x) = 0$, $s(x) = \mathcal{M}$, where the latter denotes the quark mass matrix, i.e. $\mathcal{M} = \text{diag}(m_u, m_d, m_s)$. In the presence of the external fields the generating functional can now be calculated in the path integral formalism as follows

$$Z[J] = \int [DG][Dq][D\bar{q}] e^{i \int d^4x (\mathcal{L}_0(\bar{q}, q, G) + \bar{q} J(v, a, s, p) q)} . \quad (1.5)$$

In principle Weinberg's conjecture allows one to replace the r.h.s. of the above equation by the path integral over the effective fields U incorporated in the effective Lagrangian, \mathcal{L}_{eff} , as follows

$$Z[J] = \int [DU] e^{i \int d^4x \mathcal{L}_{\text{eff}}(U, v, a, s, p)} . \quad (1.6)$$

The effective Lagrangian should be invariant under all original symmetries of the QCD Lagrangian as well as the chiral symmetry. In fact the effective Lagrangian should be invariant under *local* chiral transformations as it was demonstrated by Leutwyler in Ref. [26] through analysis of the Ward identities. For the already discussed transformation of quark fields, i.e. $q_R \mapsto R q_R$ and $q_L \mapsto L q_L$, the external fields have to transform as follows

$$\begin{aligned} v_\mu + a_\mu &\rightarrow R(v_\mu + a_\mu)R^\dagger + iR\partial_\mu R^\dagger , \\ v_\mu - a_\mu &\rightarrow L(v_\mu - a_\mu)L^\dagger + iL\partial_\mu L^\dagger , \\ (s + ip) &\rightarrow R(s + ip)L^\dagger , \end{aligned} \quad (1.7)$$

where R/L are space-time-dependent $SU(3)$ matrices.

We wish to note that the validity region of Eq. (1.6) is limited to the low energy region. The analysis of the spontaneous symmetry breaking (SSB) from $SU_L(3) \times SU_R(3)$ to $SU_V(3)$ in the

last section dictates the presence of (approximately) massless Goldstone bosons, which we have identified as π , K and η mesons. At low energies the heavy degrees of freedom are 'frozen' and the dynamics of QCD is captured by the Goldstone bosons which serve as dynamical degrees of freedom. The (low energy) expansion of the QCD Green functions in powers of masses and external momenta of these effective degrees of freedom is in principle equivalent to the transition from Eq. (1.5) to Eq. (1.6). On the other hand the heavy degrees of freedom, e.g. meson resonances, have been integrated out and their effects are captured in the coefficients of the low energy expansion. This procedure is of course valid only as long as the expansion parameter can be considered as small compared to the hadronic scale, which we previously have identified with the mass of the ρ meson (776 MeV). Another possibility is to set this scale to $4\pi F_\pi \sim 1.1$ GeV, which was discussed in Ref. [27] starting from one typical loop contribution to $\pi\pi$ scattering. Both suggestions are not that different from each other and we will assign a hadron scale as $\Lambda_\chi \sim 1$ GeV. Typically, reliable calculations can be done for energies up to ~ 200 MeV above the threshold. Later we will discuss a possibility to extend the range of validity of such strictly perturbative approach by means of unitarized chiral perturbation theory. It is also worth mentioning that the mass of the strange quark differs significantly from those of up and down quarks, i.e. (at a scale of $\mu \approx 2$ GeV, see Ref. [28]) $m_u/m_\rho = 0.005$, $m_d/m_\rho = 0.010$ and $m_s/m_\rho = 0.168$. Of course this means that we can expect the low energy expansion around the chiral limit to have a better convergence behaviour in the two-flavour sector than the one in the three-flavour sector. In fact this issue will become even more evident in the baryon sector to which we will come in the next section.

It remains to clarify how these effective fields are realized in the effective Lagrangian. Consider a symmetry group G being spontaneously broken to a subgroup $H \subset G$. Then $N = \dim(G) - \dim(H)$ Goldstone modes [29] are realized, which we assemble in $\Phi = (\phi_1, \dots, \phi_N)$, where ϕ_i is a continuous and real-valued function on Minkowski space M^4 . Obviously the set of all Φ build a vector space, denoted by Z . In fact the only non-trivial vector space axiom here is the existence of the zero element, for which we consider the ground state configuration of the Goldstone bosons³ Φ_0 . We define a mapping ζ as follows

$$\begin{aligned} \zeta : G \times Z &\longrightarrow Z \\ (g, \Phi) &\mapsto \zeta(g, \Phi) , \end{aligned}$$

which is assumed to fulfill the identity as well as associativity (group-homomorphism) axioms. Moreover, since H leaves the vacuum invariant, $\zeta(h, \Phi_0) = \Phi_0$ for all $h \in H$. Consequently for each $g \in G$

$$\zeta(gh, \Phi_0) = \zeta(g, \zeta(h, \Phi_0)) = \zeta(g, \Phi_0) , \text{ for all } h \in H ,$$

which simply means that ζ defines a mapping of the left coset space $G/H = \{gH \mid g \in G\}$ onto the space of Goldstone bosons. The dimensionality of the coset space is equal to the number of Goldstone fields and the mapping is injective since $\zeta(g_1, \Phi_0) = \zeta(g_2, \Phi_0) \Rightarrow g_1^{-1}g_2 \in H$ or $g_2 \in g_1H$. Thus the above mapping defines an unique correspondence between the generators of the coset space G/H and Goldstone bosons. Note that the latter depend in general on the coordinates in Minkowski space, however, as discussed before we consider the symmetry group also to be space-time dependent.

³In a theory consisting of Goldstone bosons only, it is a state with no excitations.

The considerations made in the last section allow us to identify $H = \{(V, V)|V \in SU(3)\}$ and $G = \{(L, R)|L \in SU(3), R \in SU(3)\}$. The choice of representative for the left coset of $g = (L, R)$ is in principle arbitrary, conventionally one takes

$$\tilde{g}H = (1, RL^\dagger) \underbrace{(LV, LV)}_{\in H} ,$$

which is of course isomorphic to $gH = \{(LV, RV)|V \in SU(3)\}$ but has now a property to be completely characterized by a unitary matrix $U = RL^\dagger$. According to the foregoing analysis this matrix is isomorphic to the Goldstone boson fields. It transforms under the chiral transformations $\tilde{g} = (\tilde{L}, \tilde{R})$ as follows

$$\begin{aligned} \tilde{g}gH &= (\tilde{L}, \tilde{R})(1, RL^\dagger)H = (\tilde{L}, \tilde{R}RL^\dagger)H = (1, \tilde{R}(RL^\dagger)\tilde{L}^\dagger)H , \\ \text{i.e. } U &\mapsto \tilde{R}U\tilde{L}^\dagger . \end{aligned}$$

Collecting now the pseudoscalar mesons in a hermitian matrix ϕ we can establish a representation of the physical states in the unitary matrix U as follows

$$U = \exp\left(i\frac{\phi}{F_0}\right) , \quad \phi = \sqrt{2} \begin{pmatrix} \frac{\pi^0}{\sqrt{2}} + \frac{\eta}{\sqrt{6}} & \pi^+ & K^+ \\ \pi^- & -\frac{\pi^0}{\sqrt{2}} + \frac{\eta}{\sqrt{6}} & K^0 \\ K^- & \bar{K}^0 & -\frac{2}{\sqrt{6}}\eta \end{pmatrix} , \quad (1.8)$$

where we again omitted the dependence on the space-time coordinates for convenience. The dimensionful quantity F_0 denotes the pion (meson) decay constant in the chiral limit as it is related to the pion decay $\pi^+ \rightarrow \mu^+ \nu_\mu$. The above representation of meson fields is not unique, e.g. frequently in the two-flavour framework one uses the so-called sigma parameterization

$$U = i \sum_{j=1}^3 \tau_j \frac{\pi_j}{F_0} + \mathbb{1}_2 \sqrt{1 - \sum_{j=1}^3 \frac{\pi_j}{F_0} \frac{\pi_j}{F_0}} , \quad (1.9)$$

where τ_i denote the Pauli matrices and π_i collect the pion fields. Clearly the differences between different descriptions of the pions (mesons) can only affect the off-shell terms. On-shell quantities are on the other hand related to physical observables and thus must be independent of the chosen parameterization, see the equivalence theorems in Ref. [30–32]. We will return to this issue in the next section, where off-shell effects will become important.

Now having specified the building blocks of effective theory, i.e. U, v, s, a, p and derivatives thereof, we demonstrate the construction principles of the chiral Lagrangian [17, 22, 23]. It contains an infinite number of structures, which can be ordered in powers of the low energy expansion parameter, denoted henceforth by q . Demanding Lorentz invariance only even numbers of derivatives can appear, thus the effective Lagrangian in the pure meson sector only contains even powers of q

$$\mathcal{L}_{\text{eff}} = \mathcal{L}^{(2)} + \mathcal{L}^{(4)} + \mathcal{L}^{(6)} + \dots .$$

In the case of massless quarks and in the absence of external fields the lowest order chiral Lagrangian reads as follows

$$\mathcal{L}^{(2)} = \frac{F_0^2}{4} \langle \partial_\mu U \partial^\mu U^\dagger \rangle ,$$

where $\langle \dots \rangle$ denotes here and in the future the trace in the flavour space. The necessity of the foregoing dimensionful prefactor, i.e. $F_0^2/4$, becomes obvious if we expand the Eq. (1.8) in meson fields explicitly, $U = 1 + i\phi/F_0 - \phi^2/(2F_0^2) + \dots$. Then the term containing only two meson fields possesses the standard form of the kinetic term. At the beginning of this section we have discussed the necessity to include the external fields and the transformation properties of these fields, see Eqs. (1.7). For non-vanishing external fields the above Lagrangian can only be invariant under the local gauge transformations if we replace the partial derivatives by the minimal form of covariant derivatives as follows

$$\partial_\mu U \longrightarrow \nabla_\mu U = \partial_\mu U - i(v_\mu + a_\mu)U + iU(v_\mu - a_\mu) , \quad (1.10)$$

which is at the very heart of gauge theories as the demand of local gauge symmetries yields in a special form of the Lagrangian which allows for a discussion of couplings of external fields to internal degrees of freedom. The scalar and pseudoscalar external fields transform exactly as the matrix U . Collecting these in the field $\chi = 2B(s + ip)$ the most general leading order (LO) chiral Lagrangian reads in its full form

$$\mathcal{L}_\phi^{(2)} = \frac{F_0^2}{4} \langle \nabla_\mu U \nabla^\mu U^\dagger \rangle + \frac{F_0^2}{4} \langle \chi^\dagger U + \chi U^\dagger \rangle . \quad (1.11)$$

The new constant B is related to the explicit chiral symmetry breaking due to the non-vanishing quark masses. We have argued before that in the real world we have to consider $s = \mathcal{M}$ and $p = 0$, i.e. $\chi = 2B\mathcal{M}$. Later we have identified the ground state of Goldstone fields by $U = 1$, consequently the energy density of the ground state is given at the leading chiral order by

$$\langle \mathcal{H}_{\text{eff}} \rangle = -\frac{F_0^2}{2} B \langle \mathcal{M} + \mathcal{M}^\dagger \rangle = -F_0^2 B (m_u + m_d + m_s) .$$

The new constant can be related to the vacuum expectation value of the chiral quark condensate $\langle \bar{q}q \rangle = \partial \langle 0 | \mathcal{H} | 0 \rangle / \partial m_q |_{m_q=0}$ to be $F_0^2 B = -\langle \bar{q}q \rangle$. Moreover, expanding the last term of Eq. (1.11) up to two mesons and using the representation (1.8) we can write down the mass term of the LO chiral Lagrangian

$$\begin{aligned} \mathcal{L}_{\text{mass}}^{(2)} = & -\frac{B}{2} \langle \phi^2 \mathcal{M} \rangle = -B(m_u + m_d) \pi^+ \pi^- - B(m_u + m_s) K^+ K^- - B(m_d + m_s) K^0 \bar{K}^0 \\ & - \frac{B}{2} (m_u + m_d) \pi^0 \pi^0 - \frac{B}{\sqrt{3}} (m_u - m_d) \pi^0 \eta - \frac{B}{6} (m_u + m_d + 4m_s) \eta \eta . \end{aligned}$$

Assuming isospin symmetry ($\hat{m} := m_u = m_d$), the $\pi^0 \eta$ mixing term vanishes and the masses of the Goldstone bosons are given at the lowest order by

$$M_\pi^2 = 2B\hat{m}, \quad M_K^2 = B(\hat{m} + m_s), \quad M_\eta^2 = \frac{2}{3}B(\hat{m} + 2m_s) ,$$

which actually correspond to the Gell-Mann, Oakes and Renner relations [15] if combined with $F_0^2 B = -\langle \bar{q}q \rangle$. On the other hand a linear combination of the above mass formulas yields the Gell-Mann-Okubo relation [14]

$$4M_K^2 = 4B(\hat{m} + m_s) = 2B(\hat{m} + 2m_s) + 2B\hat{m} = 3M_\eta^2 + M_\pi^2 ,$$

which is fulfilled in nature to a few percent accuracy.

After having introduced the framework of chiral perturbation theory the derivation of the last two well-known relations fits into few lines. Yet, this effective approach is even more powerful as it allows for a systematical improvement of the accuracy of such calculations by going to higher orders. Conceptionally, there is an even more important point of doing so, the restoration of another fundamental principle of quantum field theory, *unitarity*. Let us consider for a moment the elastic scattering of two Goldstone bosons. Above the two-particle threshold the imaginary part of the scattering amplitude is fixed by unitarity

$$\text{Im}T_{\phi\phi\rightarrow\phi\phi} \sim T_{\phi\phi\rightarrow\phi\phi}^\dagger T_{\phi\phi\rightarrow\phi\phi} .$$

On the other hand at the leading chiral order the scattering amplitude is given by a contact term from $\mathcal{L}^{(2)}$ only and thus is a real-valued number. Consequently the l.h.s. of the above equation is zero whereas the r.h.s is not. Excluding the trivial solution of this problem ($T \neq 0$), we have to include effects of intermediate particles, i.e. loop contributions. In general these loop integrals produce UV-divergences which can be absorbed into coupling constants of the effective Lagrangian. In practical calculations this requires an ordering scheme which is achieved in ChPT by Weinberg's power counting [17]. The small parameters of the low energy expansion are small meson momenta and quark masses which we both scale with a common factor α , i.e. $q \mapsto \alpha q$ and $m_q \mapsto \alpha^2 m_q$ or using the Gell-Mann-Oakes-Renner relation $M \mapsto \alpha M$ for meson masses at leading order in quark mass expansion. Every internal meson line contributes to a Feynman diagram via

$$\int \frac{d^4 k}{(2\pi)^4} \frac{i}{k^2 - M^2 + i\epsilon} \mapsto \alpha^2 \int \frac{d^4 l}{(2\pi)^4} \frac{i}{l^2 - M^2 + i\epsilon} ,$$

where a replacement of the integration momentum $k \rightarrow \alpha l$ has been performed. Obviously each vertex from a $\mathcal{L}^{(n)}$ scales with α^n but also calls for a four-momentum conserving delta function which scales as α^{-4} . Thus the S-matrix element scales as $S \mapsto S^{D'}$ with $D' = 2N_I + \sum_n N_n(n-4)$, where N_I and N_n denote the number of internal meson lines and the number of vertices of chiral order n , respectively. The S-matrix for a process involving N_e external lines is connected to the transition amplitude \mathcal{M} via $S \sim \delta^4(p_1 + \dots + p_{N_e})\mathcal{M}$, which scales then as $D = 4 + D'$ i.e.

$$D = 2 + 2N_L + \sum_n N_n(n-2) ,$$

where we have replaced $N_I = N_L + \sum_n N_n - 1$ with N_L being the number of independent loops. In full agreement with the discussion above we see that the lowest possible value of chiral order is given in the case of no loops, i.e. $D = 2$. The next most simple topology, a one-loop diagram with vertices from $\mathcal{L}^{(2)}$ contributes already at the fourth chiral order and thus calls for an inclusion of local terms from $\mathcal{L}^{(4)}$ to absorb the loop divergences. For instance, for any specific chiral order the number of diagrams and thus the number of loop diagrams can be large but remains finite. We wish to repeat that for each loop diagram there is a local term of the same chiral order which is accompanied by a coupling constant of the effective field theory. The renormalization of this allows for an absorption of the loop-divergence such that chiral perturbation theory is renormalizable order by order.

In the course of this thesis we will only require the leading order chiral Lagrangian in the pure mesonic sector and refrain for this reason of giving here the explicit form of the $\mathcal{L}^{(4)}$, $\mathcal{L}^{(6)}$ etc. . The interested reader is referred to Refs. [22, 23, 33]. Nevertheless some general remarks should be made for completeness. First, the operators of the chiral Lagrangian of order $2n$ can only consist of $2n$ derivatives of the matrix U , n quark mass matrices ($\sim \chi$) or of combinations with m derivatives and p quark mass matrices with $m + 2p = 2n$ ($m, n, p \in \mathbb{N}$). Then one has to build all possible contractions of these operators which are consistent with Lorentz invariance, C,P (and with it also T, by means of the CPT theorem) and G-parity. For simple combinatorial reasons the overall number of such operators must increase with the rising chiral order, i.e.

$$\mathcal{L}^{(2)} = \sum_{i=1}^2 L_i \mathcal{O}_i, \quad \mathcal{L}^{(4)} = \sum_{i=1}^{12} L'_i \mathcal{O}_i, \quad \mathcal{L}^{(6)} = \sum_{i=1}^{90} L''_i \mathcal{O}_i,$$

where we have denoted all chiral operators generically by \mathcal{O}_i and low energy constants by L_i . The latter cannot be determined from the symmetry principles alone and thus can be seen as free parameters of the effective approach. However, some restrictions on these parameters can be put from direct numerical evaluations of QCD Green functions on the lattice. Further restrictions can be obtained utilizing the resonance saturation hypothesis of QCD as proposed by Gasser and Leutwyler in Ref. [22] and generalized further in Refs. [34, 35]. Generally speaking, the idea is to exploit the duality of the scattering processes as a probe of the particle spectrum being on the other hand restricted by the chiral symmetry. Technically one has to introduce a resonance field coupled to the lowest order chiral Lagrangian. Then the coupling of such field to pion field (working in the two-flavour sector) is adjusted to reproduce the signal of the resonance in the hadronic spectrum. Finally the resonance field is integrated out at low momenta. Since its coupling to the Goldstone field is of the order q^2 the resonance exchange is of order q^4 and higher, one can expand the LECs of the NLO chiral Lagrangian in terms of these couplings as well as resonance masses. It turns out that the LECs are almost saturated by these resonance contributions, see Ref. [25] for a quantitative comparison.

To further extent one should keep in mind that the low energy constants in the two- and three-flavour formulation of ChPT (denoted henceforth by $SU(2)$ and $SU(3)$, respectively) are not independent of each other. In fact integrating out the strange quark from the $SU(3)$ ChPT in the same manner as the heavy quarks have been integrated out before one obtains the $SU(2)$ version automatically. A comparison of the outcome of both formulations for a specific Green function yields then a relation between the free parameters of both approaches. These so-called matching relations help to transfer the information on LECs from the three-flavour theory to the two-flavour case and vice versa. In the pure mesonic sector several constants have been matched up to the two loop level, see Refs. [36–40]. In the baryon sector matching relations have been carried out up to NLO in Ref. [41] as well as in Ref. [42] based on the analysis of pion-nucleon scattering.

A deeper understanding of meson-baryon scattering is the core issue of the present work. Moreover, it also serves as a main ingredient for our analysis of photoproduction of mesons. Thus as a next step we shall give a recipe of how to extend ChPT to the sector where baryons play a major role.

1.3 Baryon ChPT

By far the most prominent extension of chiral perturbation theory is the inclusion of baryon fields in a consistent way [43, 44]. The interest to do so grows out of the fact that most of the collected experimental results in nuclear physics involve baryons. On the other hand the baryonic spectrum itself carries a very rich structure which is described quite well in the naive quark model but still not understood properly as it does not include effects of virtual hadrons and gluons. In fact we will show later that some of these excited states can be reproduced perfectly as what we call *dynamically generated* states from the meson and baryon intermediate states.

In this work we will consider processes involving only one single baryon, for the case of more baryons included we refer to Ref. [45] as well as to the reviews [46, 47]. In contrast to the previous section, see Eq. (1.4), the object of interest is given here by the transition amplitude from an asymptotic one-baryon in-state $|\mathbf{p} \text{ in}\rangle$ to an asymptotic one-baryon out-state $|\mathbf{p}' \text{ out}\rangle$ as follows

$$Z(\mathbf{p}', \mathbf{p}; v, a, s, p) = \langle \mathbf{p}' \text{ out} | \mathbf{p} \text{ in} \rangle_{v,a,s,p}^{\text{connected}} \quad \text{for} \quad \mathbf{p}' \neq \mathbf{p} ,$$

where \mathbf{p} and \mathbf{p}' denote the three-momentum of the in- and outgoing baryon, respectively. Both are considered to be small allowing for an effective low-energy analysis.

We wish now to construct an effective chiral Lagrangian which allows for a direct access of the generating functional in the sense of Eq. (1.6). First of all we collect the baryon fields of the ground state octet, i.e. $J^P = 1/2^+$, in a traceless matrix

$$B = \begin{pmatrix} \frac{\Sigma^0}{\sqrt{2}} + \frac{\Lambda}{\sqrt{6}} & \Sigma^+ & p \\ \Sigma^- & -\frac{\Sigma^0}{\sqrt{2}} + \frac{\Lambda}{\sqrt{6}} & n \\ \Xi^- & \Xi^0 & -\frac{2}{\sqrt{6}}\Lambda \end{pmatrix} ,$$

where each element is a Minkowski space dependent Dirac field. To understand the transformation properties of this object we have to keep in mind that the effective degrees of freedom are the Goldstone bosons, parametrized in terms of matrix U . To put this in other words it is insufficient to demand the baryon fields to transform as $B \mapsto K^\dagger B K$ for $K \in SU(3) \times SU(3)$, but one has also to impose that the matrix K is also a function of the matrix U , i.e $B \mapsto K(L, R, U)^\dagger B K(L, R, U)$. The physical observables are invariant under field transformations, thus the choice of the matrix K is by no means unique. The common and very convenient choice is discussed in detail in the book by Georgi [48], it reads

$$Ru =: u' K(L, R, U) \quad \Leftrightarrow \quad K(L, R, U) = \sqrt{LU^\dagger R^\dagger R} \sqrt{U} ,$$

where we have introduced a new symbol $u^2 := U$. In the last section we have argued that the subgroup $H = \{(V, V) | V \in SU(3)\}$ leaves the ground state of Goldstone bosons invariant. Thus we demand that under this subgroup of chiral symmetry the baryons should transform independently of U , which is indeed the case since for $L = R = V \in H$

$$u \mapsto u' = \sqrt{VUV^\dagger} = \sqrt{(V\sqrt{U}V^\dagger)^2} = VuV^\dagger \quad \Rightarrow \quad K(V, V, U) = (VuV^\dagger)^{-1}Vu = V.$$

Given now the nonlinear realization of the chiral symmetry group and thus the transformation behaviour of the matter fields, i.e.

$$\begin{pmatrix} U \\ B \end{pmatrix} \mapsto \begin{pmatrix} U' \\ B' \end{pmatrix} = \begin{pmatrix} RUL^\dagger \\ K(L, U, R)BK^\dagger(L, U, R) \end{pmatrix}, \quad (1.12)$$

we can construct the most general effective baryonic Lagrangian, for which we again impose invariance under the *local* chiral symmetry group for reasons given in the last section. Consequently simple partial derivatives in the Dirac equation (recall that B consists of Dirac fields) are not independent upon the choice of coordinates and thus have to be replaced by a covariant form. In its minimal form it reads

$$D_\mu B = \partial_\mu B + [\Gamma_\mu, B] \quad \text{with} \quad \Gamma_\mu = \frac{1}{2}([u^\dagger, \partial_\mu u] - iu^\dagger(v_\mu + a_\mu)u - iu(v_\mu - a_\mu)u^\dagger),$$

which transforms as $D_\mu B \mapsto D'_\mu B' = KD_\mu BK^\dagger$, see Ref. [20] for an explicit proof. To further extent there also exists another quantity which exhibits the same transformation properties, it is called the chiral vielbein [49] and is defined as follows

$$u_\mu = iu^\dagger \nabla_\mu U u^\dagger,$$

where $\nabla_\mu U$ is defined in (1.10) in accordance with the transformation properties of the external fields as presented in (1.7). Since there are no further operators which are consistent with the local gauge symmetry, containing one derivative at most (at $\mathcal{O}(q)$), the leading order chiral meson-baryon Lagrangian reads

$$\mathcal{L}_{\phi B}^{(1)} = \langle \bar{B}(i\gamma_\mu D^\mu - m_0)B \rangle + \frac{D}{2} \langle \bar{B}\gamma_\mu\gamma_5\{u^\mu, B\} \rangle + \frac{F}{2} \langle \bar{B}\gamma_\mu\gamma_5[u^\mu, B] \rangle. \quad (1.13)$$

Here three new parameters appear which are not fixed by chiral symmetry alone, i.e. the mass of the baryon octet m_0 and the axial-vector coupling constants, D and F , in the chiral limit. In the two-flavour limit (πN chiral Lagrangian) both operators accompanied by the latter constants possess the same form such that only one constant is required, i.e. $\hat{g}_A = D + F$. At the lowest order the latter is equal to the axial-vector strength, which has been in the focus of many experiments for decades and was measured recently to high precision in the neutron β -decay using ultracold neutrons to be $g_A = 1.27590_{-0.00445}^{+0.00409}$, see Ref. [50]. The ratio F/D is predicted by the $SU(6)_f$ non-relativistic quark model (NRQM) to be $F/D = 2/3$ which is actually quite close to the value of this ratio extracted from experiments, namely $F/D = 0.58 \pm 0.05$, see Ref. [51] for a more detailed discussion. In practical calculations one is mostly satisfied with the tree level calculation [52] of semi-leptonic decays $B \rightarrow B' + e^- + \bar{\nu}_e$ which yields

$$D = 0.8 \quad \text{and} \quad F = 0.5.$$

The remaining parameter of the above Lagrangian deserves a further discussion as it induces somewhat more intricate power counting rules for the effective theory involving baryons. The main point is that in contrast to the matter fields of the purely mesonic chiral Lagrangian the baryon fields carry a mass which does not vanish in the chiral limit, i.e. $m = m_0(1 + \mathcal{O}(\hat{m}))$. The latter means that both, baryon mass as well as the operator \not{D} count as $\mathcal{O}(1)$. Naively this would destroy any power counting arguments and thus make any application of baryon ChPT

useless. However, it turns out that the operator $(i\not{D} - m_0)$ counts as $\mathcal{O}(q)$. To prove this we follow the arguments given in Refs. [44] and [53] and start with a baryon wave function Ψ of a momentum p and mass m_0 as a plane-wave solution of the free Dirac equation

$$\Psi(\vec{x}, t) = e^{-ip_\mu x^\mu} \sqrt{E + m_0} \begin{pmatrix} \chi \\ \frac{\vec{\sigma} \cdot \vec{p}}{E + m_0} \chi \end{pmatrix} \quad \text{with} \quad (i\not{D} - m_0)\Psi(\vec{x}, t) = 0 .$$

In a non-relativistic limit, i.e. small three momentum $|\vec{p}| \ll m_0$, the multiplicative factor can be split off and we can write generically $\Psi^\tau = (\phi, \psi)$, where the lower component ψ is suppressed compared to the upper one ϕ as

$$\psi = \frac{\vec{\sigma} \cdot \vec{p}}{2m_0} \phi + \mathcal{O}\left(\frac{1}{m_0^2}\right) .$$

Moreover, since Ψ fulfills the free Dirac equation it follows in the limit of small three-momenta

$$\begin{aligned} i\partial_t \phi - \vec{\sigma} \cdot \vec{p} \psi - m_0 \phi = 0 &\Rightarrow (i\partial_t - m_0)\phi = \vec{\sigma} \cdot \vec{p} \psi = \mathcal{O}(|\vec{p}|^2) , \\ i\partial_t \psi - \vec{\sigma} \cdot \vec{p} \phi + m_0 \psi = 0 &\Rightarrow (i\partial_t - m_0)\psi = -2m_0 \psi + \mathcal{O}(|\vec{p}|) = \mathcal{O}(|\vec{p}|) , \end{aligned}$$

which implies directly that $(i\partial_t - m_0)\Psi = \mathcal{O}(|\vec{p}|)$ and consequently also that $(i\not{D} - m_0)\Psi = \mathcal{O}(|\vec{p}|)$ since $(\gamma_i \partial^i)\Psi = \mathcal{O}(|\vec{p}|)$. Henceforth, we denote small three-momenta of baryons as well as the small meson momenta by q for convenience.

The chiral power counting rules of the previous section are completed with the following rules for the baryonic sector

$$m_0, B, \bar{B}, D_\mu B, \langle \bar{B} B \rangle, \langle \bar{B} \gamma_\mu B \rangle, \langle \bar{B} \gamma_\mu \gamma_5 B \rangle = \mathcal{O}(q^0) \quad \text{and} \quad (i\not{D} - m_0)B, \langle \bar{B} \gamma_5 B \rangle = \mathcal{O}(q^1) ,$$

which implies that the effective chiral Lagrangian does not only contain terms of even chiral order but reads

$$\mathcal{L}_{\phi B}^{\text{eff}} = \mathcal{L}_{\phi B}^{(1)} + \mathcal{L}_{\phi B}^{(2)} + \mathcal{L}_{\phi B}^{(3)} + \dots , \quad (1.14)$$

whereas all internal baryon lines are counted as $\mathcal{O}(q^{-1})$. That means that after an appropriate renormalization of mass and axial coupling constant, see Ref. [25] and the references therein, we can obtain the Weinberg prediction (1.3) for the πN scattering lengths starting from $\mathcal{L}_{\phi B}^{(1)}$. For an explicit calculation we refer the interested reader to e.g. Ref. [42, 54], where the threshold meson-baryon amplitudes have been calculated up to the third chiral order in the three-flavour formulation of baryon ChPT. However, doing so one is inevitably confronted with loop diagrams starting to contribute at the third chiral order whereas the second order corrections are given entirely by the local terms of $\mathcal{L}_{\phi B}^{(2)}$, which will be given later.

We wish to note that the naive assignment of a chiral order according to the counting rules defined above is not as straightforward as in the pure mesonic case once loop graphs are included. The complication arises again from the fact that the baryon mass does not vanish in the chiral limit. The appearance of this new scale of the order of $m_0 \sim \Lambda_\chi$ leads to the observation [43] that loop diagrams regularized in the framework of dimensional regularization (DR) contribute also to lower chiral orders than expected from the above power counting

rules. To be more specific, a one-loop diagram with vertices from $\mathcal{L}_{\phi B}^{(1)}$ is formally of the third chiral order, when regularized in DR it contains also terms of the second chiral order. The same holds for diagrams with more than one loop, meaning that in principle one would have to renormalize the low-energy constants due to effects of diagrams with arbitrary number of loops. Consequently every calculation beyond the leading order would lose any practical meaning. Two ways out of this dilemma have become popular in the recent years. The first one is called heavy baryon ChPT [55, 56], it relies on a non-relativistic expansion of the baryon kinematics, where the baryon momentum and baryon fields are separated into a large part and a small residual component. Whilst this method allows for a consistent power counting (as well as a massive simplification of the Dirac structures) it sacrifices manifest Lorentz invariance. On the other hand Becher and Leutwyler [57] (in principle already outlined in Refs. [43, 58, 59]) have developed a method to separate the loop integrals into an infrared singular and a regular part, referred to as the *infrared regularization*⁴. The singular part contains all non-analytic terms in quark mass and obeys 'naive' power counting, whereas the regular part can be written as a power series in the quark masses and thus can be absorbed order by order into the contact terms of the effective Lagrangian.

In the last two decades numerous calculations have been performed utilizing both regularization methods in two- and three-flavour formulation of ChPT, see e.g. Refs. [42, 54, 63–66]. An overall observation is that the convergence behaviour is hampered in the three-flavour formulation by the large kaon-loop effects in the baryon sector to even larger extent than in the pure mesonic case. Exemplary the chiral expansion of pion-nucleon scattering lengths up to the third chiral order yields in both formulations utilizing *infrared regularization*

$$SU(3) : \begin{cases} a_{\pi N}^{3/2} = -0.12(1 - 0.42 - 0.33) \\ a_{\pi N}^{1/2} = +0.21(1 + 0.23 - 0.91) \end{cases} \quad SU(2) : \begin{cases} a_{\pi N}^{3/2} = -0.12(1 - 0.54 - 0.02) \\ a_{\pi N}^{1/2} = +0.21(1 + 0.31 + 0.16) \end{cases} ,$$

which are written in form of $a_{\pi N}^{\text{Isospin}} = \mathcal{O}(q^1) + \mathcal{O}(q^2) + \mathcal{O}(q^3)$ and given in units of fm. Here, the second order LECs are taken from Refs. [42] and [67], respectively. Obviously the effects of virtual kaon and eta-mesons starting at the third chiral order are of the same order as the tree-level result in contrast to the case including only pion-loops. Consequently it is a priori not clear whether the sum of all contributions up to a certain (third) chiral order is enough to get a reliable numerical result. Nevertheless, the calculation of higher order corrections can provide useful information for example via matching relations between the LECs of the two- and three-flavour effective theories. Moreover, starting from the $SU(3)$ representation one obtains low-energy theorems for the pion-hyperon scattering as it was done in Ref. [42]. Recently these formulae became quite useful in the chiral extrapolations of pion-hyperon scattering from lattice simulations. As described in section 1.1, such numerical simulations are typically performed at higher than the physical pion mass. The low-energy theorems are perfectly suited to extrapolate these results to the physical point as it was done by the NPLQCD collaboration for the $\pi^+\Sigma^+$ and $\pi^+\Xi^0$ scattering lengths, see Fig. 1.1.

Up to now we have introduced a framework of meson-baryon analysis in the strictly perturbative sense of ChPT. Despite the shortcoming of convergence of the $SU(3)$ calculations one has to keep in mind that any calculation to a certain chiral order is restricted to low energies. To further extent the hadronic spectrum reveals a whole ladder of (excited) states on top of

⁴Similar schemes have been also developed in Refs. [58–62].

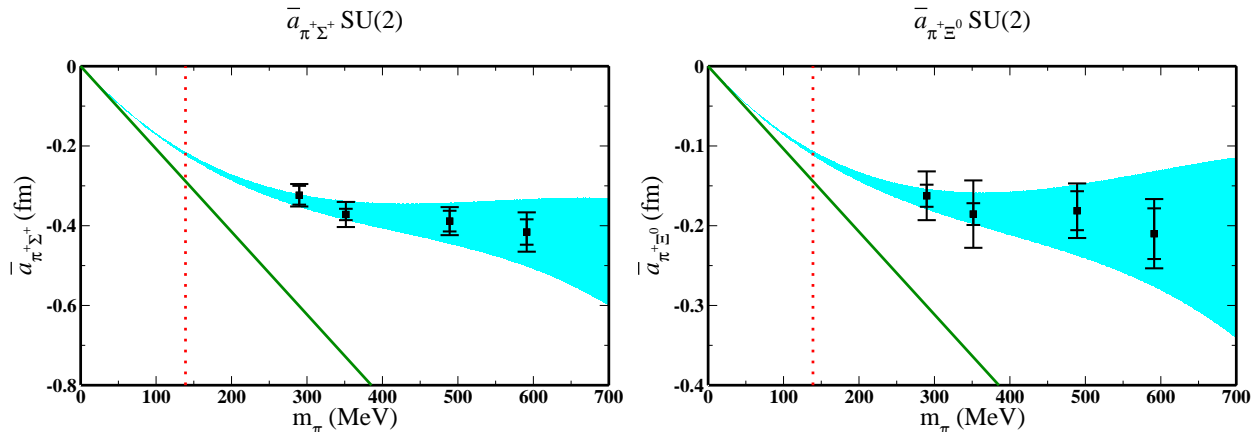


Figure 1.1: Chiral extrapolations of the $\pi^+\Sigma^+$ and $\pi^+\Xi^0$ scattering lengths from Ref. [68]. The full and dotted lines represent the leading order result and the physical point, respectively. The points with the error bars represent the lattice data and the filled bands the chiral extrapolation according to the low-energy theorems as derived in Ref. [42], respectively.

the ground state hadrons, e.g. the excited states of the nucleon $N^*(1535)S_{11}$, $\Delta(1620)S_{31}$ and $N^*(1650)S_{11}$. Dependent on their width and the reaction background these resonances can be observed in the (partial) cross sections of multi-particle collisions with appropriate quantum numbers as more or less sharp peaks. From a field theoretical point of view they can be found as poles of the scattering matrix in the complex energy plane, see chapter 3.1 and 3.8 of Ref. [69] and the discussion below. Clearly no calculation of the scattering amplitude which is truncated at a certain chiral order can yield such singular behaviour. In the next section we will demonstrate a method, called unitarized chiral perturbation theory, which allows for an extension of the range of applicability of the effective field theory and the description of resonances giving up some of the rigor of ChPT. It will even help us to shed some light on the nature (production mechanism) of some of those.

1.4 Chiral unitary approach to hadron physics

Modern physics has always been driven by a vision that the dynamics of a (meson-baryon) scattering system are constrained by a set of fundamental principles, most prominently⁵ Lorentz invariance, analyticity, unitarity and crossing symmetry. This belief is so strong that starting from the forties the axiomatic inclusion of these basic principles into the so-called S-Matrix theory was handled as a competitor of the quantum field theoretical approach. Later, with the advent of QCD this path was mostly given up, but the above principles are still believed to provide a fundamental insight into scattering processes. On the other hand the exact implementation of these turns out to be very involved. Various approaches have been proposed in the last decades, mostly favoring some of the properties with respect to the others, to name a few: Inverse Amplitude Method, K-Matrix, coupled-channel Lippmann-Schwinger Approach,

⁵For a more comprehensive list of these principles we refer the interested reader to the book by G. F. Chew [70].

Dispersion Relations. In principle, the Roy-type equations [71] implement analyticity, unitarity and crossing symmetry exactly, however, one requires an additional input from phenomenological approaches especially when going to higher energies. For a recent analysis of pion-nucleon scattering in this framework see Ref. [72]. In the present thesis we will stick to yet another method, called coupled-channel Bethe-Salpeter Equation which enables us to analyse the resonance energy region of meson-baryon scattering. Furthermore, using the solution of this equation as an effective vertex we will establish a connection to the meson photoproduction amplitude.

One of the primary principles of the S-matrix, already recognized by W. Heisenberg [73], was that of unitarity. Let us assume a transition of the state α_{in} prepared at the infinite past to a state β_{out} measured at the infinite future, its probability is given by the S-matrix element $S_{\beta\alpha} := (\beta_{out}, \alpha_{in})$. The integral over all possible intermediate states of the product of this element with the one of the reversed transition (given by $S_{\beta\alpha}^*$) yields

$$\int d\gamma S_{\gamma\beta}^* S_{\gamma\alpha} = \int d\gamma (\beta_{in}, \gamma_{out})(\gamma_{out}, \alpha_{in}) = (\beta_{in}, \alpha_{in}) = \delta(\alpha - \beta) , \quad (1.15)$$

where we have used completeness and orthogonality relation in the second and third step, respectively. In more general words that means $S^\dagger S = \mathbb{1}$, which involves the conservation of probability. Here, $\mathbb{1}$ denotes the identity matrix in the Hilbert space. To be more specific and following the conventions of Ref. [70] let us first assume a theory of only two spinless fields of mass m_1 and m_2 for simplicity. The four-line connected part is described by a scattering amplitude T as follows

$$S = (2\pi)^4 \delta^4(p_1 + p_2 - p'_1 - p'_2) \left(\mathbb{1} - iT(p'_1, p'_2, p_1, p_2) \right) ,$$

where $p_{1,2}$ and $p'_{1,2}$ are the four-momenta of the in- and outgoing particles, respectively. For the case of particles with spin T becomes a spinor function and the S-matrix is obtained by sandwiching it between initial and final spinors. In the sense of Eq. (1.15) we have to integrate over all open intermediate channels, i.e. particles which are on the mass shell and have positive energy. Thus the available phase space for each intermediate particle (i) is reduced to

$$\frac{1}{(2\pi)^3} \int d^4 p_i \delta(p_i^2 - m_i^2) \theta(p_i^0) .$$

Here and in the future the limit $d \rightarrow 4$ is taken if not stated otherwise. In principle the number of these states depends on energy and the selection rules only. However, in the present work we will be only concerned with the implications of two-particle unitarity but will comment on the effects of $\pi\pi N$ intermediate channel to pion-nucleon scattering later. We denote the four-momenta of the intermediate particles by $k_{1/2}$ and insert the last two equations into Eq. (1.15) to find

$$\begin{aligned} T(p'_1, p'_2, p_1, p_2) - T^*(p'_1, p'_2, p_1, p_2) &= -\frac{i}{(2\pi)^2} \int d^4 k_1 \delta(k_1^2 - m_1^2) \theta(k_1^0) \int d^4 k_2 \delta(k_2^2 - m_2^2) \theta(k_2^0) \\ &\quad \times T^\dagger(p'_1, p'_2, k_1, k_2) T(k_1, k_2, p_1, p_2) , \end{aligned} \quad (1.16)$$

where again T^* corresponds to a process reversed with respect to T . We can capture the dependence of the scattering amplitude on the external momenta in terms of Mandelstam

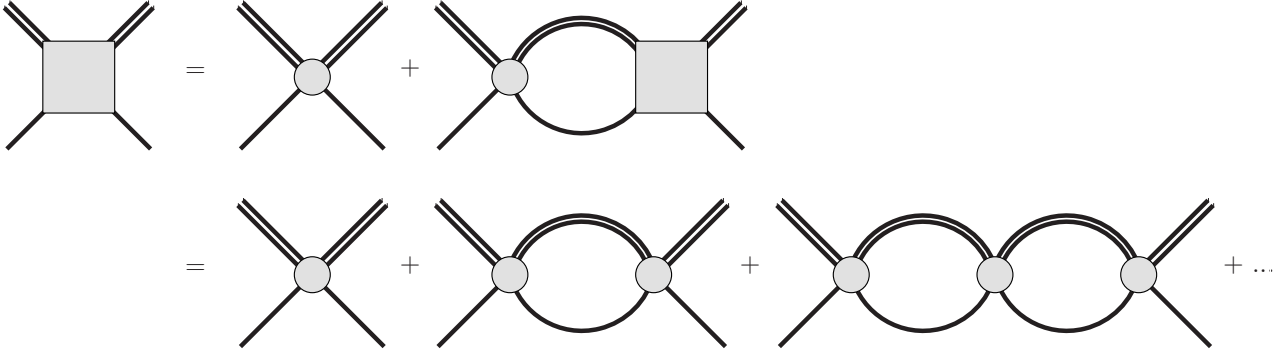


Figure 1.2: Symbolical representation of the Bethe-Salpeter equation. The shaded squares and circles represent the scattering amplitude and the interaction potential, respectively, whereas the single and double lines denote the propagation of the particles of masses m_1 and m_2 .

variables $s = (p_1 + p_2)^2$, $t = (p_1 - p'_1)^2$, $u = (p_1 - p'_2)^2$. Since only two of them are independent we choose for convenience the center-of-mass energy squared s and the cosine of the angle of the scattering in the center-of-mass system z , which can be related to the momentum transfer squared⁶ as $t = 2q_{\text{cms}}^2(z - 1)$ with q_{cms} being the modulus of the three-momentum in the center-of-mass system

$$q_{\text{cms}} := \frac{1}{2\sqrt{s}} \sqrt{(s - (m_1 + m_2)^2)(s - (m_1 - m_2)^2)}. \quad (1.17)$$

In these variables (s, z) and after some algebra the unitarity condition can be written as

$$T(s, z) - T^*(s, z) = -\frac{i}{16\pi^2\sqrt{s}} \int d\Omega_{\text{int}} T^*(s, z'') q_{\text{cms}} \theta(s - (m_1 + m_2)^2) T(s, z'), \quad (1.18)$$

where $z'(z'')$ denotes the cosine of the angle between the initial (final) and intermediate direction. Actually, q_{cms} does not depend on the integration variable and can be pulled out of the integral. However, for the general case of more than one interaction channel the last equation turns into a matrix equation, where $q_{\text{cms}} \theta(s - (m_1 + m_2)^2) \mapsto \text{diag}(q_{\text{cms}}^1, q_{\text{cms}}^2, q_{\text{cms}}^3, \dots, 0, \dots)$ with zero-elements for the energetically closed channels as ensured by the use of the Heaviside function θ .

It turns out that regardless of the production mechanism of the resonances most of their properties follow from unitarity. On the other hand it is quite obvious from Eq. (1.18) that any calculation to a finite order in (chiral) perturbation theory cannot satisfy unitarity exactly. Assume for example that the scattering amplitude is calculated up to a certain order n of some coupling g , then the l.h.s of Eq. (1.18) is of order g^n whereas the r.h.s contains terms of order g^{n+1} . Thus a non-perturbative scheme is required to fulfill unitarity exactly. One very established method utilizes the Bethe-Salpeter Equation (BSE) [74] which reads for an arbitrary interaction potential V in the formalism defined above

$$T(p'_1, p'_2, p_1, p_2) = V(p'_1, p'_2, p_1, p_2) + \int \frac{d^4 k_1}{(2\pi)^4} V(p'_1, p'_2, k_1, p - k_1) G(p, k_1) T(k_1, p - k_1, p_1, p_2), \quad (1.19)$$

⁶See also Eq. (D.1) in App. D for a general case.

where $G(p, k_1) := i/((k_1^2 - m_1^2 + i\epsilon)((p - k_1)^2 - m_2^2 + i\epsilon))$ and the pertinent diagrammatic representation is given in Fig. 1.2. Keeping in mind the definition of the overall four-momentum of the scattering $p = p_1 + p_2 = p'_1 + p'_2 = k_1 + k_2$ and the real character of the interaction potential V we can write in a rather symbolical way

$$\begin{aligned} T - T^* &= V + VGV + VGVGV + \dots - V - VG^*V - VG^*VG^*V - \dots \\ &= V(G - G^*)V + V(G - G^*)VG^*V + VGV(G - G^*)V + \dots \\ &= T(G - G^*)T^* , \end{aligned}$$

where loop integrals are suppressed for simplicity. As a matter of fact this equation is an alternative version of Eq. (1.16) and thus ensures the unitarity of the S-matrix calculated from the Bethe-Salpeter equation.

As already emphasized and also presented in the second line of the Fig. 1.2 the solution of the BSE corresponds to an infinite chain of (Feynman) bubble diagrams. Quite often Eq. (1.19) is simplified in the so-called on-shell approximation, where the intermediate particles are put on their mass shell, in which case any connection to the Feynman diagrams is lost and the solution of the BSE amounts only to a geometric series. Simply iterating a fixed on-shell kernel in such a geometric series can even lead to significant deviations from the results of Feynman graphs when iterating Born-terms, as is exemplified by an analysis of box graphs in sec. (5.2) of Ref. [75]. In the course of this work we will refrain from such approximations, inter alia in view of the analysis of the meson photoproduction, see chapter 5, which requires the full diagrammatic interpretation of the BSE solution. Nevertheless it should be mentioned that this unitarization procedure has two major drawbacks:

- The summation of bubble diagrams in Fig. 1.2 is only performed in the s -channel, thus the solution of the BSE is in general not crossing symmetric, which is a common shortcoming of all unitarization schemes. An approximate restoration of this principle is proposed in the context of meson-meson scattering in Ref. [76, 77].
- The second shortcoming of the above resummation scheme concerns analyticity. As a matter of fact the imaginary part of the one-loop function, given by

$$\tilde{G}(s = p^2) = \int \frac{d^4k}{(2\pi)^4} G(p, k) = \int \frac{d^4k}{(2\pi)^4} \frac{i}{(k^2 - m_1^2 + i\epsilon)((p - k)^2 - m_2^2 + i\epsilon)} , \quad (1.20)$$

can be deduced easily utilizing Cutkosky rules to be $\text{Im}(\tilde{G}(s)) = -q_{\text{cms}}/(8\pi\sqrt{s})$. Assuming the analyticity of the loop-function in the variable $s \in \mathbb{C} \setminus [s_{\text{thr}}, \infty]$ we can deduce its full form utilizing a dispersion relation. However, this function is logarithmically divergent in four space-time dimension, thus we subtract it once to find

$$\tilde{G}(s) = \tilde{G}(s_0) + \frac{(s - s_0)}{\pi} \int_{s_{\text{thr}}}^{\infty} ds' \frac{\text{Im}(\tilde{G}(s'))}{(s' - s)(s' - s_0)} , \quad (1.21)$$

where s_0 is the so-called subtraction point which has to lie inside the integration contour and $s_{\text{thr}} = (m_1 + m_2)^2$. Of course the r.h.s of the above equation exhibits the same kind of logarithmic divergence, which is captured in the subtraction constant $\tilde{G}(s_0)$, we will turn to the regularization of the loop-integrals later. Albeit the above solution is built from

such loop functions, see Eq. (1.19), it is so far not known how to implement this property in the solution of BSE exactly. In chapter 3 we will propose a method of approximate restoration of analyticity, also interesting steps in a similar framework have been made in Refs. [78] and [79].

Despite these shortcomings, the BSE has become quite popular in the framework of the so-called *chiral unitary approaches*, where the potential V in Eq. (1.19) is derived from the chiral Lagrangian. This technique has widened our understanding of the hadronic spectrum enormously both in the mesonic as well as in the baryonic sector, to name a few references [61, 79–84]. In the following chapters we will construct and analyse a solution of the Bethe-Salpeter equation (1.19) for meson-baryon scattering with the chiral potential of the second chiral order but before doing so we shall make a few last general remarks.

The first question we have not addressed yet is that of renormalization. We have already mentioned that the loop-integral $\tilde{G}(s)$ is divergent in four space-time dimension. There are various ways of regulating these divergences, e.g. cutoff, Pauli-Villars [85] or dimensional regularization [86]. The cutoff regularization is quite convenient for practical calculation and has been employed in the framework of BSE by different authors, see e.g. Ref. [87] and references therein. Seemingly the numerical simplicity is gained losing control of analytic structure, i.e. often very unnatural cutoff scales are required, which was pointed out in Ref. [88]. To overcome these shortcomings we will construct a regularization scheme, which is in principle similar to [57, 60, 62], starting from dimensional regularization. For an exact explanation and implications of the latter we refer the reader to the textbooks, see e.g. [69, 89, 90]. For our purposes it is sufficient to say that one starts with the continuation of the Minkowski space to d dimensions. Then the loop-integral $\tilde{G}(s)$ can be evaluated utilizing standard techniques, such as Feynman parameterization and Wick rotation. After performing the loop-integration one obtains the physical picture back taking the limit $d \rightarrow 4$ in which the UV-divergences of the loop-integral are captured in the behaviour of the gamma function, i.e. $\Gamma(y) = \int_0^\infty e^{-x} x^{y-1} dx$. In the usual (perturbative⁷) sense of renormalizable field theories one can now subtract this divergence from the loop-integral, which can then be reabsorbed into the local counter terms of the theory, see e.g. Ref. [90]. In principle the separation between the finite (\tilde{G}_{fin}) and infinite (\tilde{G}_∞) piece of the loop-integral is arbitrary. In this context the so-called \overline{MS} scheme [91] has found much use in QCD. Utilizing this scheme, the infinite part reads

$$\tilde{G}_\infty = \frac{\mu^{d-4}}{16\pi^2} \left(\frac{1}{d-4} - \frac{1}{2} (\log(4\pi) - \gamma_E + 1) \right) \quad \text{for} \quad \tilde{G} = \tilde{G}_{\text{fin}} + \tilde{G}_\infty ,$$

where μ is the regularization scale and $\gamma_E \approx 0.5772$ is the Euler-Mascheroni constant. The finite part is given by $\tilde{G}_{\text{fin}} = I_{MB}(s, m_1, m_2)$ as presented in App. A. We remind the reader that we are dealing with a non-perturbative framework where the loop-integral enters the discussion via an infinite chain of bubble diagrams with rising number of loops. Obviously this demands for an infinite number of local terms from the underlying Lagrangian to reabsorb the loop divergences and thus is not feasible from the technical point of view. To further extent the counter terms from the local Lagrangian are crossing symmetric by construction [88] in contrast to the BSE solution as emphasized above. To overcome this obstacle we shall, for a moment, take a look

⁷Up to date it is not known how to use this method in non-perturbative settings.

on the solution of the on-shell approximated BSE. The integral equation (1.19) turns into an algebraic equation with the following solution

$$T_{\text{on}} = V + V\tilde{G}T_{\text{on}} \quad \Rightarrow \quad T_{\text{on}} = \frac{1}{V^{-1} - \tilde{G}} .$$

The intuitive candidate for an absorption of infinite part of the loop-integral is the interaction potential V . Let us separate the latter as $V = V_{\text{fin}} + V_{\infty}$ for which we demand that

$$\frac{1}{V^{-1} - \tilde{G}} = T_{\text{on}} = \frac{1}{V_{\text{fin}}^{-1} - \tilde{G}_{\text{fin}}} ,$$

which determines the V_{∞} for any potential V and G_{∞} for the on-shell BSE solution. The corresponding demonstration for the off-shell BSE can be found in App. F of Ref. [92]. Consequently the infinite part of the loop-integral is canceled by an appropriate term in the potential V , thus allowing us for a calculation of the scattering amplitude from exclusively finite quantities.

On the other hand we have to keep in mind that the finite part of the loop integral is scale (μ) dependent. In perturbative calculations this scale dependence is canceled by the contact terms from the effective Lagrangian. However, since any practical treatment requires a truncation of the underlying interaction potential at some finite order the residual scale dependence reflects the influence of the higher order contributions. For this reason we will use the appearing regularization scale as a fitting parameter which is in fact similar to the discussion in Refs. [84,88] where for each loop integral a finite subtraction constant is introduced, used also as a free parameter. In chapter 5 we will reexamine this strategy adjusting the regularization scale to a fixed value.

Recently an other question has been discussed widely in the community, i.e. the field parametrization dependence. In section 1.2 we have argued that the representation of the meson fields is not unique and have presented two frequently used examples. Physical quantities do not depend upon the choice of fields as well as the on-shell solution of the BSE, where all intermediate particles are put on their mass shell. The off-shell quantities are on the other hand in general not independent of this choice and consequently also the solution of the off-shell BSE. This argument has become very popular as a justification of the on-shell scheme in the recent time. Albeit there is no general proof to rebut it we would like to make a remark here. Two most used parametrization schemes, the exponential- and the sigma-parametrization (Eq. (1.8) and (1.9)) yield the following expansion in the number of meson fields

$$\begin{aligned} u_{\text{exp}} &= 1 + i\frac{\phi}{2F} - \frac{\phi^2}{8F^2} - i\frac{\phi^3}{48F^3} + \mathcal{O}(\phi^4) , \\ u_{\sigma} &= 1 + i\frac{\pi}{2F} - \frac{\pi^2}{8F^2} + i\frac{\pi^3}{16F^3} + \mathcal{O}(\pi^4) . \end{aligned}$$

Both expansions coincide for the case of up to two meson fields, thus the result of one-loop bubble diagram is independent whether one chooses the sigma- or exponential parametrization. Such diagrams are the main ingredient of the solution of the BSE and thus we expect it to be independent of this particular choice. Please note that this argument only holds for two representatives of the whole class of field variables and thus is not a general proof.

In the main part of this thesis we will analyse various implications of such a chiral unitary approach based on the solution of the BSE with the full off-shell dependence and interaction

kernel from the NLO chiral Lagrangian. In the next chapter we will address several technical aspects for the construction of the solution of our chiral unitary framework, whereupon different applications will be presented. In the last two chapters this framework will be extended to a gauge-invariant chiral unitary framework for meson photoproduction.

Chapter 2

Solution of the Bethe-Salpeter equation

2.1 Framework

In this complementary chapter we wish to introduce the necessary formalism and the explicit solution techniques of the Bethe-Salpeter equation for meson-baryon scattering. These techniques apply also for the iteration of higher order potentials and thus may be of interest for future works.

The pivotal equation of our chiral unitary approach is the Bethe-Salpeter equation which allows for an implementation of exact two-body unitarity without loosing direct correspondence to the Feynman graphs. For the process of interest, meson-baryon scattering, we denote the in- and out-going meson momenta by q_1 and q_2 , respectively. The overall four-momentum shall be given by $p = q_1 + p_1 = q_2 + p_2$, where p_1 and p_2 are the momenta of in- and outgoing baryon, respectively. For meson-baryon scattering amplitude $T(q_2, q_1; p)$ and potential $V(q_2, q_1; p)$ the integral equation to solve reads in d dimensions

$$T(q_2, q_1; p) = V(q_2, q_1; p) + \int \frac{d^d l}{(2\pi)^d} V(q_2, l; p) \frac{i}{(l^2 - M^2 + i\epsilon)(\not{p} - \not{l} - m + i\epsilon)} T(l, q_1; p), \quad (2.1)$$

where m and M denote the mass of baryon and meson, respectively. This equation has to be understood as a matrix equation in the channel space, spanned by all assumed interaction channels, which justifies the present model as the coupled-channel approach. In our analysis these channels will be considered as combinations of the ground state octet mesons and baryons in agreement with the assumed quantum numbers as specified in the following chapters. The important point here is that every element of the above equation represents a matrix in this channel space, e.g. all propagators should be understood as diagonal matrices. The diagrammatic representation of the BSE (2.1) is of the same structure as the one given before and is depicted for meson-baryon scattering in Fig. 2.1.

For the driving term of the above equation we will consider the chiral meson-baryon potential. At the leading order the covariant derivative in the chiral Lagrangian Eq. (1.13) gives rise to the so-called Weinberg-Tomozawa potential, V_{WT} , which reads after separating the channel space

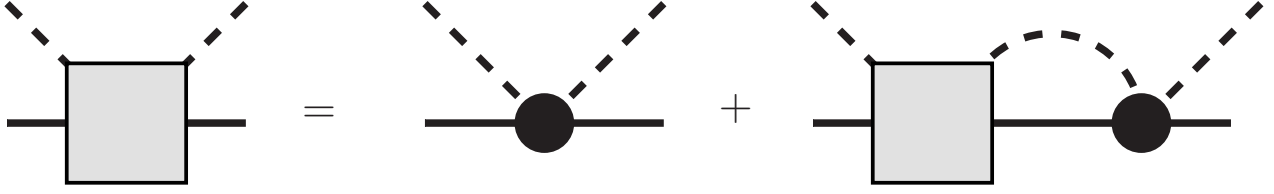


Figure 2.1: Symbolical representation of the Bethe-Salpeter equation. Here, the circle and the square represent the potential V and the scattering amplitude T , respectively. The propagation of a meson (baryon) is symbolized by a dashed (full) line.

structures from the Dirac-momentum structures as

$$V_{WT}(q_2, q_1; p) = A_{WT}(q_1 + q_2) . \quad (2.2)$$

The channel matrix A_{WT} is presented in App. C in terms of channel space matrices and meson decay constants as explained in section 1.3. The Weinberg-Tomozawa term dominates the s-wave meson-baryon interaction around the threshold. For instance the calculation of pion-nucleon scattering lengths starting from it yields the Weinberg prediction (1.3). From a more practical point of view this term allows for a quite straightforward resummation in the framework of Bethe-Salpeter type equations due to the simple momentum structure, see e.g. Ref. [92]. For these two reasons most chiral unitary approaches are restricted to the Weinberg-Tomozawa interaction kernel. However, there are two additional contributions arising from the same Lagrangian which are formally of the first chiral order, namely the u - and s -channel baryon exchange graphs. These, so-called Born-graphs have a much more involved structure which reads

$$\begin{aligned}
 & \begin{array}{c} i \quad j \\ \diagdown \quad \diagup \\ \text{---} \\ a \quad c \quad b \end{array} \quad \longrightarrow \quad q_2 \gamma_5 A_X^{b,j;c} \frac{\not{p} + m_c}{s - m_c^2} A_X^{c;a,i} \gamma_5 q_1 , \\
 & \begin{array}{c} i \quad j \\ \diagdown \quad \diagup \\ \text{---} \\ a \quad c \quad b \end{array} \quad \longrightarrow \quad \gamma_5 q_1 A_X^{b;c,i} \frac{\not{p} - q_1 - q_2 + m_c}{u - m_c^2} A_X^{c;j;a} q_2 \gamma_5 ,
 \end{aligned} \quad (2.3)$$

where we have abandoned the (channel space) matrix notation for a moment to emphasize that A_X is actually a mapping from a meson-baryon channel onto the set of baryons only, as detailed in App. C. Apart from the fact that both terms possess a much richer structure than the Weinberg-Tomozawa term they both lead to conceptual and practical difficulties in the framework of the Bethe-Salpeter type equations:

- The inclusion of the u -channel Born graphs into the kernel of the BSE leads to an infinite number of multi-loop topologies with 3 (1), 5 (2), 7 (3),... internal baryon (meson) lines. Obviously such topologies cannot be decomposed into simple series of one-loop integrals but have to be evaluated directly. To the best of our knowledge this technical issue

has not been overcome yet and calls in our opinion for an alternative non-perturbative technique to the Bethe-Salpeter type equation. An interesting idea in this direction may be the application of the Feynman-Schwinger representation approach [93] which, however, requires further investigations.

- The inclusion of the s -channel Born graphs is on the other hand technically less tangled since the denominator of the corresponding potential does only depend upon the Mandelstam s . However, it leads to conceptual difficulties as it induces graphs responsible for baryon mass renormalization. An exemplary Feynman graph occurring when a local term is iterated together with the s -channel Born graph looks as follows



Here, in addition to the notation of the Fig. 2.1 we have to distinguish between the propagation of the baryon with bare and dressed mass (thin and bold full lines). The reason is that the meson-baryon loop-graphs in the above picture contribute to mass (and wave function) renormalization of the baryons and consequently to avoid double counting we have to assign bare mass for these. Contrary the mass of the baryons within the meson-baryon loops is not renormalized by these effects as the BSE only accounts for a simple rescattering processes. Not only is this treatment very unsystematic (not all renormalization effects are accounted for) but more importantly in view of a later application to photoproduction such a non-perturbative treatment of s -channel exchanges leads to complications with gauge invariance because the selfenergies are linked (via a Ward-Takahashi identity) to the electromagnetic baryon form factors, which would also have to be treated in a corresponding (non-perturbative) fashion, see Ref. [94].

In most chiral unitary approaches these issues are overcome utilizing the on-shell formalism, see e.g. Refs. [95,96]. Then as mentioned before the direct correspondence to Feynman graphs is lost, hence neither multi-loop topologies nor renormalization of baryon fields are relevant issues anymore. A more promising method was developed in Ref. [97] and applied to meson-baryon scattering in Ref. [98], it utilizes form factors to regularize Wick rotated loop-integrals. Unfortunately this method requires cutoff parameters and introduces unphysical thresholds. Similar principles are worked out and utilized in the framework of three dimensional form of the BSE, the so-called Lippmann-Schwinger equation in Refs. [99,100].

Our wish remains the preservation of the direct correspondence of the BSE to the Feynman graphs with no cutoff, hence we do not consider the above approximations, but stick to the full off-shell BSE with local terms from the chiral meson-baryon Lagrangian as driving terms. In our earlier analysis of meson-baryon scattering [42] in the framework of strict perturbative ChPT we have seen that the NLO local terms result in sizable corrections of the scattering lengths as we have pointed out in section 1.3. Furthermore, the NLO contact terms do not only contribute to the s -waves but also to p -waves. To see which implications arise from iteration of such contributions we will also include the second order chiral potential into the kernel of the BSE. The pertinent Lagrangian density was first constructed in Ref. [44] and reads in its

minimal form [101]

$$\begin{aligned}
\mathcal{L}_{\phi B}^{(2)} = & b_0 \langle \bar{B} B \rangle \langle \chi_+ \rangle + b_D \langle \bar{B} \{ \chi_+, B \} \rangle + b_F \langle \bar{B} [\chi_+, B] \rangle \\
& + b_1 \langle \bar{B} [u_\mu, [u^\mu, B]] \rangle + b_2 \langle \bar{B} [u_\mu, \{ u^\mu, B \}] \rangle + b_3 \langle \bar{B} \{ u_\mu, \{ u^\mu, B \} \} \rangle + b_4 \langle \bar{B} B \rangle \langle u_\mu u^\mu \rangle \\
& + i b_5 \langle \bar{B} \sigma^{\mu\nu} [[u_\mu, u_\nu], B] \rangle + i b_6 \langle \bar{B} \sigma^{\mu\nu} \{ [u_\mu, u_\nu], B \} \rangle + i b_7 \langle \bar{B} \sigma^{\mu\nu} u_\mu \rangle \langle u_\nu B \rangle \\
& + \frac{i b_8}{2m_0} \left(\langle \bar{B} \gamma^\mu [u_\mu, [u_\nu, [D^\nu, B]]] \rangle + \langle \bar{B} \gamma^\mu [D_\nu, [u^\nu, [u_\mu, B]]] \rangle \right) \\
& + \frac{i b_9}{2m_0} \left(\langle \bar{B} \gamma^\mu [u_\mu, \{ u_\nu, [D^\nu, B] \}] \rangle + \langle \bar{B} \gamma^\mu [D_\nu, \{ u^\nu, [u_\mu, B] \}] \rangle \right) \\
& + \frac{i b_{10}}{2m_0} \left(\langle \bar{B} \gamma^\mu \{ u_\mu, \{ u_\nu, [D^\nu, B] \} \} \rangle + \langle \bar{B} \gamma^\mu [D_\nu, \{ u^\nu, \{ u_\mu, B \} \}] \rangle \right) \\
& + \frac{i b_{11}}{2m_0} \left(2 \langle \bar{B} \gamma^\mu [D_\nu, B] \rangle \langle u_\mu u^\nu \rangle + \langle \bar{B} \gamma^\mu B \rangle \langle [D_\nu, u_\mu] u^\nu + u_\mu [D_\nu, u^\nu] \rangle \right) \\
& + b_{12} \langle \bar{B} \sigma_{\mu\nu} [f_+^{\mu\nu}, B] \rangle + b_{13} \langle \bar{B} \sigma_{\mu\nu} \{ f_+^{\mu\nu}, B \} \rangle , \tag{2.4}
\end{aligned}$$

where $f_+^{\mu\nu}$ includes the electromagnetic field strength tensor, which vanishes for $v^\mu = 0$ but will become important for the photoproduction amplitude later, see chapter 5 for details. The Dirac-momentum structures commute with those of the channel space thus it is convenient to separate them from each other such that the second order chiral potential, which completes Eq. (2.2), reads

$$V_{NLO}(q_2, q_1; p) = A_M + A_{14}(q_1 \cdot q_2) + A_{57}[q_1, q_2] + A_{811}(q_2(q_1 \cdot p) + q_1(q_2 \cdot p)) , \tag{2.5}$$

where the low-energy constants b_i , which accompany the operators of Eq. (2.4) are included in the matrices A_{\dots} as detailed in App. C. Very little is known about the numerical values of these constants, hence we shall use them as a fit parameters of our model. In order to remain unbiased we can impose only two constraints, namely they should (i) remain of natural size, because too large values of LECs would indicate some prominent effects missing in our approach and (ii) agree with the $SU(3)$ to $SU(2)$ matching relations derived in Refs. [41, 42]. Once determined they still have to be taken with a grain of salt, because the present approach is suited to account for meson-baryon scattering (later also for the meson photoproduction) correctly but lacks universality, i.e applicability to other processes. More likely is that from the present approach one can determine only certain linear combinations of these LECs reliably.

2.2 Regularization

In the previous chapter we have already started the discussion of the regularization procedure of the loop integrals appearing in the BSE. For reasons given there we utilize the dimensional regularization for the one-meson-one-baryon loop integrals in the \overline{MS} scheme, see App. A. This, however, is not the end of story since without restricting the intermediate particles on their mass shell one also obtains a non-vanishing contribution from meson and baryon tadpole integrals, denoted henceforth by I_M and I_B , respectively. This can be seen easily utilizing the Passarino-Veltman [102] reduction of the tensor loop integrals. Consider the most simple case

which already arises in Eq. (2.1) due to the fermionic nature of the intermediate baryon, namely

$$I_{MB}^\mu := i \int \frac{d^d l}{(2\pi)^d} \frac{l^\mu}{(l^2 - M^2 + i\epsilon)((l-p)^2 - m^2 + i\epsilon)} = p^\mu I_{MB}^{(1)},$$

where the second equality is justified by Lorentz invariance. The unknown scalar function $I_{MB}^{(1)}$ can be determined if one contracts I_{MB}^μ with p^μ which results in

$$p^2 I_{MB}^{(1)} = i \int \frac{d^d l}{(2\pi)^d} \frac{p_\mu l^\mu}{(l^2 - M^2 + i\epsilon)((l-p)^2 - m^2 + i\epsilon)} = \frac{1}{2} \left(I_M - I_B + (p^2 - m^2 + M^2) I_{MB} \right).$$

where in the second step $2p_\mu l^\mu = (M^2 - m^2 + p^2 - ((l-p)^2 - m^2) + (l^2 - M^2))$ was used. The scalar component $I_{MB}^{(1)}$ is now completely determined in terms of the standard scalar loop functions. In the same sense Passarino-Veltman reduction will be applied to all possible tensor structures appearing in the numerator of the BSE, such that the full solution will be a function of scalar loop functions only.

This procedure leads to yet another difficulty which is rooted in the obscurity of non-perturbative renormalization. The crucial point here is the following: The loop integrals which enter the solution of the BSE are in general UV-divergent. Considering dimensional regularization we can map these divergences onto $(d-4)^{-1}$ poles modulo some higher order terms in $(d-4)$. In a perturbative calculation we would then take a limit of $d \rightarrow 4$, reabsorbing the infinite part by a renormalization of the coupling constants entering such calculation, see discussion in section 1.4. However, in the solution of the BSE one is inevitably confronted with an infinite number of such integrals, or more specifically with sums of products of arbitrary many UV-divergent loop integrals. Therefore strictly speaking all terms in the $(d-4)$ expansion have to be taken into account. Each one of those terms will enter the calculation in a highly nontrivial (and at present not clarified way). To overcome this obstacle we shall set $d = 4$ from the beginning which is in principle not a problem for the solution of the BSE itself, but becomes an issue for the photoproduction amplitude constructed from the hadronic solution as we will demonstrate now.

Gauge invariance, another fundamental principle of field theory which we will demand for the photoproduction amplitude, calls for the inclusion of the so-called triangle diagrams¹ when the photon is coupled to the hadronic skeleton, see chapter 5. Now dealing with the NLO driving term we are inevitably confronted with loop integrals of the form

$$I_{MMB}^{\mu\nu\sigma} := i \int \frac{d^d l}{(2\pi)^d} \frac{l^\mu l^\nu l^\sigma}{(l^2 - M_1^2 + i\epsilon)((l-k)^2 - M_2^2 + i\epsilon)((l-p)^2 - m^2 + i\epsilon)}, \quad (2.6)$$

$$I_{MBB}^{\mu\nu\sigma} := i \int \frac{d^d l}{(2\pi)^d} \frac{l^\mu l^\nu l^\sigma}{(l^2 - M^2 + i\epsilon)((l-p_1)^2 - m_1^2 + i\epsilon)((l-p)^2 - m_2^2 + i\epsilon)}, \quad (2.7)$$

where in both k denotes the photon four-momentum and $m_{\dots}(M_{\dots})$ the mass of internal baryons (mesons) in the loop. Similar to the previous case we can reduce the tensor rank of the numerator utilizing the Passarino-Veltman reduction. It yields for the second integral

$$I_{MBB}^{\mu\nu\sigma} \stackrel{d=4}{=} [\dots]^{\mu\nu\sigma} \frac{I_B(m_1^2) - I_B(m_2^2) - (m_1^2 - m_2^2) I_{BB}(k^2, m_1, m_2)}{3k^4(p_1^2 - s)} + \mathcal{O}\left(\frac{1}{k^2}\right), \quad (2.8)$$

¹Loop diagrams with three intermediate particles.

where $[\dots]^{\mu\nu\sigma}$ denotes generically the tensor structures allowed by Lorentz invariance. As a matter of fact in perturbative calculations this reduction is performed in d dimensions for all graphs of the desired order and required by the gauge invariance. Then taking the limit $d \rightarrow 4$, terms of the form presented on the r.h.s. of the above equation cancel against each other. Unfortunately, for reasons given above, we are forced to set d equal 4 already in the first steps of our calculation, hence we are confronted with the terms, formally singular for $k^2 \rightarrow 0$. On the first sight the situation should be similar for the case of $I_{MMB}^{\mu\nu\sigma}$, where one formally has to interchange the meson and baryon masses. However, considering only interactions of the second chiral order the photon is incapable to change the 'type' of the meson, hence we can assume $M_1 = M_2$. It turns out that for baryons the same holds at the leading but not at the next-to-leading order, at which the photon can induce e.g. the $\Sigma^0 \leftrightarrow \Lambda$ transition. Consequently we have to assume that $m_1 \neq m_2$, which causes the presence of formal (unphysical) singularities in the photoproduction amplitude, see Eq. (2.8) and App. B.

At this point it is instructive to recall the discussion of various regularization schemes in section 1.3 to overcome the infrared divergences in baryon ChPT. Dealing here with a non-perturbative framework these cannot be rigorously be implemented here, however, utilizing for example the EOMS [60, 62] or infrared [57] type of regularization all scalar loop integrals containing only baryons are set to zero, such that terms singular for $k^2 \rightarrow 0$ vanish exactly, see Eq. (2.8). Inspired by this, we shall utilize dimensional regularization and apply the \overline{MS} subtraction scheme setting all baryon loops, i.e. I_B and I_{BB} , to zero. All required scalar loop integrals as well as the reduction rules are collected in App. A and B.

2.3 Solution

Having clarified the regularization scheme we are now in the position to present a technique for the solution of the Bethe-Salpeter equation (2.1) with the full off-shell dependence. This method does not rely on any approximation of the BSE which are used very often in the literature, i.e. on-shell approximation or a three-dimensional reduction of the BSE to the Lippmann-Schwinger equation. It is also applicable for any kernel with only one restriction: The interaction kernel must consist of local terms only. Thus the solution of the BSE corresponds to an infinite chain of the Feynman bubble diagrams as presented in Fig. 2.1. To keep this section short we will restrict the form of the kernel to the one used in the main text of this work. Up to the next-to-leading chiral order the meson-baryon local potential is given by the sum of potentials presented in Eq. (2.2) and (2.5) and can be written in general form as follows

$$V(q_2, q_1; p) = \sum_{i=1}^6 A_i \mathcal{D}_i(q_2, q_1; p) , \quad (2.9)$$

$$\begin{aligned} \text{with} \quad & \mathcal{D}(q_2, q_1; p) = (q_1, q_2, (q_1 \cdot q_2), q_2 q_1, id, q_2(q_1 \cdot p), q_1(q_2 \cdot p)) \\ \text{and} \quad & A = (A_{WT}, A_{WT}, (A_{14} + 2A_{57}), A_{57}, A_M, A_{811}, A_{811}) , \end{aligned}$$

where id is supposed to be defined in the space of Dirac matrices. As already discussed the solution of the BSE corresponds to an infinite chain of Feynman diagrams which formally reads

$$T(q_2, q_1; p) = V(q_2, q_1; p) + i \int \frac{d^d l}{(2\pi)^d} V(q_2, l; p) \frac{\not{p} - \not{l} + m}{((p-l)^2 - m^2 + i\epsilon)(l^2 - M^2 + i\epsilon)} V(l, q_1; p) + \dots ,$$

where we again have suppressed the channel indices keeping in mind that T and V are matrices in channel space. From this equation one easily sees that the iterative use of the interaction potential introduces new Dirac-momentum structures additionally to those of \mathcal{D} . The number of these structures is limited such that it is convenient to rewrite the scattering matrix as follows

$$T(q_2, q_1; p) = \sum_{i=1}^{20} T_i(s) \aleph_i(q_2, q_1; p) , \quad (2.10)$$

$$\begin{aligned} \text{with } \aleph(q_2, q_1; p) := & (\not{q}_1, \not{p}\not{q}_1, \not{q}_2\not{p}\not{q}_1, \not{q}_2\not{q}_1, \not{p}\not{q}_1(q_2 \cdot p), \not{q}_1(q_2 \cdot p), \\ & \not{q}_2(q_1 \cdot p), \not{q}_2\not{q}_1, (q_1 \cdot p)(q_2 \cdot p), \not{p}(q_1 \cdot p)(q_2 \cdot p), (q_1 \cdot p), \\ & \not{p}(q_1 \cdot p), (q_2 \cdot q_1), \not{p}(q_2 \cdot q_1), \not{q}_2\not{p}, \not{q}_2, \not{p}(q_2 \cdot p), (q_2 \cdot p), id, \not{p}) . \end{aligned}$$

Please note that in contrast to the decomposition of the potential V , the coefficients T_i still depend on the center-of-mass energy squared. Reinserting the latter equation into the BSE (2.1) and collecting all $T_i(s)$ on the r.h.s. we obtain the following expression

$$\begin{aligned} \sum_{i=1}^{20} V_i \aleph_i(q_2, q_1; p) = & \quad (2.11) \\ \sum_{i=1}^{20} \left(\aleph_i(q_2, q_1; p) - \sum_{j=1}^{20} V_j \left(i \int \frac{d^d l}{(2\pi)^d} \frac{\aleph_j(q_2, l; p)(\not{p} - \not{l} + m)\aleph_i(l, q_1; p)}{(l^2 - M^2 + i\epsilon)((p-l)^2 - m^2 + i\epsilon)} \right) \right) T_i(s) , \end{aligned}$$

where V is expressed in terms of the vector \aleph . The term in the inner brackets has a crucial property that due to Lorentz invariance it is also an element of the Dirac-momentum subspace spanned by the elements of the vector \aleph

$$\forall_{a \in \aleph(q_2, l; p), b \in \aleph(l, q_1; p)} : \exists_{C \in \mathbb{C}^{20}} \int \frac{d^d l}{(2\pi)^d} \frac{a(\not{p} - \not{l} + m)b}{((p-l)^2 - m^2)(l^2 - M^2)} = \sum_{k=1}^{20} C_k \aleph_k(q_2, q_1; p) . \quad (2.12)$$

The coefficients C_i are complex valued functions of scalar quantities only, i.e. $s, M, m, I_{MB}, I_M, I_B$ for every two-particle channel. They can be determined utilizing Passarino-Veltman reduction as exemplified in the previous section and presented explicitly in App. B. Consequently the r.h.s. of Eq. (2.11) can be rewritten as follows

$$\sum_{i=1}^{20} V_i \aleph_i(q_2, q_1; p) = \sum_{i=1}^{20} \sum_{j=1}^{20} \left(\delta_{ij} - \tilde{C}_{ij} \right) T_j(s) \aleph_i(q_2, q_1; p) ,$$

where the coefficients \tilde{C}_{ij} are matrices in channel space, obtained from Eq. (2.12) replacing $a = V$ and $b = \aleph_i$. In fact, the latter expression is a system of 20 coupled linear equations which we can rewrite in an even more elegant way as

$$\mathbf{X}_i^j T_j(s) = V_i , \quad (2.13)$$

where we have utilized the Einstein summation convention for $i, j \in [1, 20]$ and $\mathbf{X} \in \text{Mat}^{20 \times 20}$, whereas each element is a complex valued channel space matrix defined by $\mathbf{X}_{ij} = (\delta_{ij} - \tilde{C}_{ij})$. The solution of the latter equation is conceptionally unproblematic, however, it turns out that it contains a large number of very convoluted matrix operations in the channel space. One observation² can simplify the situation to some extent, namely that some Dirac-momentum structures are decoupled from the others. For example, none of the structures of the form $\{\aleph_i | i \geq 15\}$ can induce any other than these structures, meaning that coefficients \tilde{C}_{ij} vanish for $i \geq 15$ and every j . This and similar patterns imply that the only non-vanishing elements of the matrix \mathbf{X} are the following

$$\mathbf{X}_{ij} \neq 0 \text{ for } \begin{cases} 1 \leq i \leq 6 \text{ and } 1 \leq j \leq 6 \\ 7 \leq i \leq 12 \text{ and } 7 \leq j \leq 12 \\ 1 \leq i \leq 14 \text{ and } 13 \leq j \leq 14 \\ 15 \leq i \leq 20 \text{ and } 15 \leq j \leq 20 \end{cases},$$

hence we can obtain the solution of Eq. (2.13) in computationally more efficient in four steps according to the above rules. However, even then the solution contains, dependent upon the case, up to a few thousand matrix operations including several hundred matrix inversions per $T_i(s)$. As a matter of fact in the realistic case of e.g. six open channels as required in the following chapters the solution is technically only feasible if all parameters and constants are fixed to the corresponding numerical values. In principle this is not a problem, but in the case of the dimension d of the Minkowski space it calls for a modified regularization scheme as presented in the previous section which is the technical reason for the use of this scheme. Once having solved the equation (2.13) the scattering amplitude T is obtained back reinserting the coefficients $T_i(s)$ into Eq. (2.10). The scattering amplitude can then be used in the full off-shell form as an effective vertex for the photoproduction amplitude. Alternatively setting the external particles on their mass shell we can study the physical observables of meson-baryon scattering directly as it will be done in the next chapter.

²This is the actual reason for the somewhat awkward ordering of the vector \aleph in Eq. (2.10).

Chapter 3

πN scattering and properties of the $N^*(1535)$ and $N^*(1650)$ resonances¹

3.1 Introduction

Pion-nucleon scattering has traditionally been the premier reaction to study the resonance excitations of the nucleon. In particular, in the S_{11} partial wave, one finds two close-by resonances at 1535 and 1650 MeV, which overlap within their widths of about 100 MeV. It was pointed out early in the framework of unitarized coupled-channel chiral perturbation theory [81] that the $N^*(1535)S_{11}$ might not be a three-quark (pre-existing) resonance but rather is generated by strong channel couplings, with a dominant $K\Sigma - K\Lambda$ component in its wave function. This analysis was extended in Ref. [103], where within certain approximations the effects of 3-body $\pi\pi N$ channels were also included. Further progress was made in Ref. [84], where the S_{11} phase shift was fitted from threshold to about $\sqrt{s} \simeq 2$ GeV together with cross section data for $\pi^- p \rightarrow \eta n$ and $\pi^- p \rightarrow K^0 \Lambda$ in the respective threshold regions. This led to a satisfactory description of the S_{11} phase and a reasonable description of the inelasticity up to the ηN threshold. Two poles were found corresponding to the $N^*(1535)S_{11}$ and the $N^*(1650)S_{11}$ (henceforth called $S_{11}(1535)$ and $S_{11}(1650)$ for brevity) resonances together with a close-by unphysical pole on the first Riemann sheet. More recently, it was pointed out in a state-of-the-art unitary meson-exchange model that there is indeed strong resonance interference between the two S_{11} resonances, as each of these resonances provides an energy-dependent background in the region of the other, see Ref. [99].

In view of these developments we consider in this chapter the two s-waves S_{11} and S_{31} in pion-nucleon scattering. We will utilize the framework of a coupled-channel Bethe-Salpeter equation (BSE) including in the driving potential all local terms of second order in the chiral counting, thus going beyond the often used approximation of simply including the leading order Weinberg-Tomozawa interaction. Further, we do not perform the often used on-shell approximation for reasons given in the previous chapters. Note that $K^- p$ scattering including such dimension two terms was already analyzed in a framework equivalent to the on-shell approximation of the Bethe-Salpeter equation in Refs. [95, 96, 104, 105], we will turn to this interaction channels

¹Most of the contents of this chapter have been published in Ref. [2].

in the next chapter. Our investigation is restricted to center-of-mass energies below 1.8 GeV, as required for the future meson photoproduction studies. As we will show, both resonances in the S_{11} partial wave are dynamically generated, even if the scattering data are fitted only up to $W_{\text{cms}} = \sqrt{s} = 1.56$ GeV. Quite in contrast, the $S_{31}(1620)$ resonance is not generated by the coupled-channel dynamics. We also analyze the structure of the dynamically generated resonances as revealed through their coupling to the various meson-baryon channels.

3.2 Formalism

We consider the process of meson-baryon scattering at low energies. As already explained before, the s-wave interaction near the thresholds is dominated by the Weinberg-Tomozawa contact term, derived from the effective chiral Lagrangian Eq. (1.13). Most chiral unitary approaches restrict their meson-baryon potential to this interaction, which generates the leading contribution to the s-wave scattering lengths. This approach has been remarkably successful in many cases, see e.g. Ref. [61, 79–83]. However, at first chiral order, there are also the Born graphs, describing the s -channel and u -channel exchanges of an intermediate nucleon. The full inclusion of these graphs in the driving term of the Bethe-Salpeter equation leads to conceptual and practical difficulties, which have not yet been solved to the best of our knowledge, see the discussion in section 2.1. Therefore, we will approximate our interaction kernel by a sum of contact terms. To go beyond the simple Weinberg-Tomozawa potential, we shall include the full set of meson-baryon vertices from the second order chiral Lagrangian. These terms may lead to sizeable corrections to the leading-order results, see e.g. the calculation of NNLO corrections on meson-baryon scattering lengths within SU(3) ChPT [42]. The pertinent Lagrangian density was first constructed in Ref. [44] and is presented in its minimal form [101] in Eq. (2.4).

Dealing with the specific case of meson-baryon scattering we set all external sources to zero except the scalar one, which is equal to the quark mass matrix, i.e. $s = \mathcal{M} := \text{diag}(m_u, m_d, m_s)$, hence, leaving out some terms formally of third chiral order, our considered interaction potential reads

$$V(q_2, q_1; p) = A_{WT}(q_1 + q_2) \tag{3.1} \\ + A_{14}(q_1 \cdot q_2) + A_{57}[q_1, q_2] + A_M + A_{811}(q_2(q_1 \cdot p) + q_1(q_2 \cdot p)) ,$$

where $A_{..}$ denote matrices in the channel space. As the premier goal of our present discussion is the analysis of pion-nucleon scattering we restrict ourselves to meson-baryon channels with strangeness $S = 0$ and electric charge $Q = +1$. This leaves us with the following channels:

$$p\pi^0, n\pi^+, p\eta, \Lambda K^+, \Sigma^0 K^+, \Sigma^+ K^0 .$$

The channel matrix A_{WT} depends upon the meson decay constants F_π, F_K, F_η , whereas all other channel matrices also depend upon 14 new constants b_i , as presented in App. C. The decay constants will be fixed to their physical values as specified below. However, the numerical values of the next-to-leading order low-energy constants² b_i cannot be derived from symmetry

²The LECs $b_{0,D,F}$ are the so-called *symmetry breakers* while the b_i ($i = 1, \dots, 11$) are referred to as *dynamical* LECs.

principles alone and shall be used here as free fitting parameters imposing only that they remain of natural size and fulfill the matching relations from Ref. [42] as argued in section 2.1.

The strict perturbative chiral expansion is only applicable at low energies. Moreover, it certainly fails in the vicinity of resonances. The purpose of the present chapter is the extension of the range of applicability of the low-energy effective theory by means of a coupled-channel Bethe-Salpeter equation (BSE). Introduced in [74] it has been proven to be very useful both in the purely mesonic and in the meson-baryon sector [61, 79–83]. In contrast to perturbative calculations this approach implements two-body unitarity exactly and in principle allows to generate resonances dynamically. Due to the exact correspondence of the Bethe-Salpeter scattering amplitude with an infinite sum of dimensionally regularized Feynman graphs, we can use our solution of the BSE as an extended vertex in a model amplitude for meson photoproduction and arrive at a natural and straightforward way to implement gauge invariance in a chiral unitary framework. For details on the construction principles the reader is referred to chapter 5.

Now we wish to recall the formalism of the Bethe-Salpeter approach as it was introduced in section 2.1. We denote the in- and outgoing meson momenta by q_1 and q_2 , respectively, whereas the overall four-momentum is given by $p = q_1 + p_1 = q_2 + p_2$, where p_1 and p_2 are the momenta of in- and out-going baryon, respectively. For meson-baryon scattering amplitude $T(q_2, q_1; p)$ and chiral potential $V(q_2, q_1; p)$ the integral equation to be solved is presented in Eq. (2.1). The loop diagrams appearing there are in general divergent and require renormalization. In case of a strict chiral perturbation expansion, they can be renormalized in a quite straightforward way, order by order, including at a given order of the calculation all the counterterms absorbing the loop divergences. On the other hand the treatment of the divergences of the BSE is known to be a complicated issue, see e.g. Refs. [88, 106]. There are various ways to treat the divergent integrals and the large baryon mass scale appearing. In the previous chapter we have developed a proper regularization scheme which preserves the analytic structure of the loop integrals utilizing dimensional regularization and just replacing the divergent part by a subtraction constant. The purely baryonic integrals are set to zero from the beginning. Thus, our treatment of the loop integrals is, in effect, similar to the EOMS regularization scheme advocated in Ref. [62]. As it was argued in Ref. [106] it is not possible to express the terms necessary to absorb the divergences in the BSE as counterterms derived from a local Lagrangian. However, it is possible to alter the loop integrals in the solution of the BSE in a way that is in principle equivalent to a proper modification of the chiral potential itself (for an explicit demonstration, see section 1.4 as well as App. F of Ref. [92]). In this spirit we apply the usual \overline{MS} subtraction scheme, keeping in mind that the modified loop integrals are still scale-dependent. This regularization scale (μ) dependence would be canceled by the corresponding scale dependence of higher-order contact terms in the perturbative approach. In our non-perturbative framework, the scale μ is used as a fitting parameter, reflecting the influence of higher order terms not included in our potential. Note that in Refs. [84, 88], the 12 loop integrals (4 for each meson-baryon, meson and baryon case) appearing there, gave rise to 12 finite subtraction constants, which were then also used as fitting parameters of their approach.

Having specified the kernel and the regularization procedure we can solve the Bethe-Salpeter equation with the full off-shell dependence. The solution techniques are described in detail in

section 2.3. To our knowledge this is the first time the NLO corrections of the chiral potential are included and unitarized within the full relativistic BSE, without making use of the on-shell approximation or s-wave projection of the chiral potential, so that also a p-wave is iterated. Once the BSE has been solved, we can of course set the *external* particles on their mass shell, which leaves us with only two independent structures for the on-shell amplitude, i.e. $\mathbb{1}$ and \not{p} . Starting from these we will derive more accessible quantities, such as partial wave amplitudes and then compare them with the outcome of other (more phenomenological) approaches as described below.

3.3 Numerics

Throughout the present work we use the following numerical values for the masses and the meson decay constants:

$$\begin{aligned}
F_\pi &= 0.0924 \text{ GeV}, & M_{\pi^0} &= 0.135 \text{ GeV}, & m_p &= 0.9383 \text{ GeV}, \\
F_\eta &= 0.12012 \text{ GeV}, & M_{\pi^+, \pi^-} &= 0.1396 \text{ GeV}, & m_n &= 0.9396 \text{ GeV}, \\
F_K &= 0.113 \text{ GeV}, & M_\eta &= 0.5478 \text{ GeV}, & m_\Lambda &= 1.1157 \text{ GeV}, \\
& & M_{K^0, \bar{K}^0} &= 0.4977 \text{ GeV}, & m_{\Sigma^0} &= 1.1926 \text{ GeV}, \\
& & M_{K^+, K^-} &= 0.4937 \text{ GeV}, & m_{\Sigma^+} &= 1.1894 \text{ GeV}, \\
& & & & m_{\Sigma^-} &= 1.1975 \text{ GeV}.
\end{aligned}
\tag{3.2}$$

The use of physical masses rather than of those in the chiral limit is motivated by the wish to reproduce the physical thresholds correctly. On the other hand the baryon mass in the chiral limit, m_0 in Eq. (2.4), can be fixed to 1 GeV without loss of generality, as any other value only amounts to a rescaling of some unknown LECs.

There are 17 free parameters in the present approach, given by the 14 LECs, as well as three subtraction constants for the regularized loop integrals, corresponding to the logarithms of the undetermined regularization scales (in GeV), i.e. $\log(\mu_\pi/(1\text{GeV}))$, $\log(\mu_K/(1\text{GeV}))$ and $\log(\mu_\eta/(1\text{GeV}))$. Here, we take the regularization scale of each channel to be fixed by the respective meson, i.e. in addition to $\mu_{\pi N} =: \mu_\pi$ and $\mu_{\eta N} =: \mu_\eta$, we take $\mu_{K\Sigma} = \mu_{K\Lambda} =: \mu_K$. The latter constraint appears to be natural in view of our forthcoming work on meson photoproduction, where loops are present in which a photon-induced $\Lambda \leftrightarrow \Sigma^0$ transition occurs, the detailed discussion of this issue can be found in section 2.3.

For the fits, we consider the very established analysis of the pion-nucleon data provided by the SAID program at GWU. Their partial wave analysis relying on the so-called K-matrix approach has been performed both for single energy bins (energy independent solution) as well as for a wide energy range simultaneously (energy dependent solution), see Ref. [107] as well as [108] for a more recent analysis. In principle our amplitude does not only accounts for s- but also for p-waves as the interaction kernel of the BSE (2.1) exhibits an explicit angular dependence. However, the P_{11} as well as the P_{33} partial waves are dominated by Roper and Δ resonances, respectively. At our present state of knowledge both have different origin than the considered meson-baryon dynamics of the BSE, e.g. the Δ is a three-quark state. Thus

without explicitly including these resonances³ the BSE solution will be spoiled drastically if one includes the information in these partial waves. Hence as a first step we shall consider only the s-waves (both real and imaginary parts) of the SAID analysis on πN scattering for energies up to $W_{\text{cms}} = 1.56$ GeV in the energy dependent solution. Comparing an earlier analysis by the Karlsruhe group [109] to the current one, we assign for the energies below $W_{\text{cms}} = 1.28$ GeV an absolute systematic error of 0.005 and for higher energies an error of 0.030 to the partial wave amplitudes. To some extent this is in agreement with error estimates done in Ref. [84], which are motivated by the expectation of pronounced three-body effects above the $\pi\pi N$ threshold, see also Ref. [25].

The BSE solution turns out to be dependent upon the free parameters of the model in a very tangled way. Hence very elaborative techniques are required to adjust the parameters such that the experimental (phenomenological) input is reproduced correctly. The most established and convenient method is the minimization of a suitable χ^2 function. There are various ways how this function can be defined with various advantages and disadvantages, however, in this theoretical work we find it most convenient to use the following definition

$$\chi_{DOF}^2 := \frac{\sum_i n_i}{N(\sum_i n_i - p)} \sum_i \frac{\chi_i^2}{n_i}, \quad (3.3)$$

where p is the number of free parameters, n_i is the number of data points available for the observable i and N is the number of observables. This choice of χ^2 ensures the equal weight of all fitted observables. To be more specific in the present case $p = 17$, $N = 4$ and $n_i = 30$ for all $i \in \{\text{Re}S_{11}, \text{Im}S_{11}, \text{Re}S_{31}, \text{Im}S_{31}\}$. Our solution is fully analytical but very complicated and time-consuming. In both versions, as a Mathematica(TM) and a C++ routine, the calculation takes $\sim 30 - 60$ seconds for one specific parameter set and fixed energy. The Mathematica (TM) version serves more as an analysis tool whereas the C++ routine is written solely for the minimization procedure of χ_{DOF}^2 , which is performed utilizing the MINUIT C++ library, see Ref. [110]. Since this numerical procedure requires typically several thousands steps (each of them taking up to $n_i = 30$ minutes), we have parallelized the calculation routine on the HSKP cluster such that for each energy it is performed on a separate thread of the cluster. Then all results are combined and inserted into Eq. (3.3), which is then passed through to the MINUIT driven main routine. There a variable-metric method MIGRAD [111] is utilized to find the minimum of χ_{DOF}^2 in the 17-dimensional parameter space.

3.4 Results

For the best fit, found using the MINUIT library, with a $\chi_{DOF}^2 = 1.23$ we obtain the following parameter set (all μ_i in GeV)

$\log(\mu_\pi/(1\text{GeV}))$	$= +0.924$
$\log(\mu_\eta/(1\text{GeV}))$	$= -0.218$
$\log(\mu_K/(1\text{GeV}))$	$= +0.581$

³The inclusion of explicit resonances leads to other conceptional difficulties within the present framework and lies outside of the scope of the present work. For an attempt to do so see Ref. [79].

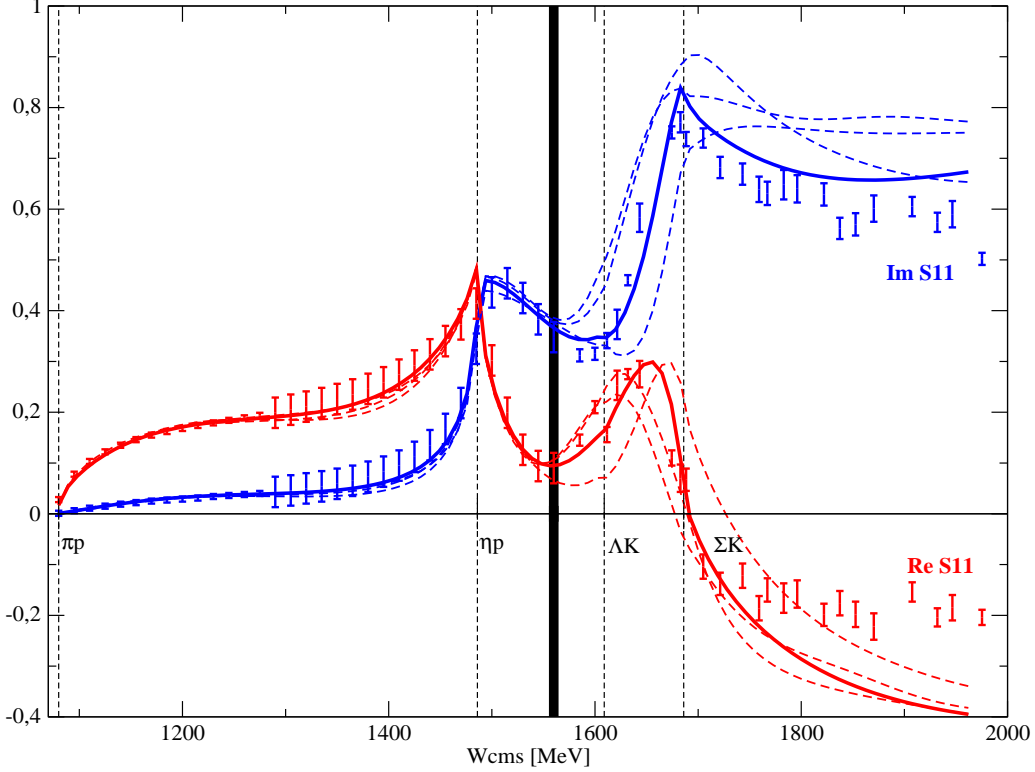


Figure 3.1: Real and imaginary part of the S_{11} partial wave amplitude compared with the SAID-data (WI08-analysis). Full curves correspond to the best fit, the dashed ones to fits with slightly larger χ^2_{DOF} . The bold vertical line limits the region of the fit, where in the not fitted region single energy values are taken from the SAID analysis.

$b_1 = -0.082 \text{ GeV}^{-1}$	$b_8 = +0.609 \text{ GeV}^{-1}$
$b_2 = -0.118 \text{ GeV}^{-1}$	$b_9 = -0.633 \text{ GeV}^{-1}$
$b_3 = -1.890 \text{ GeV}^{-1}$	$b_{10} = +1.920 \text{ GeV}^{-1}$
$b_4 = -0.215 \text{ GeV}^{-1}$	$b_{11} = -0.919 \text{ GeV}^{-1}$
$b_5 = -0.963 \text{ GeV}^{-1}$	$b_0 = -0.768 \text{ GeV}^{-1}$
$b_6 = +0.218 \text{ GeV}^{-1}$	$b_D = +0.641 \text{ GeV}^{-1}$
$b_7 = -1.266 \text{ GeV}^{-1}$	$b_F = -0.098 \text{ GeV}^{-1}$

All parameters are of natural size and the LECs agree with the estimates from the SU(3) to SU(2) matching relations provided in Ref. [42]. At this point we are only able to estimate the computational errors on the above parameters within the MIGRAD (MINUIT) minimization procedure, which appear to be negligible. As a consequence of the sizeably increased computing time, when fitting the full amplitudes rather than the on-shell approximations to them, we are not able to perform a full error analysis as e.g. done in Ref. [105] for K^-p scattering. However, in the course of this thesis we will develop and perform a more systematic error analysis.

In Figs. 3.1 and 3.2 we present the results of our approach for the S_{11} and S_{31} partial waves. Clearly the uncertainty of our predictions grows with increasing energy. For an indication of the error bands on the partial wave amplitudes we present the second, third and fourth best fits in Figs. 3.1 and 3.2 as dashed lines. As already seen in earlier publications on the BSE

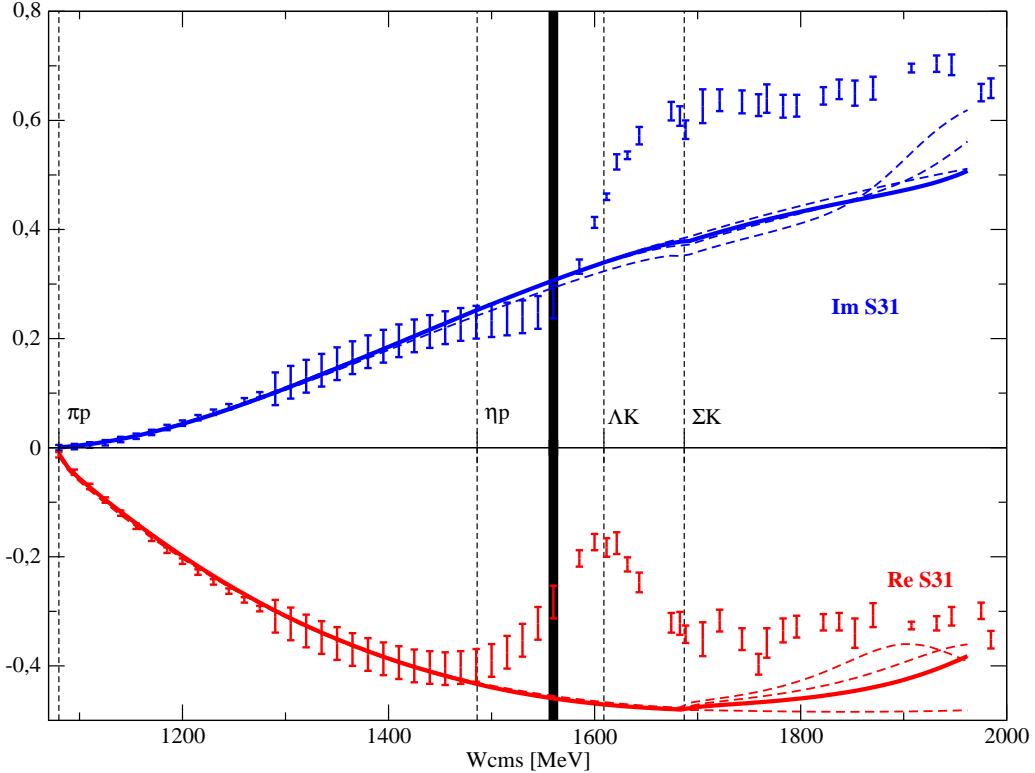


Figure 3.2: Real and imaginary part of the S_{31} partial wave amplitude compared with the SAID-data (WI08-analysis). Full curves correspond to the best fit, the dashed ones to fits with slightly larger χ^2_{DOF} . The bold vertical line limits the region of the fit, where in the not fitted region single energy values are taken from the SAID analysis.

approach with leading order chiral potential [84], the low-energy region (e.g. $W_{\text{cms}} < 1.4$ GeV) is reproduced for both isospin 3/2 and 1/2 reasonably well. For the two s-wave scattering lengths, we obtain

$$a_{1/2} = 145.8 \times 10^{-3}/M_{\pi^+} \quad \text{and} \quad a_{3/2} = -91.6 \times 10^{-3}/M_{\pi^+} ,$$

to be compared with the direct extraction of these scattering lengths from the GWU solution, $a_{1/2} = (174.7 \pm 2.2) \times 10^{-3}/M_{\pi^+}$ and $a_{3/2} = (-89.4 \pm 1.7) \times 10^{-3}/M_{\pi^+}$.⁴ The theoretically cleanest determination of these observables stems from the analysis of pionic hydrogen and pionic deuterium data based on effective field theory [112], $a_{1/2} = (179.9 \pm 3.6) \times 10^{-3}/M_{\pi^+}$ and $a_{3/2} = (-78.5 \pm 3.2) \times 10^{-3}/M_{\pi^+}$. The description of the πN amplitude at low energies will certainly be improved by a more complete treatment of the Born terms, which is beyond the scope of this work. One might also think about constraining the well-known pion-nucleon scattering lengths, e.g. by adopting a matching procedure to the perturbative expansion. However, since we did not put a special weight on the threshold region in our fits, and the overall description of the partial waves seems to work well over a rather broad energy range, we regard the obtained results for the scattering lengths as satisfactory.

⁴We thank Ron Workman for providing us with these values.

Moreover, and more importantly, within the fit region we reproduce the $S_{11}(1535)$. At the same time the $S_{31}(1620)$ resonance is not reproduced by our approach, which is in agreement with the current state of knowledge that the first S_{31} resonance does not have a prominent dynamically generated component. To emphasize this we exclude the data on S_{31} and recalculate the χ_{DOF}^2 for the above parameter set, we end up with $\chi_{DOF}^2(S_{11}) = 0.59$. Let us remark at this point that the $S_{11}(1535)$ is reproduced without any use of explicit vector meson resonances or even taking into account the $\pi\pi N$ channels as for example in Ref. [103]. As a matter of fact the neglect of these inelastic channels is expected to lead to an overestimate of the $\pi N \rightarrow \eta N$ cross section not considered here (see e.g. Ref. [113]). We will turn to this issue in more detail in chapter 5.

At this point one realizes an even more interesting fact: After fixing the S_{11} partial wave in the energy region up to $\sqrt{s} = 1.56$ GeV every curve with minimized χ_{DOF}^2 possesses a second structure between the $K\Lambda$ and $K\Sigma$ threshold. Obviously this corresponds to the well-known $S_{11}(1650)$ resonance and is predicted here only by demanding a good description in the low-energy and the first resonance region. To some extent this is in agreement with Ref. [84], where the $S_{11}(1650)$ was reproduced in the fit of the phase shifts and inelasticities for the full region of $1.077 < \sqrt{s} < 1.946$ GeV. While only the leading order chiral potential was considered there, the authors introduced additional parameters appearing for every loop integral. Apparently these parameters contain some of the information that has to be attributed to neglected terms of higher order in the chiral potential. Additionally, in contrast to our approach this method does not allow to identify the higher partial waves than the s-wave, which might become important for higher energies as emphasized in Ref. [106].

Up to now we have been very sloppy using the word 'resonances' for the structures in the s-wave projected scattering amplitudes. Indeed it is common to denote a bump in the spectrum of an observable (e.g. cross section) by the word 'resonance'. Then it is quite convenient to fit this Breit-Wigner formula which is parametrized by two parameters W_R related to the mass of the resonance and Γ_R called the resonance width which is inverse to the resonance mean life time. Actually, this is an approximation which is well enough to describe the resonances, if the width is not too large and as long as the background is weakly energy-dependent. From the field theoretical point of view it is much cleaner to assign the resonances to the poles of the scattering amplitude in the complex plane, see e.g Refs. [69, 70]. The real part of the pole position is equal to the mass of resonance and the negative imaginary part to half its width. However, these poles have to lie on the unphysical (second) Riemann sheet as the microcausality forbids the complex-valued poles on the first Riemann sheet. In Figs. 3.3 and 3.4 we present the modulus of the analytic continuation of $T_{\pi N}^{11}$ into the complex s -plane. In Fig. 3.3 two poles appear on the (222-111) Riemann sheet, which labels the unphysical Riemann sheet connected to the physical (scattering) axis in the energy region between the third (ηp) and fourth ($K\Lambda$) threshold. For the position of the two poles we extract:

$$\begin{aligned} W_{1535} &= (1.506 - i 0.140) \text{ GeV}, \\ W_{1650} &= (1.692 - i 0.046) \text{ GeV}. \end{aligned} \tag{3.4}$$

Choosing the (2222-11) Riemann sheet, i.e. the unphysical sheet reached by analytic continuation from the region $(M_K + m_\Lambda)^2 < s < (M_K + m_\Sigma)^2$, see Fig. 3.4, we obtain one single pole structure, which is located at

$$W_{1650} = (1.682 - i 0.042) \text{ GeV} . \tag{3.5}$$

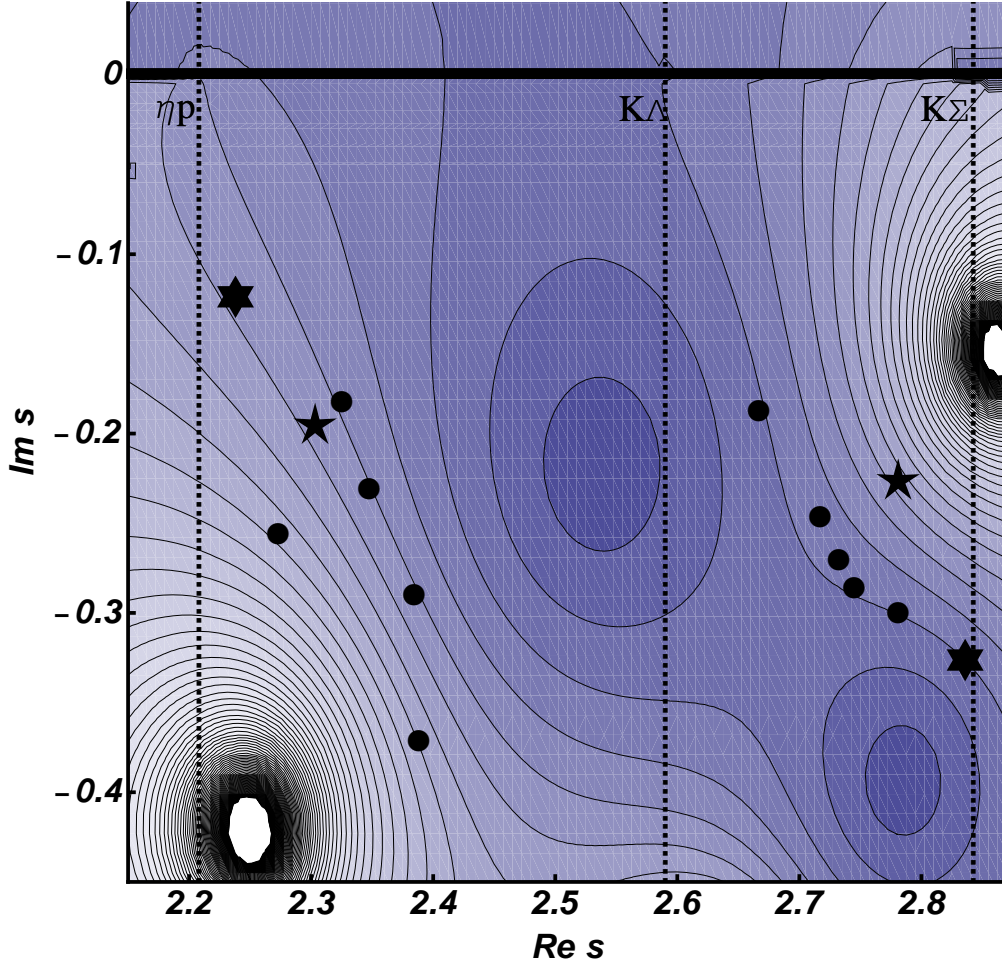


Figure 3.3: (222-111) Riemann sheet of the s -plane. The five-star and the six-star correspond to the values obtained in Refs. [99] and [88], respectively, the dots represent results of phenomenological models listed in Ref. [28].

We conclude that the $S_{11}(1650)$ can also be described as a dynamically generated resonance, just like the $S_{11}(1535)$. Recall that this resonance appears in our framework, although no information is included from phenomenology in this energy region.

It is further interesting to analyze the structure of these states. To do that, we consider the on-shell scattering matrix in the vicinity of the two poles, where it takes the form

$$T_{ij}^{\text{on}}(s) \simeq \frac{g_i g_j}{s - s_R}, \quad (3.6)$$

with g_i (g_j) the complex coupling constant for the initial (final) transition of the meson-baryon system, including a complex wave function renormalization constant. For the $S_{11}(1535)$, we obtain the following ordering

$$|g_{\Lambda K^+}|^2 > |g_{p\eta}|^2 > |g_{\Sigma^+ K^0}|^2 \simeq |g_{n\pi^+}|^2 > |g_{\Sigma^0 K^+}|^2 \simeq |g_{p\pi^0}|^2. \quad (3.7)$$

We remark that the inequalities between couplings to different πN and $K\Sigma$ channels are mostly due to Clebsch-Gordan coefficients in the associated isospin decompositions. However, isospin

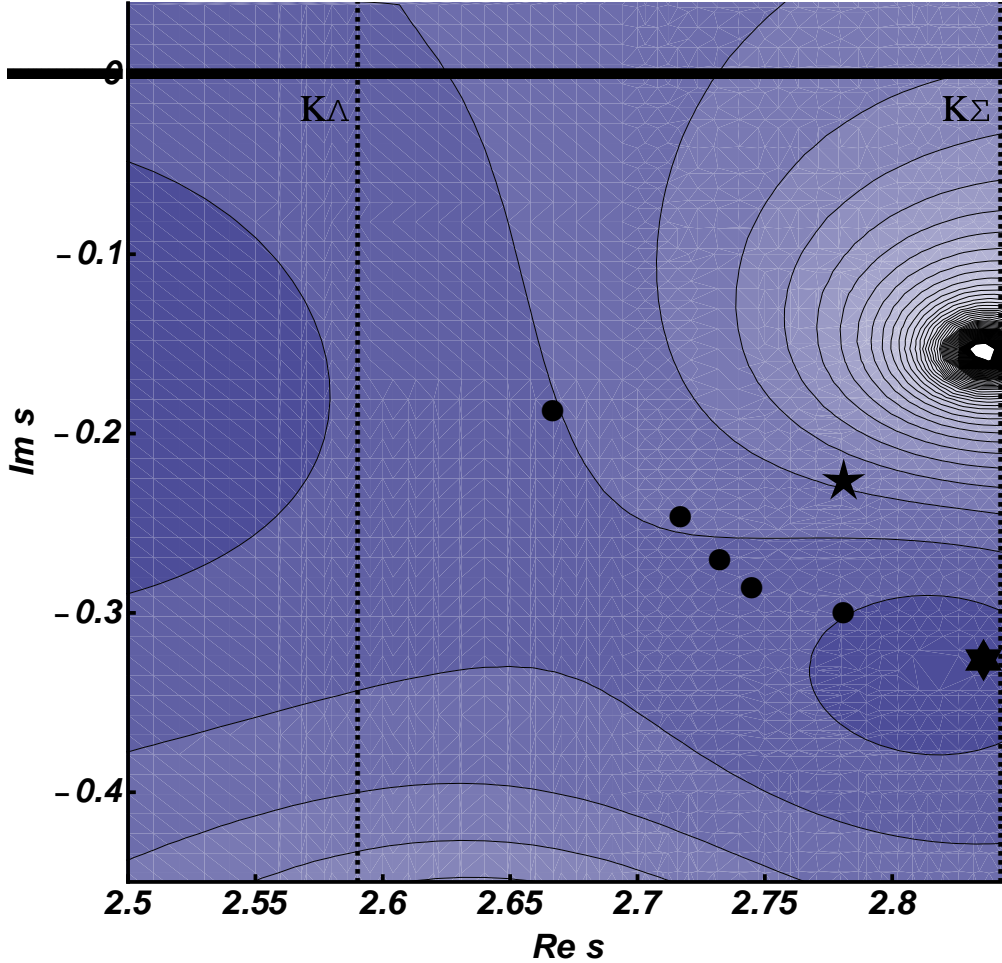


Figure 3.4: (2222-11) Riemann sheet of the s -plane. The five-star and the six-star correspond to the values obtained in Ref. [99] and Ref. [88], respectively, the dots represent results of phenomenological models listed in Ref. [28].

symmetry is not exact in the present approach. We find that the largest component is the $K\Lambda$ one and that the coupling to ηN is significantly bigger than the πN ones, in agreement with the empirical fact that the $S_{11}(1535)$ couples dominantly to ηN . The pattern for the $S_{11}(1650)$ looks different,

$$|g_{\Sigma^+ K^0}|^2 > |g_{p\eta}|^2 > |g_{\Sigma^0 K^+}|^2 \simeq |g_{n\pi^+}|^2 > |g_{p\pi^0}|^2 \gg |g_{\Lambda K^+}|^2, \quad (3.8)$$

i.e. for this resonance the $K\Sigma$ component is dominant and the $K\Lambda$ one is completely negligible, which for instance is indicated by the fact that the pole associated with the $S_{11}(1650)$ is accompanied by a second one on a neighboring sheet, with almost the same coordinates. As for the lower-lying resonance, the coupling to ηN is bigger than the one to πN .

3.5 Summary and outlook

In this chapter, we have analyzed s-wave pion-nucleon scattering in coupled-channel unitarized chiral perturbation theory. The driving kernel includes all local interactions terms of first and second order from the chiral effective Lagrangian. We consider all two-body channels with strangeness zero and charge plus one, but do not include inelasticities generated from three-body $\pi\pi N$ states. The Bethe-Salpeter equation has been solved including the full off-shell dependence of the chiral potential. The parameters are fitted to the real and imaginary part of the S_{11} and the S_{31} partial waves for cms energy below 1.56 GeV. We show that both the $S_{11}(1535)$ and the $S_{11}(1650)$ are generated dynamically, even though the fit range does only include the first resonance. We have also analyzed the structure of these states, which exhibit some marked differences as indicated by the couplings given in Eqs. (3.7,3.8). Quite differently, no resonance is generated in the S_{31} partial wave. We consider this an important step in our program of describing pion photoproduction from coupled-channel unitarized chiral perturbation theory. Clearly, in the future more work is needed to properly include the Born terms and to perform a systematic error analysis. The first issue is an ongoing project and for the latter the reader is referred to chapter 5.

Chapter 4

$\bar{K}N$ scattering and properties of the $\Lambda(1405)$ resonance¹

4.1 Introduction

The unitarization procedures are in general of an enormous use for systems, where the resonances are located around two-particle thresholds. In such cases the radius of convergence of a strict perturbative calculation is restricted by the presence of a nearby resonance. This fact becomes most evident in the case of $\bar{K}N$ scattering as clearly shown in Refs. [65] and [42]. There the real part of the scattering length of $\bar{K}N$ scattering for Isospin $I = 0$ came with right magnitude but with the wrong sign in both approaches, which is due to the presence of the very near (~ 50 MeV) lying subthreshold resonance $\Lambda(1405)$.

With the recent precise measurement of kaonic hydrogen observables in the SIDDHARTA experiment at DAΦNE [114], an accurate determination of the so important antikaon-nucleon scattering amplitude is now possible. The appropriate framework to perform this task is unitarized coupled-channel chiral perturbation theory, which combines the strictures from the chiral SU(3) dynamics of QCD with coupled channel effects, that e.g. generate the much discussed $\Lambda(1405)$ resonance, as first pointed out by Dalitz and Tuan [115]. From earlier studies by various groups, it is already known that simply taking the leading order chiral interactions in the effective potential of the respective scattering equation is insufficient to achieve the desired accurate theoretical description, see e.g. Refs. [96, 104, 105]. In fact, Ikeda et al. [95, 116] have performed such a combined analysis based on the next-to-leading order chiral effective meson-baryon Lagrangian, nicely demonstrating that indeed a more precise description of the K^-p and K^-n interaction arises. Here, we perform a similar analysis, but in contrast to Refs. [95, 116], we use a Bethe-Salpeter framework without an on-shell approximation for the intermediate meson-baryon states. The framework we use has already been successfully applied to pion-nucleon scattering for the s-waves in the previous chapter and thus it is quite natural to extend this analysis to antikaon-nucleon scattering.

¹Most of the contents of this chapter can be found in Ref. [3].

4.2 Framework

In chapter 1 we have introduced a unitarization procedure which relies on the solution of the Bethe-Salpeter equation. In the following, chapter 2, we have derived the solution of this equation for the driving term derived from the chiral Lagrangian of the leading and next-to-leading order, which was then applied successfully in chapter 3 to pion-nucleon scattering. Here, we wish to refine this procedure and utilize it for the description of the meson baryon scattering in the strangeness $S = -1$ sector. For completeness the basic ingredients of our model shall be specified in the following in a more succinct style to avoid (larger) repetitions.

In chiral perturbation theory the meson-baryon interaction at the leading chiral order is encoded in the Lagrangian (1.13). For the present case of hadronic scattering we set the external currents to zero except for the scalar one, which is set equal to the quark mass matrix, i.e. $s = \mathcal{M} := \text{diag}(m_u, m_d, m_s)$. Starting from the covariant derivative $D_\mu B$, the so-called Weinberg-Tomozawa term can be derived. This term dominates the s-wave interaction near the thresholds, therefore in most chiral unitary approaches the meson-baryon interaction is restricted to this term. Secondly, a meson can couple to a baryon via the axial vector current $\sim D, F$, generating the s - and u -channel exchanges of the intermediate baryons, see Eqn. (2.3). The inclusion of these so-called Born graphs in the driving term of the Bethe-Salpeter equation leads to conceptual and practical difficulties, which are described in detail in section 2.1. The latter are usually overcome, making use of the on-shell approximation or via projection of the kernel to the s-wave, see e.g. Ref. [105] and Ref. [116] for a more recent study. However, the particular attention of the present work lies on the solution of the Bethe-Salpeter equation with the full off-shell dependence. Thus we will restrict the interaction kernel to a sum of contact terms, but refrain from the approximations mentioned above.

Aside from the Weinberg-Tomozawa term, we will take into account the full set of meson-baryon vertices from the second-order chiral Lagrangian. The pertinent Lagrangian density was first constructed in Ref. [44] and is presented in its minimal form [101] in Eq. (1.13). There all operators are accompanied by dimension-two low energy constants (LECs), b_i . On the one hand such terms may lead to sizable corrections to the leading-order result, see e.g. Ref. [42] for the calculation of meson-baryon scattering lengths up to the third chiral order. On the other hand, including such terms with full off-shell dependence we hope to account for some of the structures created by the missing Born graphs.

Let us denote the in- and out-going meson momenta by q_1 and q_2 , respectively. The overall four-momentum is given by $p = q_1 + p_1 = q_2 + p_2$, where p_1 and p_2 are the momenta of in- and out-going baryon, respectively. Separating the momentum space from the channel space structures, the chiral potential considered here takes the form:

$$V(q_2, q_1; p) = A_{WT}(q_1 + q_2) + A_{14}(q_1 \cdot q_2) + A_{57}[q_1, q_2] + A_M + A_{811} \left(q_2(q_1 \cdot p) + q_1(q_2 \cdot p) \right),$$

where the first matrix A_{WT} only depends on the meson decay constants $F_{\pi,K}$, whereas A_{14} , A_{57} , A_{811} and A_M also contain the NLO LECs as specified in appendix C. In going from the Lagrangian (2.4) to the above vertex rule, we have left out some terms, which are formally of third chiral order. The channel space is defined in accordance with the quantum numbers as

well as the energy range of interest. For the purpose of gaining some insight into the nature of the $\Lambda(1405)$ it is spanned by six vectors corresponding to the following meson-baryon states:

$$K^- p, \bar{K}^0 n, \pi^0 \Lambda, \pi^0 \Sigma^0, \pi^+ \Sigma^-, \pi^- \Sigma^+$$

It should be noted that in principle there are four additional channels which have the same quantum number and can be build from the ground state octet of mesons and baryons, i.e. $\eta \Lambda, \eta \Sigma^0, K^+ \Xi^-, K^0 \Xi^0$. However, these channels are much heavier (≥ 1.663 GeV) than the six given above (≤ 1.437 GeV) and thus their effects can be considered to be absorbed in the LECs to be fitted.

The strict perturbative chiral expansion is only applicable at low energies and certainly fails in the vicinity of (subthreshold) resonances. We extend the range of applicability by means of a coupled-channel Bethe-Salpeter equation (BSE). Introduced in Ref. [74] it has been proven to be very useful both in the purely mesonic and also in the meson-baryon sector. In contrast to perturbative calculations this approach implements two-body unitarity exactly and in principle allows to generate resonances dynamically. For the meson-baryon scattering amplitude $T(q_2, q_1; p)$ and the chiral potential $V(q_2, q_1; p)$ the integral equation to be solved is presented in Eq. (2.1). To treat the loop diagrams appearing there, we utilize the regularization scheme developed in section 2.2. It relies on the dimensional regularization but sets all purely baryonic integrals to zero. In the spirit of the discussion there, we apply the usual $\overline{\text{MS}}$ subtraction scheme, keeping in mind that the modified loop integrals are still scale-dependent. The scale μ reflects the influence of the higher-order terms not included in our potential and is used as a fitting parameter of our approach. As mentioned before, this treatment is similar to those adopted in similar approaches, e.g. [84, 95], where subtraction constants are assigned to the loop integrals and used then as a fitting parameters. In any case we should impose that these free parameters remain of natural size, otherwise it would indicate that some important effects are missing.

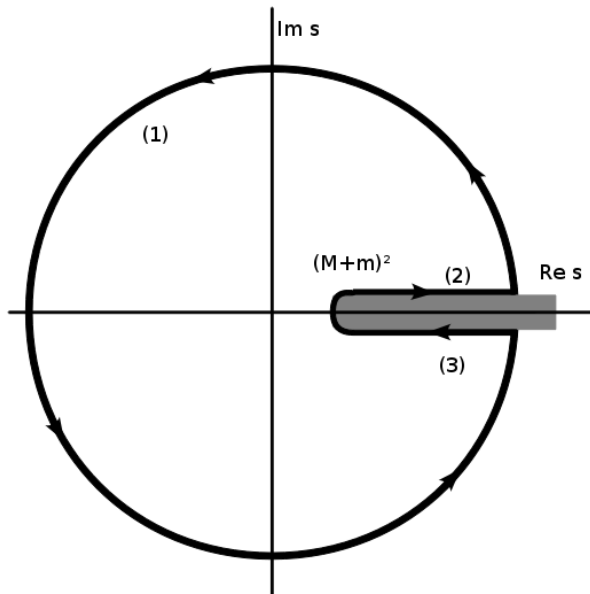
The solution of the BSE Eq. (2.1) with full off-shell dependence is obtained following the construction principles described in chapter 2. As an extension of this approach we wish also to address an other issue here, namely analyticity, which is one of the fundamental principles of modern physics as described in section 1.4. Let us first start with the one-meson-one-baryon loop-function $I_{MB}(s = p^2)$ in four dimensions

$$I_{MB}(s) := \int \frac{d^4 l}{(2\pi)^4} \frac{i}{(l^2 - M^2 + i\epsilon)((p-l)^2 - m^2 + i\epsilon)}. \quad (4.1)$$

Applying the Cutkosky rules, one immediately obtains the imaginary part of this integral, given by

$$\text{Im}(I_{MB}(s)) = -\frac{q_{\text{cms}}(p^2)}{8\pi\sqrt{s}} \quad \text{for} \quad q_{\text{cms}} = \frac{\sqrt{(s - (m+M)^2)(s - (m-M)^2)}}{2\sqrt{s}}.$$

Working in the complex s -plane we can apply Cauchy's integral formula for holomorphic functions which states that their values in their domain of analyticity are completely determined by their value on the boundary of that domain. Now since the above function exhibits a cut along the real axis starting from the threshold $(m+M)^2$ (gray area), the boundary has the following shape:



The idea is then to widen the contour to infinity, where for the fast enough decreasing functions the value of the function on the contour part (1) vanishes. Then the function value at any point within the integration contour is given entirely by its functional behaviour along the integration parts (2) and (3). The Schwarz reflection principle allows on the other hand to replace the integration along the paths (2) and (3) by the integration along the path (2) over the imaginary part of the function in question. These arguments are at the heart of dispersion relations.

Taking yet another look on Eq. (4.1) one realizes that the function I_{MB} diverges logarithmically for $s \rightarrow \infty$. Hence the dispersion relation has to be subtracted to ensure that the contour integral is well-defined. Restricting to the real part the dispersion relation for the function $I_{MB}(s)$ can be written as follows

$$\text{Re}(I_{MB}(s)) = \text{Re}(I_{MB}(s_0)) + \frac{(s - s_0)}{\pi} \text{p.v.} \int_{s_{\text{thr}}}^{\infty} ds' \frac{\text{Im}(I_{MB}(s'))}{(s' - s)(s' - s_0)},$$

where $s_{\text{thr}} = (M + m)^2$ and s_0 is a subtraction point chosen not to lie on the integration contour and 'p.v.' denotes the principal value. As a matter of fact the loop integral I_{MB} depends upon the regularization scale μ as argued above. This dependence is now carried by the subtraction constant $\text{Re}(I_{MB}(s_0))$ on the r.h.s. of the last equation.

The solution of the BSE Eq. (2.1) corresponds to a bubble sum of the form exemplified in the Fig. 1.2, containing exactly the same one loop-functions I_{MB} . Thus, demanding microcausality of the scattering amplitude one should in principle be able to write an equation similar to the last one for the scattering amplitude

$$\text{Re}(T(s)) = \text{Re}(T(s_0)) + \frac{(s - s_0)}{\pi} \text{p.v.} \int_{s_{\text{thr}}}^{\infty} ds' \frac{\text{Im}(T(s'))}{(s' - s)(s' - s_0)}, \quad (4.2)$$

where for the moment we have suppressed the $q_{1,2}$ dependence. We have checked numerically that the above integral is well-defined as $|T(s)|$ decreases with increasing $|s|$ in the whole

complex plane. However, to the best of our knowledge, it is not possible to implement the last relation Eq. (4.2) into the BSE Eq. (2.1) directly. To put it in other words, the BSE ansatz is known to produce poles on the physical Riemann sheet, which are forbidden by the postulate of maximal analyticity. Thus a scattering amplitude, which solves Eq. (2.1), does not satisfy Eq. (4.2) exactly.

Nevertheless it is possible to find a solution of the BSE Eq. (2.1), which fulfills Eq. (4.2) at least approximately, as we wish to describe now. One way to do so is to keep only those solutions of the BSE, which do not produce poles on the first Riemann sheet 'near' the real (physical) axis. E.g. in Ref. [105] solutions producing poles for $\text{Im}(W_{\text{cms}}) < 250 \text{ MeV}$ were excluded by hand. To overcome such unsatisfactory intervention into the fitting procedure we continue differently. First, for a fixed s_0 and several values of s along the whole fitting region we define the following quantity

$$\chi_{\text{DISP}}^2 = \left(\frac{\text{Re}(T(s) - T(s_0)) - \frac{(s-s_0)}{\pi} \text{p.v.} \int_{s_{\text{thr}}}^{\infty} ds' \frac{\text{Im}(T(s'))}{(s'-s)(s'-s_0)}}{\text{Re}(T(s) - T(s_0))} \right)^2. \quad (4.3)$$

Then the fitting parameters of our model are adjusted to minimize the quantity $\chi_{\text{FULL}}^2 = \chi_{\text{DISP}}^2 + \chi_{\text{DATA}}^2$, where the latter is based on the experimental data. It should be clear that such a procedure is not suited to overcome the unphysical poles. It ensures, however, that they are moved far away from the real axis in a systematic manner, without manual intervention. We consider this as an improvement of the model.

4.3 Fit strategy

We are now able to confront our approach with the experimental results. The baryon mass in the chiral limit, m_0 in Eq. (2.4), is fixed to 1 GeV, whereas the remaining meson and baryon constants are fixed to their physical values, see Eqs. (3.2). For the experimental data we consider total cross sections for the processes $K^-p \rightarrow K^-p$, $K^-p \rightarrow \bar{K}^0 n$, $K^-p \rightarrow \pi^0 \Sigma^0$, $K^-p \rightarrow \pi^+ \Sigma^-$ and $K^-p \rightarrow \pi^- \Sigma^+$ taken from Refs. [117–120]. Moreover, we consider the following threshold decay ratios

$$\begin{aligned} \gamma &= \frac{\Gamma(K^-p \rightarrow \pi^+ \Sigma^-)}{\Gamma(K^-p \rightarrow \pi^- \Sigma^+)} = 2.38 \pm 0.04, \\ R_n &= \frac{\Gamma(K^-p \rightarrow \pi^0 \Lambda)}{\Gamma(K^-p \rightarrow \text{neutral states})} = 0.189 \pm 0.015, \\ R_c &= \frac{\Gamma(K^-p \rightarrow \pi^+ \Sigma^-, \pi^- \Sigma^+)}{\Gamma(K^-p \rightarrow \text{inelastic channels})} = 0.664 \pm 0.011, \end{aligned} \quad (4.4)$$

where the first one is taken from Ref. [121] and the last two from Ref. [122]. Additionally to these quite old data we use a recent determination of the energy shift and width of the kaonic hydrogen in the 1s state, i.e. $\Delta E - i\Gamma/2 = (283 \pm 42) - i(271 \pm 55) \text{ eV}$ from the SIDDHARTA experiment at DAΦNE [114]. These are related to the K^-p scattering length via the modified Deser-type relation [123]

$$\Delta E - i\Gamma/2 = -2\alpha^3 \mu_c^2 a_{K^-p} [1 - 2a_{K^-p} \alpha \mu_c (\ln \alpha - 1)],$$

where $\alpha \simeq 1/137$ is the fine-structure constant, μ_c is the reduced mass and a_{K^-p} the scattering length of the K^-p system.

There are 17 free parameters in the present approach. First of all, the low-energy constants represent the heavy degrees of freedom of QCD, which are integrated out. Thus they have to be fixed in a fit to the experimental data. As a matter of fact, the fitting parameters of our approach correspond to the SU(3) low-energy constants, renormalized by the effects of the not included channels $\{\eta\Lambda; \eta\Sigma^0; K^+\Xi^-; K^0\Xi^0\}$, which one has to keep in mind when using these constants for the further analysis. Additionally, three subtraction constants have to be determined from a fit, which correspond to the logarithms of the undetermined regularization scales, i.e. $\{\mu_{\pi\Lambda}, \mu_{KN}, \mu_{\pi\Sigma}\}$.

To reproduce the experimental data as well as to preserve the property of analyticity as described above, we minimize the following quantity $\chi_{\text{FULL}}^2 = \chi_{\text{DISP}}^2 + \chi_{\text{DATA}}^2$, where the first part is given in Eq. (4.3) and the second part by the quantity

$$\chi_{\text{DATA}}^2 := \frac{\chi^2}{\text{d.o.f}} = \frac{\sum_i n_i}{N(\sum_i n_i - p)} \sum_i \frac{\chi_i^2}{n_i}.$$

Here p is the number of the free parameters, n_i is the number of data points available for the observable i and N is the number of observables. There is a huge number of data points on cross sections of the above reaction channels, which have been collected for the last 50 years. For practical reasons we consider only up to 12 typical data points distributed over the range of $100 \leq p_{\text{lab}} \leq 300$ MeV for the total cross sections in addition to the threshold parameters ΔE , Γ , γ , R_n and R_c . The unequal number of the data points for the cross sections and threshold parameters makes the present choice of χ_{DATA}^2 absolutely inevitable as it ensures the equal weight of different observables. The minimization itself is performed using MINUIT [110], especially the MIGRAD strategy in two steps, which is due to the quite complicated structure of the BSE solution with full off-shell dependence. First, parameters are found to minimize the χ_{FULL}^2 in the on-shell parametrization. In the second step we turn on the ‘‘off-shellness’’ slowly, minimizing in each step the χ_{DATA}^2 and taking the parameters of the best fit from the previous step as starting values. Such a procedure guarantees preservation of the right analytic properties of the solution, found in the first step.

4.4 Results

For the best fit, i.e. $\chi_{\text{DATA, BEST}}^2 = 0.524$, we obtain the following parameter set (all μ_i in GeV) with the corresponding uncertainties as calculated in the *hesse* subroutine of the MINUIT library

$\log(\mu_{KN}/(1\text{GeV}))$	$= +1.155 \pm 0.181$
$\log(\mu_{\pi\Sigma}/(1\text{GeV}))$	$= -0.008 \pm 0.002$
$\log(\mu_{\pi\Lambda}/(1\text{GeV}))$	$= -0.010 \pm 0.003$

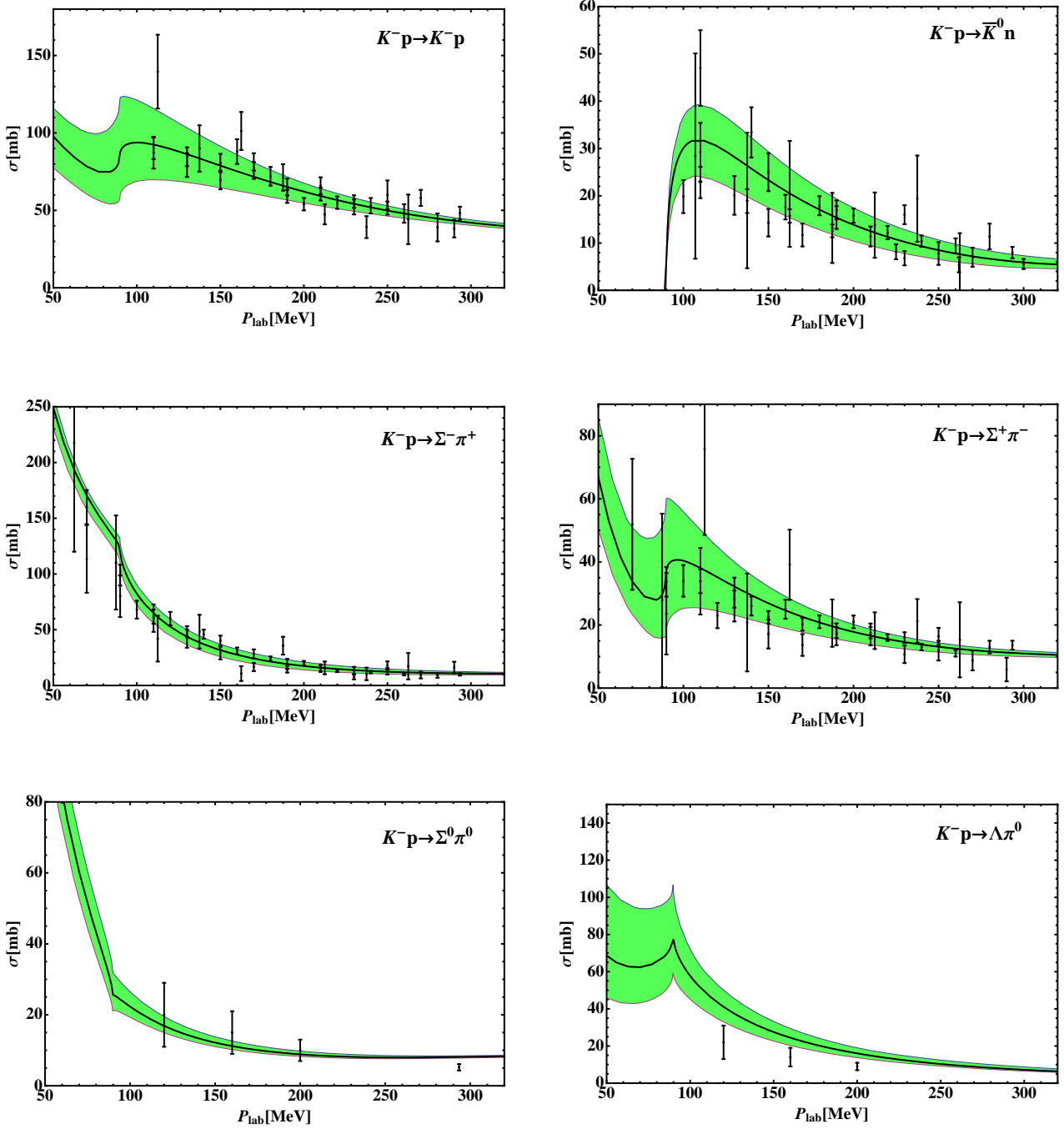


Figure 4.1: Total cross sections for the scattering of K^-p to various channels versus the K^- laboratory momentum. The black points with error bars denote the experimental data from Refs. [117–120] considered for the fits. Shaded (green) bands denote the 1σ error bands calculated as described in the text. The reaction $K^-p \rightarrow \Lambda \pi^0$ is not a part of our fit and presented here only for completeness.

$b_1 = +0.582 \pm 0.052 \text{ GeV}^{-1}$	$b_8 = -0.332 \pm 0.045 \text{ GeV}^{-1}$
$b_2 = -0.310 \pm 0.092 \text{ GeV}^{-1}$	$b_9 = +0.298 \pm 0.087 \text{ GeV}^{-1}$
$b_3 = +0.227 \pm 0.038 \text{ GeV}^{-1}$	$b_{10} = +0.198 \pm 0.058 \text{ GeV}^{-1}$
$b_4 = -0.939 \pm 0.069 \text{ GeV}^{-1}$	$b_{11} = +0.516 \pm 0.058 \text{ GeV}^{-1}$
$b_5 = +0.023 \pm 0.007 \text{ GeV}^{-1}$	$b_0 = +0.710 \pm 0.211 \text{ GeV}^{-1}$
$b_6 = +0.001 \pm 0.001 \text{ GeV}^{-1}$	$b_D = -0.291 \pm 0.068 \text{ GeV}^{-1}$
$b_7 = -2.518 \pm 0.110 \text{ GeV}^{-1}$	$b_F = -0.057 \pm 0.014 \text{ GeV}^{-1}$

We note that the LECs are all of natural size, indicating that all relevant physical mechanisms are included in the calculations. The experimental data on total cross sections are reproduced quite nicely, see Fig. 4.1. We first wish to remark that due to the very small number of data points and since our focus lies only on the Isospin ($I=0$) channel, the data on the process $K^-p \rightarrow \Lambda\pi^0$ are not considered as experimental input in the fit procedure. For completeness, we present the outcome of our approach for this channel in Fig. 4.1. Secondly, all of the cross sections presented here are due to the strong interaction only. Additionally, Coulomb interaction was taken into account in Refs. [95, 105] via a non-relativistic quantum mechanical formula. Since this alone cannot count for an interference between the strong and the electromagnetic interactions, we relegate the proper inclusion of the electromagnetic contributions to a future work. We also note that the data are at sufficiently high momenta, so that effects due to Coulomb interaction should be negligible.

In the previous chapter we have pointed out the importance of a more systematic error analysis. To address here for this we have calculated the error bars (confidence bands) on all observables in the following manner. First we generate a large number ($\sim 10,000$) of randomly distributed parameter sets in the error region given above. Then for each of these parameter sets we calculate the χ^2_{DATA} and keep only those sets, for which $\chi^2_{\text{DATA}} - \chi^2_{\text{DATA, BEST}} \leq 1.05$. Quantities calculated for these parameter sets are assumed to lie in the 1σ region around the central value. Sometimes the latter definition is applied w.r.t. the χ^2 instead of χ^2_{DATA} , however, we have checked numerically that in this case the error bars do not change drastically. In view of the very different number of observables we wish to stick to the above prescription for the determination of error bars.

The results for the threshold quantities are in excellent agreement with experimental data, see Eqs. (4.4), and read

$$\Delta E - i\Gamma/2 = +296_{-49}^{+56} - i 300_{-54}^{+42} \text{ eV},$$

$$\gamma = +2.44_{-0.67}^{+0.73}, \quad R_n = +0.268_{-0.086}^{+0.110}, \quad R_c = +0.643_{-0.019}^{+0.015}.$$

As a matter of fact, the shape of the 1σ region for the energy shift and width of kaonic hydrogen cannot be assumed to be rectangular a priori. Its actual form is depicted in Fig. 4.2, where also the constraints from two older experiments (DEAR and KEK) are presented for completeness. The resulting scattering lengths for isospin $I = 0$ and $I = 1$, i.e. a_0 and a_1 , are displayed in Fig. 4.3, in comparison to some older determinations and the determination based on scattering data alone [105]. The inclusion of the SIDDHARTA data leads to much smaller errors, especially for a_1 . Our values for the scattering lengths are

$$a_0 = -1.81_{-0.28}^{+0.30} + i 0.92_{-0.23}^{+0.29} \text{ fm},$$

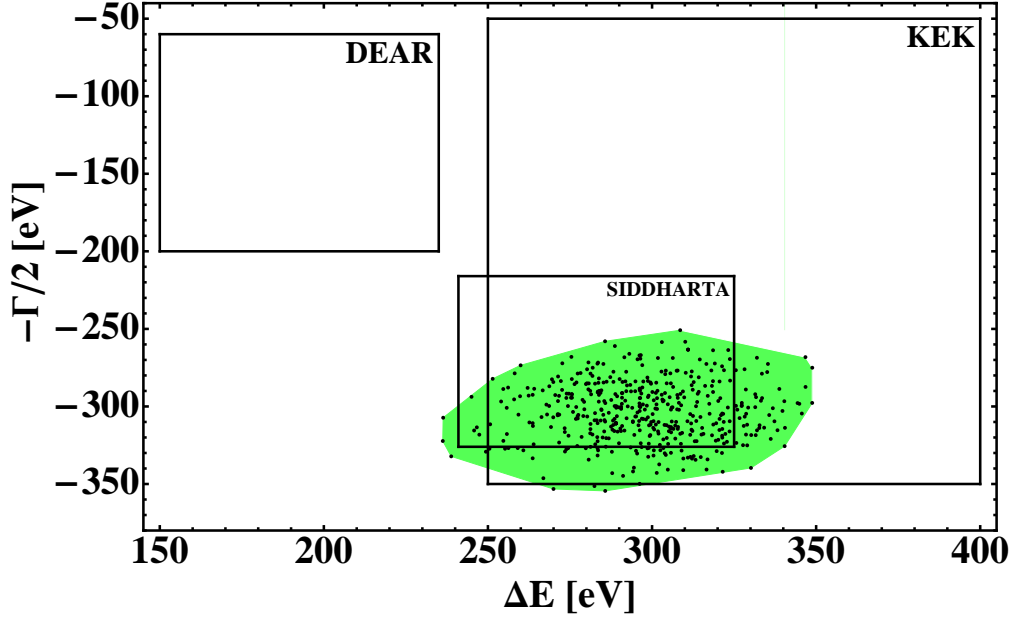


Figure 4.2: Energy shift and width of kaonic hydrogen as determined from the DEAR [124], the KEK [125] and the SIDDHARTA [114] experiments. The shaded area denotes the 1σ region of our approach around the best fit value.

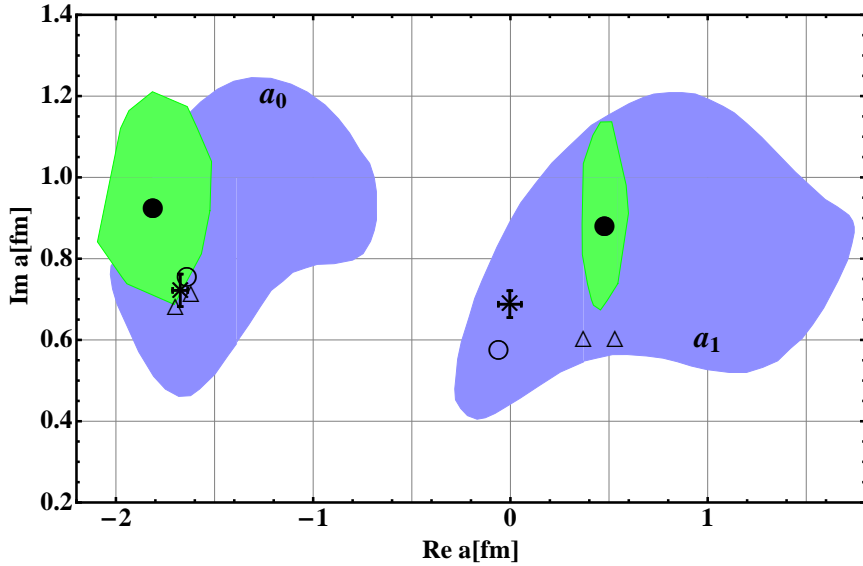


Figure 4.3: Real and imaginary part of isospin 0 and 1 $\bar{K}N \rightarrow \bar{K}N$ scattering lengths. The light shaded (green) areas correspond to the 1σ region of our approach around the central value (full circles). The darker (blue) areas correspond to the 1σ region around central value (empty circle) from Ref. [105]. The cross and empty triangles denote older experimental values from Refs. [126] and [127], respectively.

$$a_1 = +0.48_{-0.11}^{+0.12} + i 0.87_{-0.20}^{+0.26} \text{ fm} . \quad (4.5)$$

The inclusion of the $\Lambda\pi^0$ data in the fitting procedure could yield an additional constraint on the isospin $I = 1$ amplitudes and fix the value of a_1 as done in Ref. [105]. We have not considered this channel as an experimental input for the reasons given above. The scattering length for the elastic K^-p channel reads $a_{K^-p} = -0.68_{-0.17}^{+0.18} + i 0.90_{-0.13}^{+0.13}$ fm. For comparison, taking the SIDDHARTA data only, one obtains $a_{K^-p} = -0.65_{-0.15}^{+0.15} + i 0.81_{-0.18}^{+0.18}$ fm, while Ikeda et al. find² $a_{K^-p} = -0.70_{-0.13}^{+0.13} + i 0.89_{-0.16}^{+0.16}$ fm. Therefore, these fundamental chiral SU(3) parameters can now be considered to be determined with an accuracy of about $\sim 15\%$,

Having fixed the parameters of our model, we can extrapolate the amplitudes of elastic K^-p scattering to the subthreshold region, i.e. center-of-mass energies $1330 \leq W_{\text{cms}} \leq 1450$ MeV. The result is presented in Fig. 4.4. For both real and imaginary parts of the amplitude the maximum lies close to the $\bar{K}N$ threshold and is quite narrow, which indicates the presence of a close-by pole. It is also worth mentioning that the error band gets smaller to low energies, different to the recent analysis by Ikeda et al. [95, 116].

To obtain a more complete picture about the structure of $\Lambda(1405)$, the amplitudes are analytically continued to the complex W_{cms} -plane. As already argued in the last chapter, microcausality forbids poles on the first Riemann sheet, that is for $\text{Im}(W_{\text{cms}}) > 0$. This is fulfilled in our model automatically due to the restoration of analyticity as described above. On the other hand some pole structure has to be responsible for the functional form of the scattering amplitudes $f_{K^-p \rightarrow K^-p}$, see Fig. 4.4. Two poles are found on the second Riemann sheet for isospin $I = 0$, which is achieved via analytic continuation to $\text{Im}(W_{\text{cms}}) < 0$. We denote the second Riemann sheet connected to the physical axis in the region between the $\Sigma\pi$ and $\bar{K}N$ threshold as $\mathcal{R}_{\Sigma\pi}$ and the one connected to the physical axis for $W_{\text{cms}} > (M_{\bar{K}} + m_N)$ as $\mathcal{R}_{\bar{K}N}$. The absolute value of the scattering amplitude is presented on both these sheets in Fig. 4.5. We find that two poles lie on different Riemann sheets, the pole position reads

$$\begin{aligned} \mathcal{R}_{\Sigma\pi} : W_1 &= 1428_{-1}^{+2} - i 8_{-2}^{+2} \text{ MeV} . \\ \mathcal{R}_{\bar{K}N} : W_2 &= 1497_{-7}^{+11} - i 79_{-9}^{+9} \text{ MeV} . \end{aligned}$$

The real part of the position of the first pole agrees quite well with determination from Refs. [79, 95, 105, 116]. Its imaginary part agrees roughly with the determination of Refs. [79, 105] and is significantly smaller than extracted by Ikeda et al. [95, 116]. For the second pole, the situation is different, its imaginary part is in agreement with Refs. [95, 105, 116], but the real part is much larger.

We have investigated the origin of these observations qualitatively. First, from our previous analysis of πN scattering in the same framework, see chapter 3, we know that off-shell effects can account for large modifications of the pole positions. Setting the tadpole integrals to zero, we obtain immediately the solution of the BSE in the on-shell factorization. Note that this solution is still different to the one by Ikeda et al. [95, 116] since no s-wave projection is performed. We found that in the present case the off-shell effects do not alter the pole position drastically. More precisely, the imaginary part of the first pole decreases and the one of the second increases by about 10 MeV. The real parts of both poles do not change significantly. Secondly, we noticed much smaller values of the NLO LECs found by Ikeda et al. additionally

²Here, the error bars are extracted from Fig. 4 of Ref. [95].

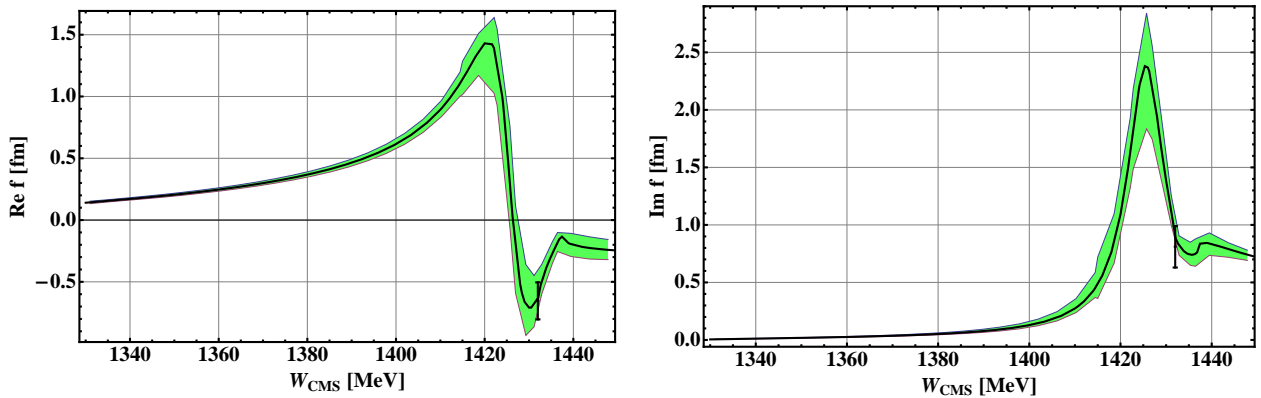


Figure 4.4: Real and imaginary part of the $K^-p \rightarrow K^-p$ scattering amplitude. The shaded band indicates the uncertainty of the calculation. The data point at $W_{\text{cms}} = M_K + m_p$ is determined from the energy shift and width of kaonic hydrogen from the SIDDHARTA experiment.

to the fact that the LECs b_i ($i = 5, \dots, 11$) were neglected there due to the s-wave projection. To keep track of this we scale down our LECs continuously from the values found above to zero. Such a solution of the BSE is of course by no means physical since no further fitting to experimental data is done here. Qualitatively, however, we observe that both poles move (the second one by about 100 MeV) to lower values of $\text{Re}(W_{\text{cms}})$. The conclusion to be drawn is that the s-wave projection in the on-shell approximation of the interaction kernel is the main reason for the difference in pole positions extracted in Ikeda et al. compared to the one extracted from our approach. Despite all these differences the calculated $\pi\Sigma$ mass distributions from the reaction $\Sigma^+(1660) \rightarrow \pi^+(\pi^-\Sigma^+)$ [128], see Fig. 4.6, are of similar quality as the one obtained by Ikeda et al. .

To further elaborate on the two obtained poles, we have analyzed the structure of both resonances utilizing the following representation of the scattering matrix

$$T_{ij} \sim \frac{g_i g_j}{s - s_R},$$

where g_i and g_j are coupling constants of the in- and out-going states, respectively. For each pole (isospin $I = 0$) we extract the coupling constants to the $\bar{K}N$ and $\pi\Sigma$ channel as follows

$$\begin{aligned} W_1 : & \quad |g_{\bar{K}N}| = 3.02 \quad \text{and} \quad |g_{\pi\Sigma}| = 1.61, \\ W_2 : & \quad |g_{\bar{K}N}| = 1.89 \quad \text{and} \quad |g_{\pi\Sigma}| = 4.39. \end{aligned}$$

At the position of the first pole (the one located at the smaller imaginary value of W_{cms}) the coupling to the $\bar{K}N$ channel is nearly twice as large as to the $\pi\Sigma$ channel. For the second pole this pattern is reversed. Qualitatively both observations agree quite nicely with the ones made in Refs. [104, 129].

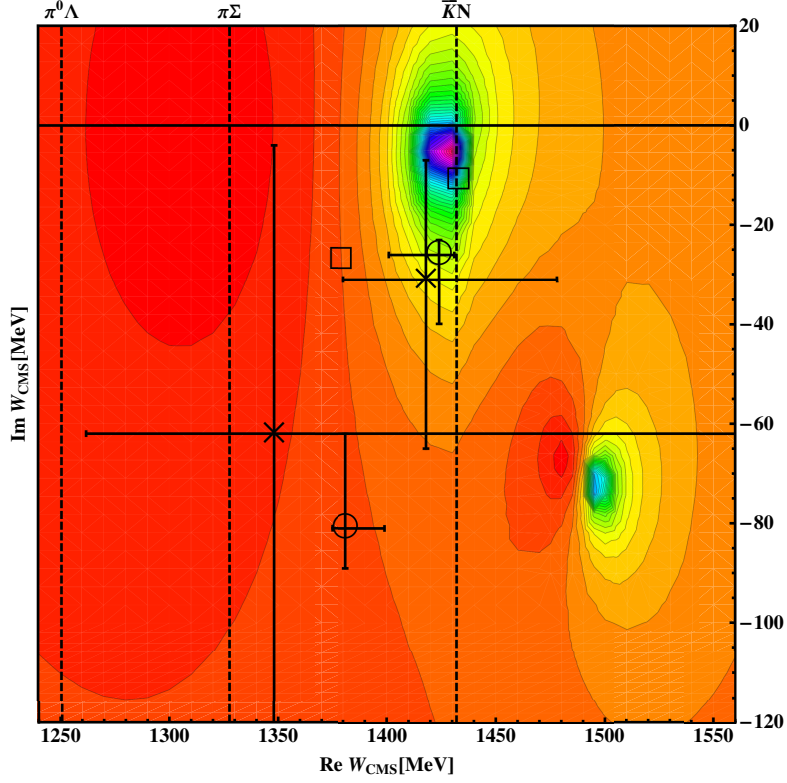


Figure 4.5: Contour plot of the absolute value of the scattering amplitude for isospin $I = 0$ in the complex W_{cms} plane. Both Riemann sheets $\mathcal{R}_{\Sigma\pi}$ and $\mathcal{R}_{\bar{K}N}$ are 'glued' together along the $\bar{K}N$ threshold line. The pole positions of comparable models are presented in the plot via squares [79], circles [95, 116] and crosses [105].

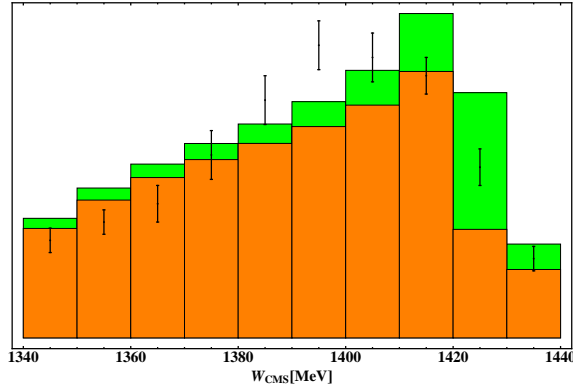


Figure 4.6: The prediction of our approach for the $\pi\Sigma$ ($I = 0$) mass distribution with (shaded area) as constructed from the $\pi\Sigma \rightarrow \pi\Sigma$ and $\bar{K}N \rightarrow \pi\Sigma$ amplitudes in comparison to the experimental data from Ref. [128]. Units are arbitrary and the green bands represent the uncertainty of our prediction.

4.5 Summary and outlook

In this section we have applied our chiral unitary framework as developed in chapter 1 and 2 to antikaon-nucleon scattering. We have fitted the scattering data for $K^-p \rightarrow K^-p$, \bar{K}^0n , $\Sigma^\pm\pi^\mp$, and $\Sigma^0\pi^0$ for laboratory momenta $p_{\text{lab}} \leq 300$ MeV together with the SIDDHARTA data, which allows for a good description of the antikaon-proton cross section data (cf. Fig. 4.1) and an accurate determination of the scattering lengths, cf. Eq. (4.5). We can give a precise prediction for the real and imaginary part of the $K^-p \rightarrow K^-p$ scattering amplitude for center-of-mass energies $1330 \leq W_{\text{cms}} \leq 1450$ MeV, cf. Fig. 4.4. We have investigated the two-pole structure of the $\Lambda(1405)$ [79, 129]. While the first pole is in agreement with other determinations, we find the real part of the second pole at larger energies than usually obtained. We trace this back to the contributions from the NLO terms in the driving potential. In contrast to most other works we neither restrict those to be small nor perform an s-wave projection of the kernel. We determine the coupling of both isospin $I = 0$ poles to the $\bar{K}N$ and $\pi\Sigma$ channels. We observe a nice qualitative agreement with the observation made in Refs. [104, 129].

The $\pi\Sigma$ invariant mass distributions can be of the great interest to shed more light on the structure of the $\Lambda(1405)$. Currently available data [128] are in agreement with our as well as with the earlier analyses [95, 105, 116]. New results have been reported recently [130, 131]. Once analysed these may help to put narrow constraints on the position of both $\Lambda(1405)$ poles. From a more conceptual point of view we consider the approximate restoration of analyticity as an improvement of the present analysis. It may be also of interest for the analysis of related processes as it allows for an additional restriction of the typically very large parameter space.

Chapter 5

Pion photoproduction off the proton in a gauge-invariant chiral unitary framework¹

5.1 Introduction

Pseudoscalar meson photoproduction off protons is one of the premier tools to unravel the spectrum and properties of baryons made of the light up, down and strange quarks, as witnessed e.g. by the dedicated baryon resonance programs at ELSA (Bonn) and CEBAF (Jefferson Laboratory). Some of the low-lying resonances like the Roper $N^*(1440)$, the $S_{11}(1535)$ or the $\Lambda(1405)$ exhibit features that cannot easily be reconciled with a simple constituent quark model picture. Therefore, it was speculated since long that some of these peculiar states and their properties can be explained if one assumes that they are generated through strong coupled-channel dynamics. Arguably the best tool to address such a dynamical generation of resonances is unitarized chiral perturbation theory [2, 3, 61, 79–83, 95].

Over the years, we have developed and applied a gauge-invariant chiral unitary coupled-channel approach based on the leading order (LO) chiral effective Lagrangian of QCD to kaon [106] and eta photoproduction, see Ref. [132]. To go beyond LO, one first has to refine the description of meson-baryon scattering in this framework as the strong hadronic final-state interactions are a crucial ingredient in evaluating the complete photoproduction amplitudes. Therefore, we have developed a framework to analyse meson-baryon scattering incorporating next-to-leading order (NLO) contributions of the chiral Lagrangian [133]. Our scheme is based on the solution of the Bethe-Salpeter equation (BSE), with a kernel derived from the contact terms of the NLO chiral Lagrangian. We have summed up the full infinite series of Feynman diagrams generated by the BSE without resorting to any of the commonly made approximations as e.g. the on-shell approximation. In this way we were able to reproduce successfully both s-waves of pion-nucleon scattering (S_{11} and S_{31}) between the πN and ηN thresholds. For higher energies we have observed that only the resonance $S_{11}(1535)$ but not the $S_{31}(1620)$ could be

¹Most of the contents of this chapter can be found in Ref. [4] which has been accepted for publication in Physical Review D.

described well. We have concluded that the $S_{31}(1620)$ does not have a prominent dynamically generated content. As a matter of fact after fixing the S_{11} partial wave in the first energy region, i.e. $W_{\text{cms}} < 1.56$ GeV, the S_{11} amplitude for the higher energies came out in astonishing agreement with current partial wave analyses. The examination of the complex energy plane showed that also the pole position of the second s-wave resonance, i.e. the $S_{11}(1650)$, agrees rather well with those given by the particle data group [28]. It is therefore natural to extend this approach to s-wave photoproduction of pions, where a large data base already exists. This is the main issue of the present chapter.

This chapter is organized as follows: In section 5.2, the underlying approach to analyse meson-baryon scattering is described. Two fit strategies to pin down the occurring parameters are presented and fits to data and predictions for some scattering lengths and the fundamental ηN scattering amplitude are given. The approach is extended to photoproduction in section 5.3, where parameter-free predictions for pion and η production off protons are given. Many technicalities are relegated to the appendices.

5.2 Hadronic scattering

In the present section we wish to present the basic formalism for meson-baryon scattering as it will serve us as the most important ingredient in our analysis of the photoproduction processes. For details and fundamental properties we refer the reader to the introductory chapter 2. We wish also to give a more systematic error analysis of our results as it was done in chapter 3. Moreover, from this first study we know that our coupled-channel approach is applicable to relatively high energies, when including the full NLO terms from the chiral Lagrangian. Thus we will extend our analysis also to the process $\pi N \rightarrow \eta N$, studied within a simplified approach in Ref [132].

5.2.1 Formalism

Inspired by Chiral Perturbation Theory, which gives the driving terms of the meson-baryon interaction, our framework relies on the coupled-channel Bethe-Salpeter equation [74]. The latter implements the requirement of two-body unitarity exactly and in principle allows to generate resonances dynamically. It already improved our understanding of the purely mesonic and meson-baryon sector in recent years, see e.g. Refs. [2, 3, 61, 79–83, 95]. We denote the in- and out-going meson momenta by q_1 and q_2 , respectively. Moreover, the overall four-momentum is given by $p = q_1 + p_1 = q_2 + p_2$, where p_1 and p_2 are the momenta of in- and out-going baryons, respectively. To iterate the meson-baryon potential $V(q_2, q_1; p)$ we utilize once again the Bethe-Salpeter equation in d dimensions as presented in Eq. (2.1) and visualized in Fig. 2.1. Restricting the meson-baryon states to have the quantum numbers of the proton, the channel space reduces to the 6-dimensional space spanned by the following channels $\{\pi^0 p, \pi^+ n, \eta p, K^+ \Lambda, K^+ \Sigma^0, K^0 \Sigma^+\}$. Note that the loop integration in Eq. (2.1) is performed in d dimensions, without restricting the loop momenta to be on the mass shell. Such an approximation would certainly reduce the technical effort to solve the BSE, however, it spoils the direct correspondence of the solution of the BSE Eq. (2.1) to the series of Feynman graphs,

which we evaluate as it stands. Thus, every term in our solution of the BSE is related, in a one-to-one correspondence, to a properly evaluated Feynman diagram. It comes as an advantage of this prescription that the implementation of gauge invariance in a combined analysis of hadronic scattering and meson photoproduction is straightforward and very natural: It follows essentially the guidelines from quantum field theory textbooks, see e.g. sec. (7.4) of Ref. [89], and will be explained in sec. 5.3. Moreover, it is also straightforward to compare our amplitude to the perturbative expansion at any fixed chiral order. We complete our discussion of the off-shell-dependence of the effective vertices with the remark that the use of the on-shell-approximation is not more “physical” than taking the off-shell-dependence into account, though reducing the effort of the calculation significantly down to the evaluation of a geometric series. Simply iterating a fixed on-shell kernel in such a geometric series can even lead to significant deviations from the results of Feynman graphs when iterating Born-terms, as is exemplified by an analysis of box graphs in sec. (5.2) of Ref. [75]. In our case, off-shell behavior of the potential reflects itself in tadpole - integral terms in the full scattering amplitude. These terms might in general depend on the chosen parameterization of fields as long as only a subset of Feynman graphs is summed up, see section 1.4. Setting them to zero as done using the on-shell approximation is just one possible “choice of gauge” (in the space of field parameterizations) in a non-invariant result, which, however, is not in line with the proper evaluation of loop diagrams we aim at here. As the analytic energy-dependence of the tadpole-terms is trivial, it should be possible to compensate for this non-invariance effect by an adjustment of coupling constants in the kernel. As a byproduct of our procedure for finding fits², we have checked numerically that this is indeed the case. Thus, while the exact numerical values of the coupling constants should be taken with a grain of salt (they should be considered as model parameters in our approach) the overall properties of the amplitude are solely based on the unambiguous analytic properties of the selected infinite subset of loop graphs.

Relying on the previous analyses, see chapter 3 and 4, we will approximate the driving term of the meson-baryon interaction, i.e. the potential $V(q_2, q_1; p)$ by the sum of contact terms from the leading and next-to-leading order chiral Lagrangian, see Eqn. (1.13) and (2.4), respectively. The one-baryon exchange graphs, both in the s and u channel will be omitted from this potential since they induce several (up to now not solved) technical and practical difficulties in the framework of Bethe-Salpeter type equations as described in extenso in section 2.1. Hence the interaction potential of the first and second chiral order takes the form

$$V(q_2, q_1; p) = A_{WT}(q_1 + q_2) + A_{14}(q_1 \cdot q_2) + A_{57}[q_1, q_2] + A_M + A_{811}(q_2(q_1 \cdot p) + q_1(q_2 \cdot p)) , \quad (5.1)$$

where $A_{...}$ denote matrices in channel space as defined in App. C. The matrix A_{WT} depends upon the meson decay constants, which will be fixed to their physical values in the following. However, the remaining matrices $A_{...}$ depend also upon the so-called low-energy constants, b_i , which appear in this low-energy effective field theory while integrating out the heavy degrees of freedom of the underlying theory (QCD). As a matter of fact the importance of the second order terms in the kernel of the BSE is twofold. First of all, as can be seen in Ref. [42], such terms lead to sizable corrections of the meson-baryon scattering amplitudes. Secondly, the contact interactions of the second chiral order not only contribute to the s-wave but also to the

²See the discussion in section 4.3.

p-waves, which are then iterated in the BSE. In App. D we demonstrate in a toy model that the presence of the first two partial waves is sufficient to reproduce the correct behavior of the differential cross sections at sufficiently low energies.

In the second chapter of this thesis we have developed the recipe for the solution of the BSE with the interaction kernel consisting of local terms. As described there we utilize dimensional regularization to treat the divergent loop integrals, where the purely baryonic integrals are set to zero from the beginning, while only an energy-independent constant is subtracted from the fundamental meson-baryon loop integral. This prescription to treat the large baryon mass scale is similar to the EOMS regularization scheme described in Ref. [62]. On the other hand it resolves several technical problems, which appear in the course of the study of the photo-production amplitudes described in the next section. To further extent, the solution of the BSE corresponds to an infinite chain of one-meson-one-baryon loop diagrams, see e.g. Fig. 1.2. From the point of view of the usual perturbative treatment this would demand an infinite number of counterterms from a local Lagrangian to absorb the loop divergences. This is of course not feasible in an effective field theory. In our non-perturbative framework, the ignorance of higher-order terms in the scattering kernel, which would serve to cancel the divergences and the scale-dependence of the loop integrals in a perturbative setting, reflects itself by the appearance of a new free parameter for every loop-integration, parametrized here by the logarithm of the renormalization scale. This pragmatic approach is commonly adopted in the literature, see e.g. Refs. [2, 3, 84, 88, 95]. The new free parameters are not completely arbitrary, however: At least, we must impose that the values for the renormalization scale correspond to neglected higher order terms of natural size. Should this not be the case, and a scale of e.g. $\mu \sim \text{TeV}$ emerge from some fits, we must discard that solution as unnatural. As a side remark, we note that any modification of the loop integrals corresponds to a specific modification of the potential V in the solution of the BSE. For an explicit demonstration of this procedure we refer to App. F of Ref. [92]. The requirement that the modification of the potential is not dominating the leading order terms also yields the mentioned constraints on the free scales. In conclusion, the foregoing discussion suggests that it is sufficient in the present work to apply the subtraction scheme described above, keeping in mind that the modified loop integrals still depend on the renormalization scale, which constitutes a free fitting parameter. In the next subsection we will re-examine this as well as the possibility to adjust this scale to a fixed value due to constraints on the loop dressing of vertex functions.

The essential advantage of the above treatment is the preservation of the analytic structure of the loop integrals, which allows for a continuation of the scattering amplitudes into the complex energy plane. The solution of the BSE is presented in section 2.3. It can be written in terms of elementary functions (that is without resorting to a numerical solution) of the loop integrals, which are collected in App. A. Once the BSE has been solved we put the external particles on their mass shell and calculate partial wave amplitudes as well as differential cross sections for hadronic scattering. For the evaluation of the photoproduction amplitudes we will require the full off-shell dependence of the hadronic solution, as will be described later.

5.2.2 Fit

It is important to clarify the physical input to the scattering amplitudes. Throughout this chapter we will use physical hadron masses (in GeV), as specified in Eq. (3.2). The baryon mass in the chiral limit, m_0 in Eq. (1.13), can be fixed to 1 GeV without loss of generality, as any other value only amounts to a rescaling of the unknown LECs. In contrast to the earlier work [106], the meson decay constants are also fixed to their physical values, see Eq. (3.2).

To pin down the free parameters of our approach we have to specify experimental input available on the market for the considered meson-baryon channels. From the experimental point of view elastic πN scattering is by far the best explored reaction. On the other hand it is clear that the low-energy region is dominated by the p-wave resonances, namely Roper and Delta. Our investigations presented in chapter 3 have shown that we are not able to dynamically generate these resonances consistently with the s-wave resonances. Since these degrees of freedom are not included in our approach, we restrict ourselves to the analysis of s-waves. We fit our results for these πN partial waves to the widely accepted partial wave analysis (WI08) by the SAID collaboration [108]. Comparing an earlier analysis by the Karlsruhe group [109] to the current one, we assign for the energies below $W_{\text{cms}} = 1.28$ GeV an absolute systematic error of 0.005 and for higher energies an error of 0.030 to the partial wave amplitudes. To some extent this is in agreement with error estimates done in Ref. [84], which are motivated by the expectation of pronounced three-body effects above the $\pi\pi N$ threshold.

Another widely explored channel is $\pi^- p \rightarrow \eta n$, for which we consider quite recent but already very established results on differential cross sections measured by Prakhov et al. in Ref. [134]. For all seven measured incident pion beam momenta p_{lab} we assign a measurement error as well as the systematic error of 6% as pointed out in Ref. [134]. Moreover, one should keep in mind that also p_{lab} itself entails an uncertainty, which hampers the clear pairwise separation between most of the given beam momenta [135]. We do not consider this uncertainty in our fitting routine as the inclusion would require an additional model-dependent input. The necessary formalism is collected in App. D.

To fit the above data we follow two different fit strategies, which allow us to make additional tests of the stability of our solution.

Fit strategy (I): We start from the best fit obtained in chapter 3 and additionally include the $\pi^- p \rightarrow \eta n$ differential cross sections by Prakhov et al. adjusting all 17 parameters of the model ($\log(\mu_\pi), \log(\mu_K), \log(\mu_\eta)$ as well as the 14 LECs). The fitting region in the elastic πN channel is chosen to be $(m_p + M_\pi) < W_{\text{cms}} < 1.56$ GeV for both S_{11} and S_{31} . It is obvious that the new data will restrict our parameter set additionally, possibly corrupting the agreement of the elastic πN to the SAID data compared to the fit obtained in chapter 3.

Fit strategy (II): One of the main observations of the analysis in chapter 3 was that the S_{11} but not the S_{31} partial wave of πN scattering can be described well in the resonance region. On the other hand the main goal of the present work is to see how hadronic resonances manifest themselves in the photoproduction amplitude. Moreover, since the ηN final state is an isospin 1/2 state we fit the elastic S_{11} partial wave in the energy region $(m_p + M_\pi) < W_{\text{cms}} < 1.7$ GeV together with $\pi^- p \rightarrow \eta n$ differential cross

sections of Prakhov et al.. The S_{31} is considered only in the near-threshold region for $W_{\text{cms}} < 1.2$ GeV. Furthermore, we reduce the number of the free parameters of the model to LECs fixing the regularization scales from the beginning. It turns out that the corrections to the tree-level result of the photoproduction multipole E_{0+} due to the dressing of the $B \rightarrow \phi B$ vertex are large already at the πN threshold. Thus we choose the scales such that the meson-baryon loop integral evaluated at $s = m_p^2$ vanishes in every meson-baryon channel, to assure that the axial vertex-function does not deviate much from the corresponding tree-level expression.

For both fit strategies we minimize $\chi^2 := \chi_{DOF}^2$ as specified in Eq. (3.3). This choice of χ^2 ensures the equal weight of both fitted observables, compensating for the different number of data points. Albeit the solution of the BSE is fully analytical, it costs a huge amount of computational power. Thus the fitting as well as error estimation routine is performed in a parallelized version on 20-30 threads of the HSKP cluster utilizing the (migrad) minimization routine of the MINUIT C++ library [110]. The uncertainty of the model is estimated as established already in chapter 4. First, after obtaining the best fit (χ_{BEST}^2) the errors on the parameters are calculated in the *hesse* subroutine of the MINUIT package. Then within these errors we generate a large number of parameter sets ($\sim 10,000$) and calculate for each the corresponding χ_{DOF}^2 . Then each set corresponding to a $\chi^2 < \chi_{BEST}^2 + 1.15$ is considered to produce results in the 1σ region around the central value³.

5.2.3 Results

Solution I: Following the first fit strategy, we obtain the best fit as presented in Figs 5.1 and 5.2. As already discussed, the differential cross sections on $\pi^- p \rightarrow \eta n$ are taken at seven different pion beam energies, which by themselves entail a non-negligible uncertainty. The latter, however, is not included into the definition of the χ^2 for the reasons given above. Therefore, we refrain from giving any numerical value for this quantity⁴. The corresponding parameters (all μ_i in GeV) are of natural size and read:

	$\log(\mu_\pi/(1\text{GeV}))$	$= +1.003 \pm 0.331$
	$\log(\mu_\eta/(1\text{GeV}))$	$= +1.034 \pm 0.298$
	$\log(\mu_K/(1\text{GeV}))$	$= -0.168 \pm 0.080$
b_1	$= -0.126 \pm 0.039 \text{ GeV}^{-1}$	$b_8 = +0.610 \pm 0.012 \text{ GeV}^{-1}$
b_2	$= -0.139 \pm 0.045 \text{ GeV}^{-1}$	$b_9 = -0.677 \pm 0.037 \text{ GeV}^{-1}$
b_3	$= -2.227 \pm 0.133 \text{ GeV}^{-1}$	$b_{10} = +2.027 \pm 0.100 \text{ GeV}^{-1}$
b_4	$= -0.288 \pm 0.080 \text{ GeV}^{-1}$	$b_{11} = -0.847 \pm 0.027 \text{ GeV}^{-1}$
b_5	$= -1.402 \pm 0.094 \text{ GeV}^{-1}$	$b_0 = -1.063 \pm 0.038 \text{ GeV}^{-1}$
b_6	$= +0.474 \pm 0.118 \text{ GeV}^{-1}$	$b_D = +0.771 \pm 0.042 \text{ GeV}^{-1}$
b_7	$= -1.751 \pm 0.368 \text{ GeV}^{-1}$	$b_F = -0.169 \pm 0.054 \text{ GeV}^{-1}$

³One might argue, whether or not one should divide by the number of degrees of freedom. It turns out that the error bars do not change significantly.

⁴We wish to note that χ^2 restricted to the SAID data lies only slightly above the one given in chapter 3, where no other than elastic πN channels were included as observables.

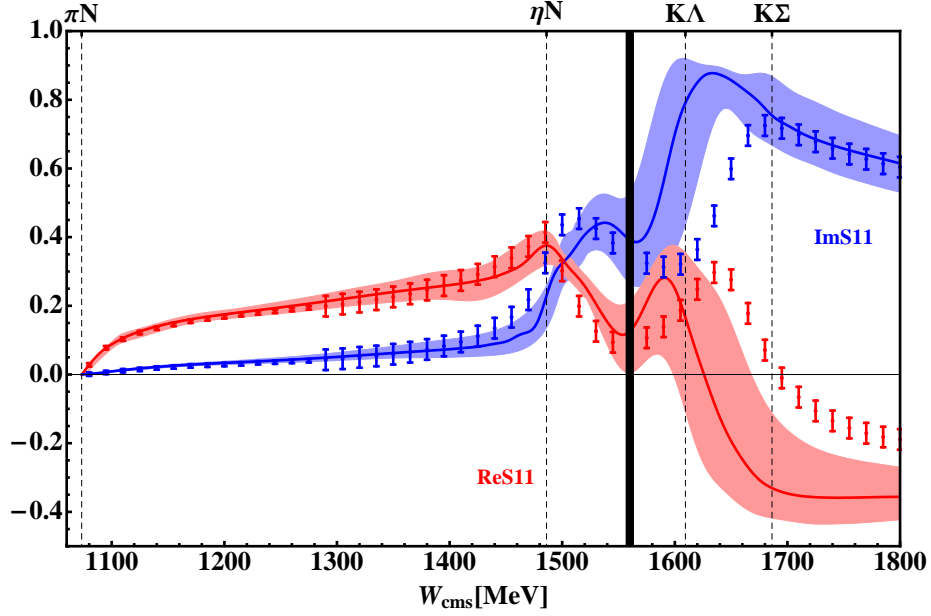


Figure 5.1: Best fit according to fit strategy (I) to the real and imaginary part of the S_{11} partial wave compared to the WI08 analysis done by the SAID collaboration [108]. The dashed vertical lines correspond to the two particle thresholds and the bold vertical line limits the energy range up to which the fit has been performed. The blue and red bands represent the 1σ uncertainty of our approach as described in the main text.

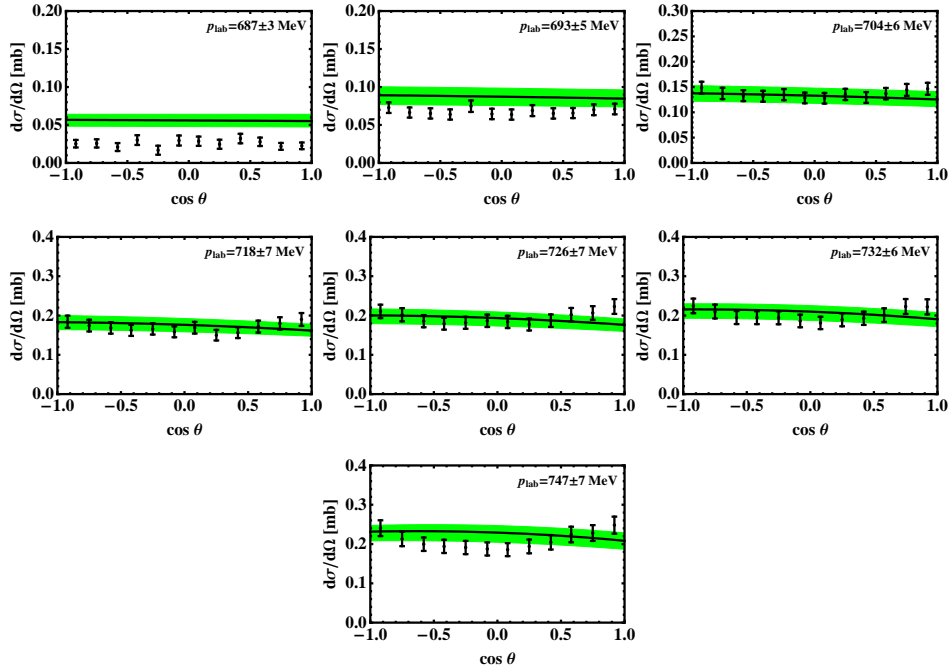


Figure 5.2: Best fit according to fit strategy (I) to the differential cross sections for $\pi^- p \rightarrow \eta n$ from Ref. [134]. The error bars of experimental data include the systematic error of 6% as argued in Ref. [134]. The green bands represent the 1σ uncertainty of our approach as described in the main text.

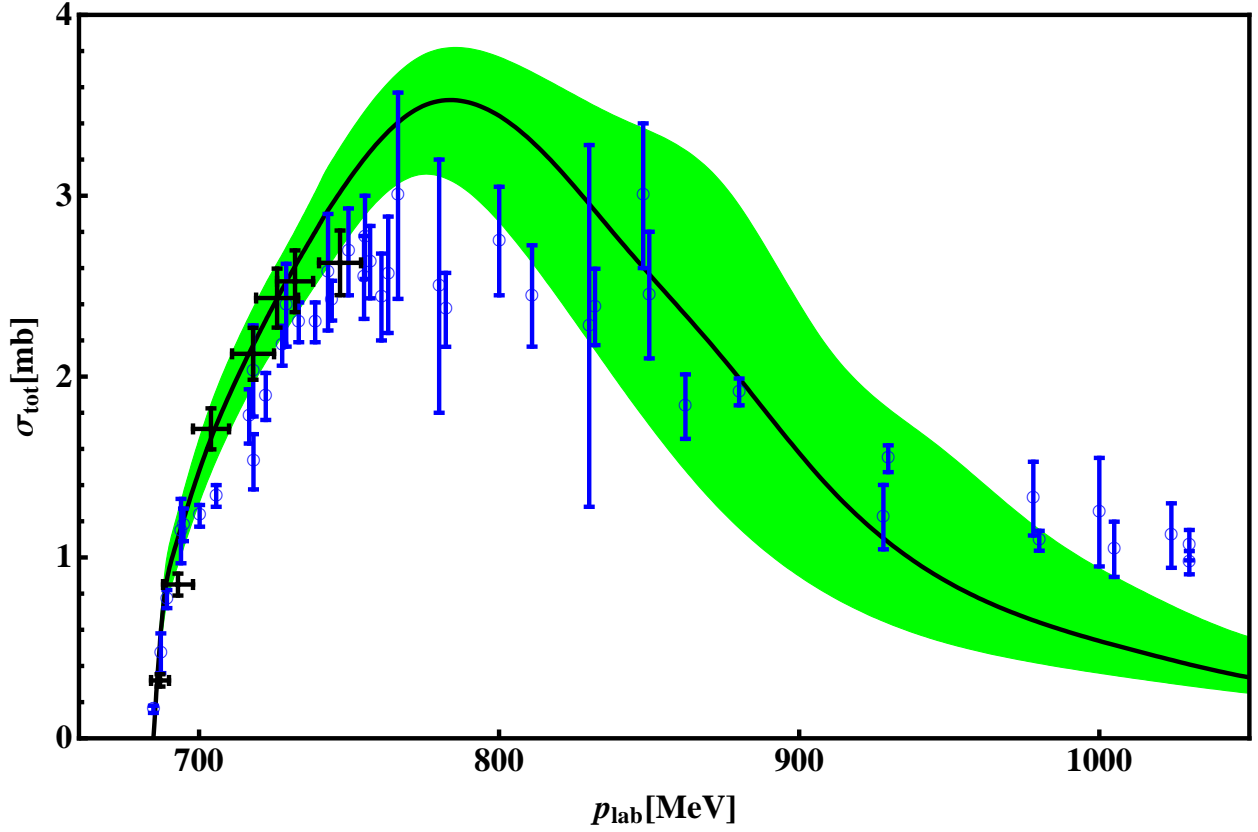


Figure 5.3: Total cross section of the best fit for $\pi^- p \rightarrow \eta n$ according to fit strategy (I). The model is fixed to reproduce the differential cross section and thus the total cross section as measured by Prakhov et al. (black symbols). The black curve including the uncertainty band is the result of our model. The blue circles correspond to older measurements as selected by the SAID collaboration which are presented for completeness.

The observation in the elastic πN channels is similar the one made in chapter 3. Between the πN and ηN thresholds both partial waves can be fitted nicely to the SAID partial wave analysis. For the πN scattering lengths of isospin I , a_I (in units of $10^{-3}/M_{\pi^+}$), we obtain:

$$a_{3/2}^{\pi N} = -87.0_{-4.2}^{+4.3} \quad \text{and} \quad a_{1/2}^{\pi N} = +174.5_{-32.8}^{+15.2}. \quad (5.2)$$

The theoretically cleanest determination of these observables stems from the analysis of pionic hydrogen and pionic deuterium data based on effective field theory [112], $a_{1/2} = (179.9 \pm 3.6) \times 10^{-3}/M_{\pi^+}$ and $a_{3/2} = (-78.5 \pm 3.2) \times 10^{-3}/M_{\pi^+}$, which is in nice agreement with our determination for the $I = 1/2$ channel, but our result is slightly too small for $I = 3/2$. For both isospins our determination agrees perfectly with those from the direct extraction by the SAID collaboration: $a_{1/2} = (174.7 \pm 2.2) \times 10^{-3}/M_{\pi^+}$ and $a_{3/2} = (-89.4 \pm 1.7) \times 10^{-3}/M_{\pi^+}$.⁵

In the higher energy region the lowest S_{11} but not S_{31} resonances could be reproduced as dynamically generated states in our model. The pole positions can be extracted via analytic

⁵We thank Ron Workman for providing us with these values.

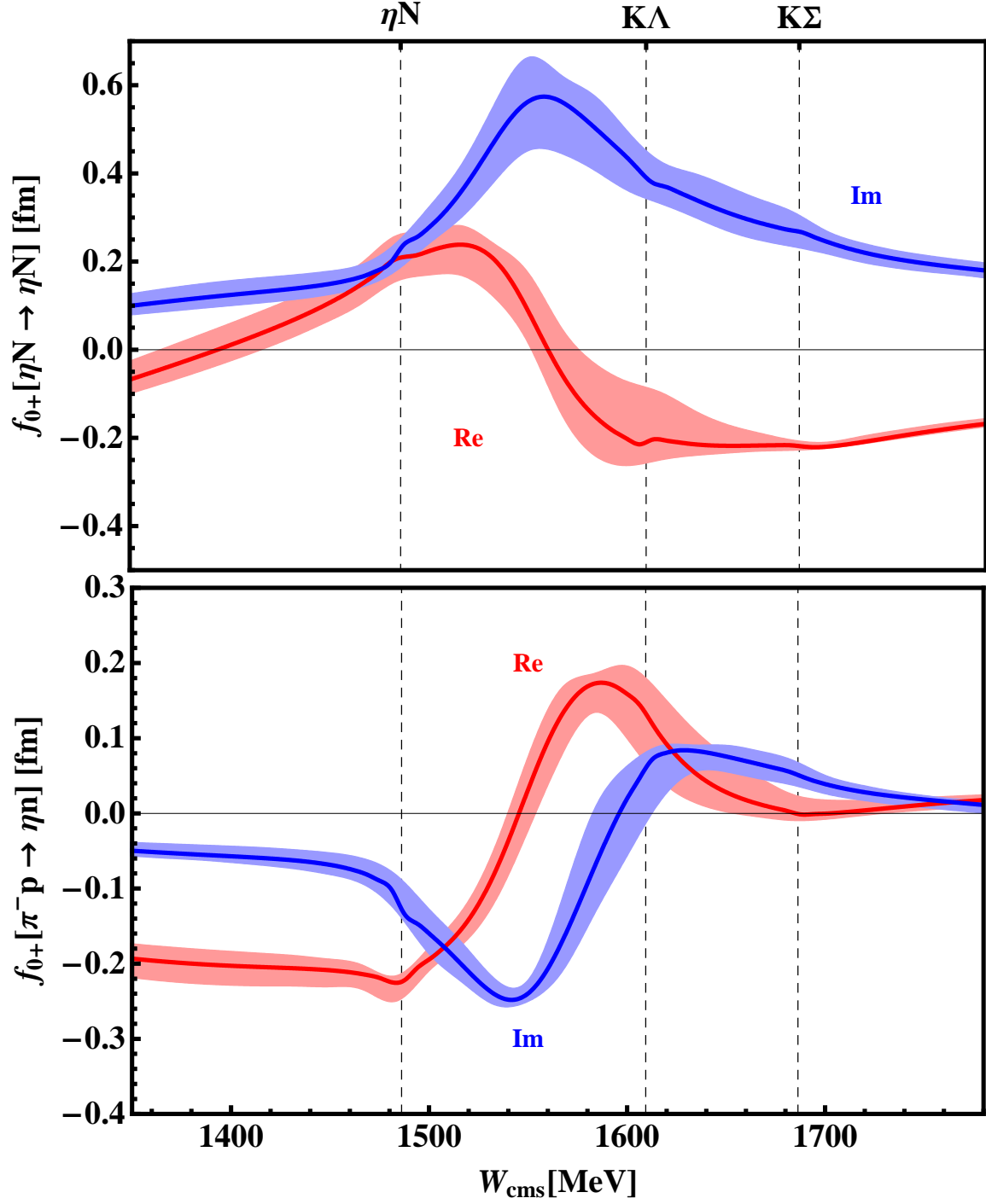


Figure 5.4: The result of our model in the fit strategy (I) for the real and imaginary part of the s-wave scattering amplitude of the ηN (top) and $\pi^- p \rightarrow \eta n$ (bottom) channels. The error bands represent the uncertainty due to the variation of the model parameters as described in the text.

continuation of the scattering amplitude to the complex W_{cms} plane and read

$$\begin{aligned} W_{1535} &= (1.547_{-0.021}^{+0.004} - i0.046_{-0.017}^{+0.004}) \text{ GeV}, \\ W_{1650} &= (1.597_{-0.020}^{+0.017} - i0.045_{-0.015}^{+0.010}) \text{ GeV}. \end{aligned} \quad (5.3)$$

Obviously the inclusion of ηN observables into the analysis forces the pole of $N^*(1535)$ to the higher and the pole of $N^*(1650)$ to the lower energies compared with the previous analysis in this thesis. This observation is in some agreement with the analysis in Ref. [113]. There in a meson-exchange model the analysis of the inelasticities has shown that a simultaneous description of the ηN and πN scattering amplitude is hampered by the missing $\pi\pi N$ channels, which are also missing in our approach. However, let us repeat that the starting values of the present fit strategy are chosen to be those from the analysis done in chapter 3. Although there is no reason to doubt about them for the description of elastic πN scattering one should keep in mind that the inclusion of additional, i.e. ηN data, alter the amplitudes in the πN channel as well.

For the pion induced eta production, Fig. 5.2, we observe that the outcome of the model agrees with the experimental data, keeping in mind the uncertainty on the pion beam momenta. The inclusion of the latter is crucial especially for the lowest pion beam momenta, where the slope of the total cross section is enormous as can be seen in Fig. 5.3. There we present the outcome of the model for higher beam momenta than included in the fit. Obviously the total cross section agrees with the experimental data within the error bars. We also observe a large qualitative agreement of the outcome of the model with the older and less precise measurements, selected by the SAID collaboration. The overshooting of the total $\pi N \rightarrow \eta N$ cross section by 30% as discussed in Ref. [113] is overcome obviously via moving of the $N^*(1535)$ peak towards higher energies, which is a direct consequence of the present fit strategy. In App. D we show that the present model is in principle capable to simulate a $\cos^2 \theta$ like behavior in the differential cross sections, usually referred to as the influence of the D_{13} resonance. The observation to be made from Fig. 5.2 is that the inclusion of the elastic πN channels prevents (or at least damps) such behavior. One should notice that the curvature in the data is of comparable size as the uncertainty in the data as well as the uncertainty band of our approach.

We can make a prediction of the s-wave amplitudes for elastic ηN as well as $\pi^- p \rightarrow \eta n$ scattering as presented in Fig. 5.4. Here and in the future we use the standard Höhler partial waves denoted by f_{0+} in contrast to the S_{11} partial wave used by SAID collaboration, see e.g. Fig. 5.1, which is $f_{0+}(I = 1/2)$ multiplied by q_{cms} . In both channels the real and imaginary part shows a similar behavior to the one shown in Ref. [136]. However, the position of the S_{11} peak is systematically shifted to higher energies in our approach, which is again a feature of the present fit strategy. For the scattering lengths we obtain the following values (in commonly used units of fm)

$$\begin{aligned} a_{\eta N \rightarrow \eta N} &= (+0.219_{-0.068}^{+0.047} + i0.235_{-0.055}^{+0.148}) \text{ fm}, \\ a_{\pi^- p \rightarrow \eta n} &= (-0.234_{-0.024}^{+0.020} - i0.129_{-0.104}^{+0.048}) \text{ fm}. \end{aligned} \quad (5.4)$$

There is a large spread in the results on ηN scattering lengths debated for a long time, see Ref. [137] for a nice collection of those. One can note that most models predict a positive real and imaginary part of the scattering length, which is in agreement with our result as well.

Solution II: As argued above, the number of free parameters is reduced in this fit strategy by the three regularization scales. They are fixed such that for each meson-baryon channel (i): $I_{MB}(m_p^2, m_i, M_i) \stackrel{!}{=} 0$ in the nomenclature of App. A, which yields the following values

$$\log(\mu_\pi) = -0.368, \quad \log(\mu_\eta) = 0.056, \quad \log(\mu_K) = 0.210.$$

The best fit of the 14 LECs, which are the only free parameters of the model in the present fit strategy, is presented in Fig. 5.5 and 5.6. All parameters are of natural size and read including the error bars:

$b_1 = -0.014 \pm 0.023 \text{ GeV}^{-1}$	$b_8 = +0.272 \pm 0.015 \text{ GeV}^{-1}$
$b_2 = -0.207 \pm 0.051 \text{ GeV}^{-1}$	$b_9 = -0.483 \pm 0.032 \text{ GeV}^{-1}$
$b_3 = -1.063 \pm 0.032 \text{ GeV}^{-1}$	$b_{10} = +1.054 \pm 0.021 \text{ GeV}^{-1}$
$b_4 = -1.312 \pm 0.023 \text{ GeV}^{-1}$	$b_{11} = +0.328 \pm 0.015 \text{ GeV}^{-1}$
$b_5 = -0.628 \pm 0.060 \text{ GeV}^{-1}$	$b_0 = -1.228 \pm 0.005 \text{ GeV}^{-1}$
$b_6 = +0.508 \pm 0.045 \text{ GeV}^{-1}$	$b_D = +1.097 \pm 0.011 \text{ GeV}^{-1}$
$b_7 = +1.041 \pm 0.191 \text{ GeV}^{-1}$	$b_F = -0.858 \pm 0.011 \text{ GeV}^{-1}$

In the elastic πN channel the S_{11} partial wave agrees almost perfectly in the whole energy range with the one from the analysis by the SAID collaboration. The corresponding scattering lengths are extracted to be (in units of $10^{-3}/M_{\pi^+}$)

$$a_{3/2}^{\pi N} = -93.0_{-6.3}^{+4.7} \quad \text{and} \quad a_{1/2}^{\pi N} = +168.9_{-6.4}^{+5.9}. \quad (5.5)$$

A comparison with the result of other calculations, given before, shows the same pattern as in the previous fit. Both scattering lengths agree within the error bars with the direct extraction by the SAID collaboration and are smaller than the values extracted in Ref. [112].

Both $N^*(1535)$ and $N^*(1650)$ are reproduced as dynamically generated states of the lowest meson and baryon octet states. The pole positions of both N^* resonances read

$$\begin{aligned} W_{1535} &= (1.512_{-7}^{+8} - i0.070_{-5}^{+9}) \text{ GeV}, \\ W_{1650} &= (1.715_{-24}^{+32} - i0.116_{-24}^{+15}) \text{ GeV}. \end{aligned} \quad (5.6)$$

As a matter of fact we expect the pole positions from the present fit strategy to be even more realistic than those from the previous fit strategy as well as from the analysis done in chapter 3, where no physical information was included for energies in the region of the second resonance. The pole position of the $N^*(1535)$ is perfectly within the uncertainty band presented in Ref. [28], i.e. $W_{1535} = (1.490\dots 1.530) - i(0.045\dots 0.125)$ GeV. On the other hand the position of $N^*(1650)$ differs slightly from the one given there, i.e. $W_{1650} = (1.640\dots 1.670) - i(0.050\dots 0.085)$ GeV. Note that both bands in Ref. [28] are mostly based on a selection of partial wave analyses. The pole positions from two comparable theoretical works read $W_{1535} = 1.519 - i0.064$ GeV and $W_{1650} = 1.669 - i0.068$ GeV from Ref. [138] as well as $W_{1535} = 1.496 - i0.041$ GeV and $W_{1650} = 1.686 - i0.096$ GeV from Ref. [88].

For the pion induced eta production we observe that, taking into account the uncertainty of the pion beam energy, all seven differential cross sections agree with the data by Prakhov et al., see Fig. 5.6. Again the $\cos^2\theta$ behavior does not appear. We have discussed in App. D

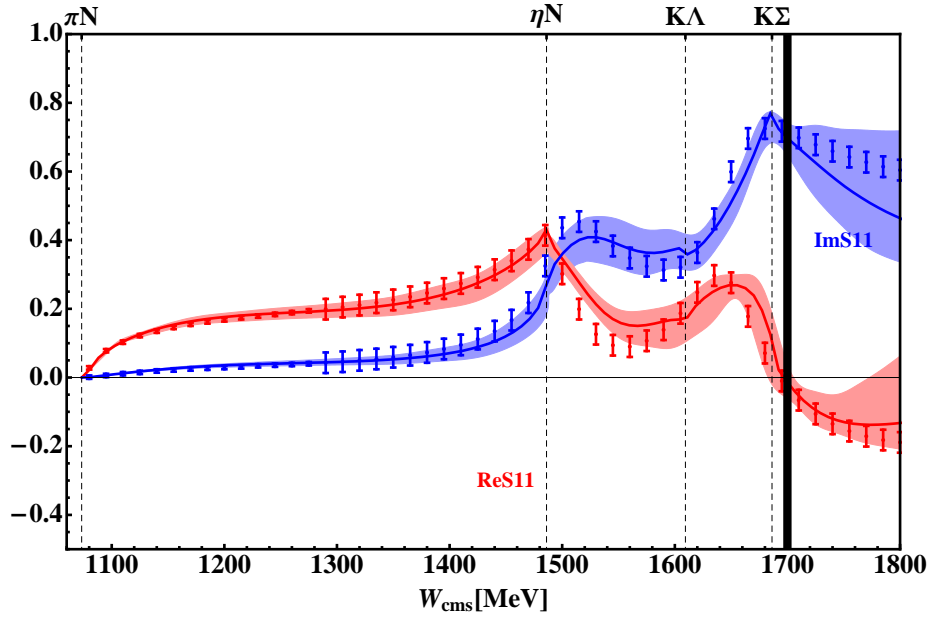


Figure 5.5: Best fit according to fit strategy II to the real and imaginary part of the S_{11} partial wave compared to the WI08 analysis done by the SAID collaboration [108]. The dashed vertical lines correspond to the two particle thresholds and the bold vertical line limits the energy range up to which the fit has been performed. The blue and red bands represent the 1σ uncertainty of our approach as described in the text.

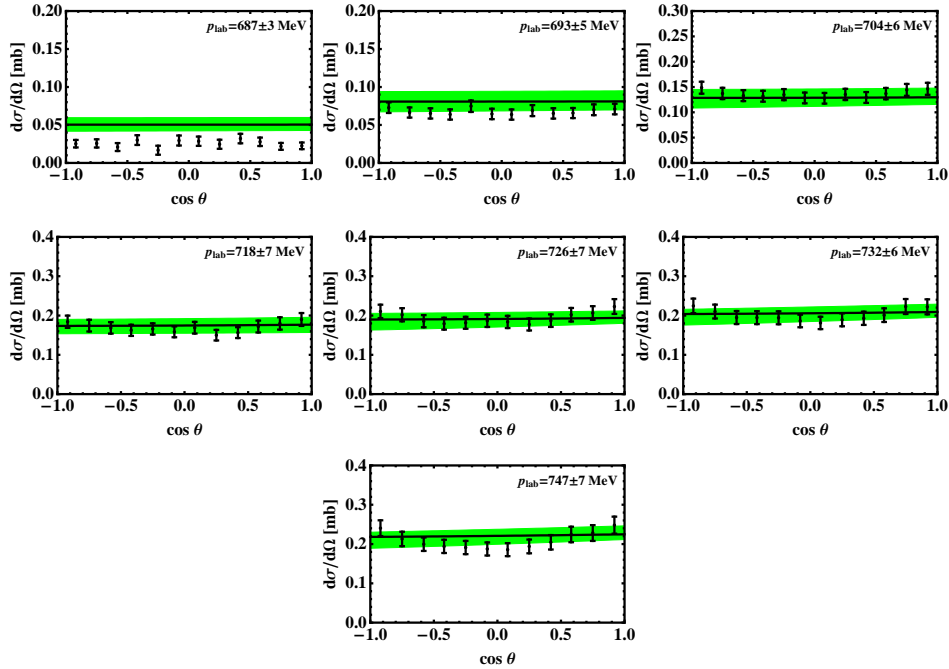


Figure 5.6: Best fit according to fit strategy II to the differential cross sections for $\pi^- p \rightarrow \eta n$ from Ref. [134]. The error bars of experimental data include the systematic error of 6% as argued in Ref. [134]. The green bands represent the 1σ uncertainty of our approach as described in the text.

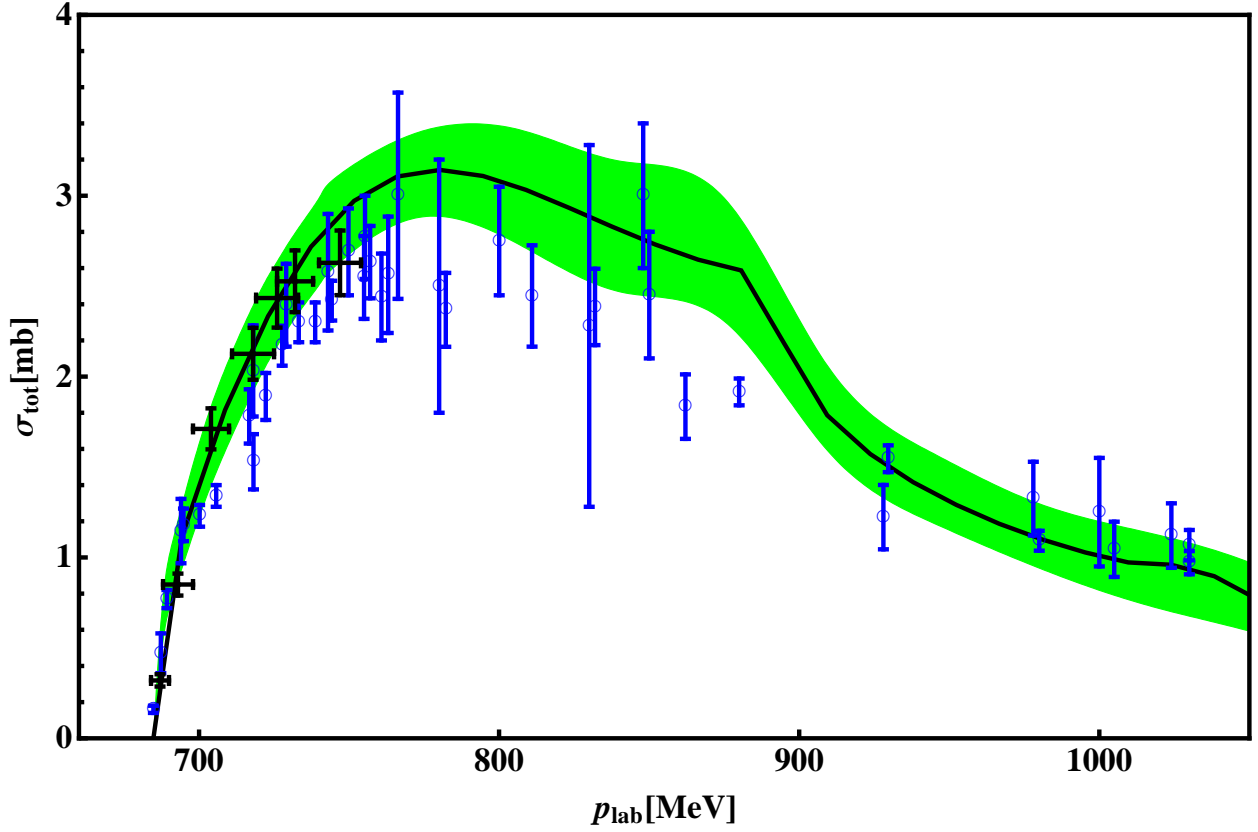


Figure 5.7: Total cross sections of the best fit for $\pi^- p \rightarrow \eta n$ according to fit strategy (II). The model is fixed to reproduce the differential cross section and thus also the total cross section as measured by Prakhov et al. (black symbol). The black curve including the uncertainty band is the outcome of the model. The blue circles correspond to the older measurements as selected by the SAID collaboration which are only presented for completeness.

that in principle such a behavior could be reproduced in our amplitude by means of enhanced contributions from the p-waves, which are iterated in our approach. We conclude from this observation that such a behavior is excluded in this combined πN and ηN fit. In Fig. 5.7 we present the total cross section for the same process beyond the fitting region. In contrast to the previous fit, we observe here a behavior of the resulting cross section $\sigma(p_{\text{lab}})$ much more in line with our earlier analysis⁶. As a matter of fact we do not see any overprediction of the total cross section at the position of the $N^*(1535)$ peak which has been pointed out before, relying on the analysis of [113].

As a further prediction we extract the scattering lengths of the ηN channels, which read

$$\begin{aligned} a_{\eta N \rightarrow \eta N} &= (+0.378^{+0.092}_{-0.101} + i0.201^{+0.043}_{-0.036}) \text{ fm}, \\ a_{\pi^- p \rightarrow \eta n} &= (-0.208^{+0.016}_{-0.017} - i0.138^{+0.025}_{-0.029}) \text{ fm}. \end{aligned} \quad (5.7)$$

⁶That means that no forced shift of the $N^*(1535)$ pole to higher energies emerges from the fits.

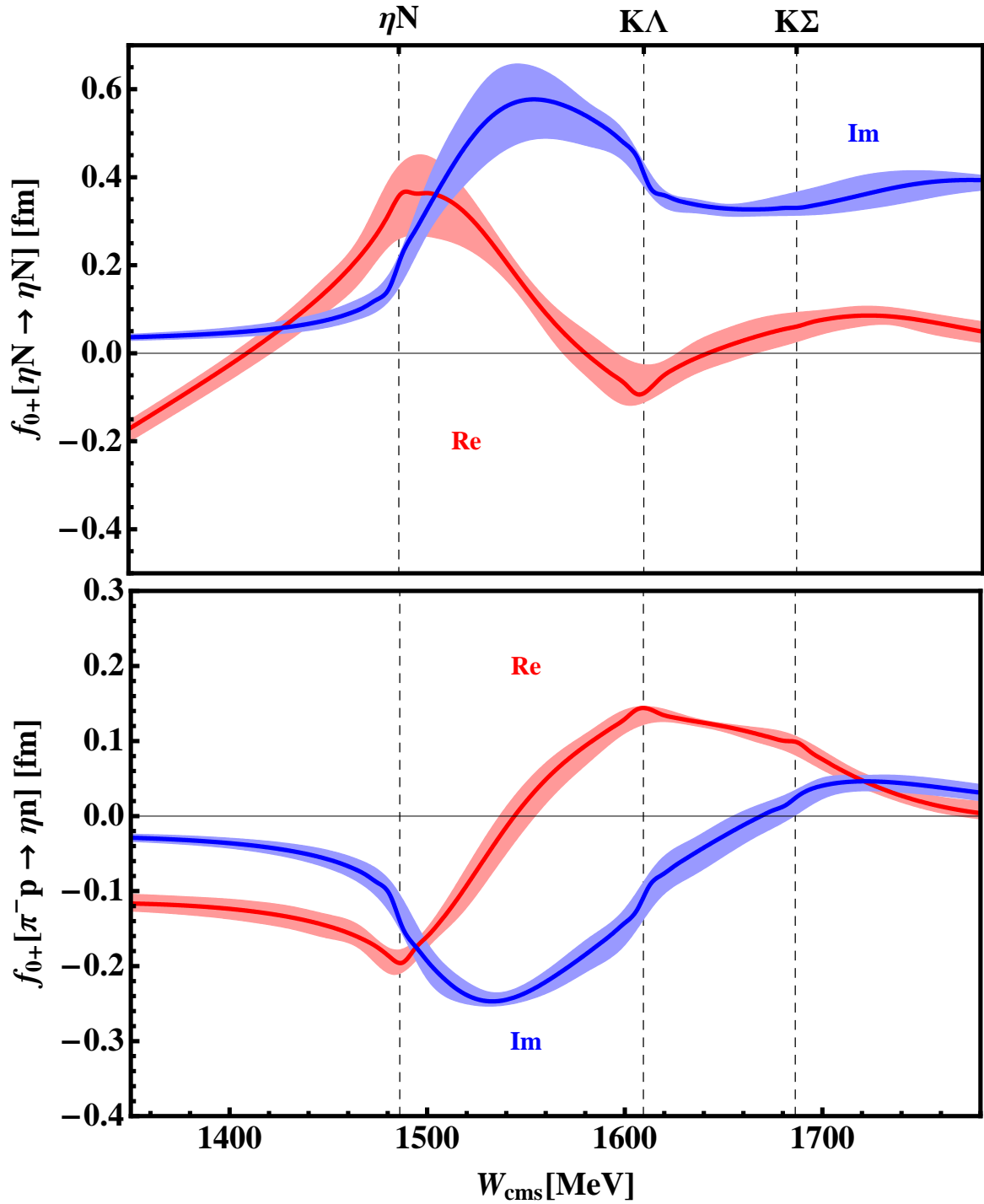


Figure 5.8: The result of the model employing fit strategy (II) for the real and imaginary part of the s-wave scattering amplitude of the ηN (top) and $\pi^- p \rightarrow \eta n$ (bottom) channels. The error bands express the uncertainty due to variation of the model parameters as described in the text.

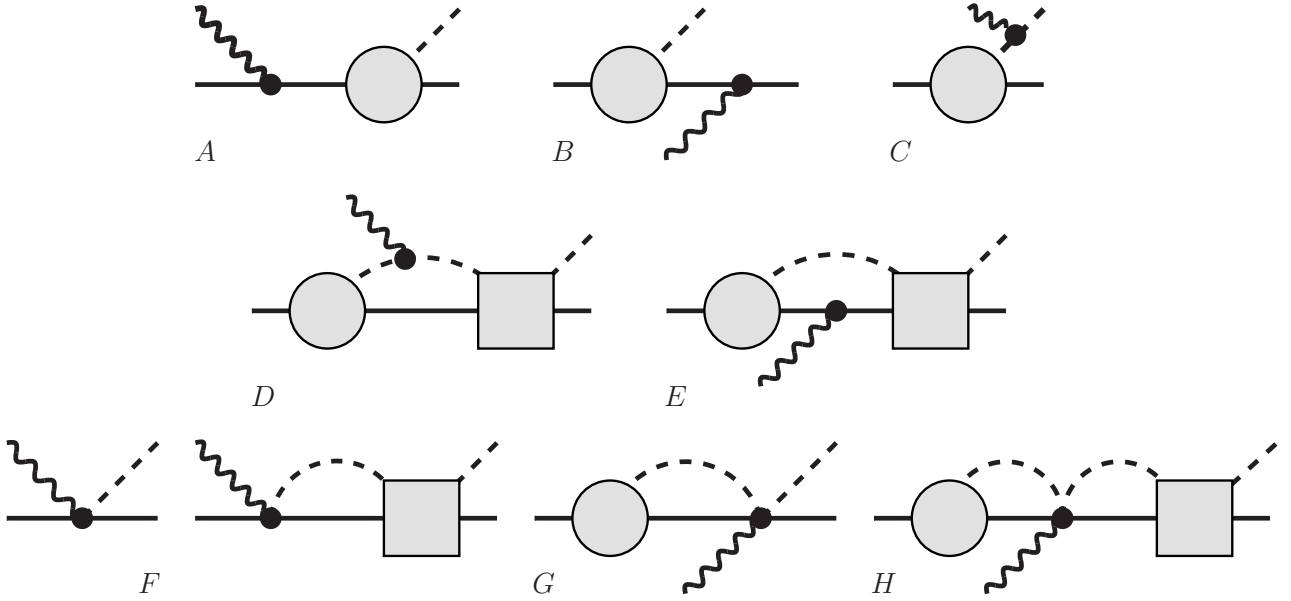


Figure 5.9: Types of diagrams of the turtle approximation. Shaded circles, squares and black dots represent the dressed meson-baryon vertex Γ , scattering amplitude T and the photon vertex as described in the main text.

The observation to be made is that both are consistent with the extraction from other (more phenomenological) approaches [137]. The s-wave amplitude in both channels can be found in Fig. 5.8. For energies lower than the $K\Lambda$ threshold we observe similar behavior as for the amplitudes extracted in fit strategy I, see Fig. 5.4.

5.3 Pion photoproduction off the proton

Pion photo- and electroproduction off protons has been one of the premier objects of study in hadron physics for decades. One of the major issues was [139, 140] and still is the interplay between the hadronic scattering and the photoproduction of mesons off the baryons. It is unquestionable that the meson-baryon interaction plays a crucial role in the photoproduction processes via the rescattering processes. At the production threshold, pion photoproduction can be successfully analysed within strictly perturbative ChPT as has been done to one loop about twenty years ago [141, 142]. Going to higher energies, one is again confronted with the problems already appearing in the hadronic sector as discussed in the previous section, namely, resonance phenomena. Thus a non-perturbative framework is required to implement the rescattering mechanism adequately. In the early years the unitarized hadronic amplitude was simply used as the final state interaction (FSI) multiplied on top of the $\gamma p \rightarrow \pi N$ contact interaction, which in general violates the Ward-Takahashi identities and thus gauge invariance. Recently a framework for pion photoproduction based on the Jülich model was constructed in Ref. [143]. There the hadronic part of the amplitude is also used as the FSI coupled to a special form of contact terms and fulfilling the gauge Ward-Takahashi identities by construction.

Our approach follows a different direction, where gauge invariance is not enforced via *ad hoc* conditions on vertex functions and propagators, but follows most straightforwardly from the selected infinite subset of Feynman graphs which are summed up. The basic ideas can be traced back from Refs. [144–147]. Essentially, one adopts a generalization of the construction of a gauge-invariant amplitude (as spelled out e.g. in sec. (7.4) of Ref. [89]) to the present non-perturbative setting. It was first applied to the analysis of kaon photoproduction, relying on the leading s-wave terms from the three-flavour chiral Lagrangian, in Ref. [106]. There, the selected subset of Feynman graphs was referred to as “turtle approximation”. In principle this is the most natural way of constructing a gauge-invariant photoproduction amplitude as the photon is coupled to any point of the $p \rightarrow \phi B$ amplitude, ensuring current conservation. Nevertheless, it requires as an input the underlying hadronic amplitude with the full off-shell dependence. Such an amplitude was provided in the previous section. It fulfills the two-body unitarity requirement exactly and the parameters are fixed such as to reproduce the s-wave of πN as well as $\pi N \rightarrow \eta N$ scattering. Without any further fitting, we wish to investigate what we can learn about the multipole amplitudes by just plugging in our fixed hadronic amplitude as an effective vertex function.

The outstanding feature of our analysis is the precise analysis of the pion-nucleon scattering amplitudes and the determination of both lowest S_{11} resonances. Obviously the hadronic interaction is a part of a more involved photoproduction amplitude, hence both resonances will certainly appear in the spectrum of the photo-induced meson production. It is, however, a priori not clear whether they will be enhanced or suppressed. To put it in the words of Berends et al. [140] the question we are addressing here is:

“How do these resonances manifest themselves in photopion (and electropion) production?”

There they refer this question among others to the (in that time) novel and not very precise measured resonances $S_{11}(\approx 1500)$ and $S_{11}(\approx 1650)$.

5.3.1 Formalism

Closely following the formalism explained in Ref. [106], the gauge-invariant photoproduction amplitude $\mathcal{M}^\mu(q', k; p)$, is a sum of nine different types of Feynman diagrams, see Fig. 5.9. Here, q' is the four-momentum of the produced meson and p is again the overall four-momentum. The four-momentum of the incoming photon is denoted by k . The scattering amplitude T has been calculated in the previous section, consequently there are only two building blocks left to be clarified, i.e. Γ denoting the dressed meson-baryon vertex and the photon vertices $W_{\gamma\phi\rightarrow\phi}$, $W_{\gamma B\rightarrow B}$, $W_{\gamma B\rightarrow B\phi}$ and $W_{\gamma B\phi\rightarrow B\phi}$.

The exact two-body unitarity is a crucial property of the hadronic amplitude. For this to be preserved in the photoproduction amplitude as well, the axial meson-baryon coupling has to be dressed properly. The tree level axial meson-baryon potential stems from the leading order chiral Lagrangian Eq. (1.13) and reads

$$V_{ax}(q') = A_X \not{q}' \gamma^5, \quad (5.8)$$

where we have separated off the channel space structure, which is specified in App. C. Dressing of this amplitude in the ‘turtle approximation’ [106] is presented in a rather intuitive pictorial

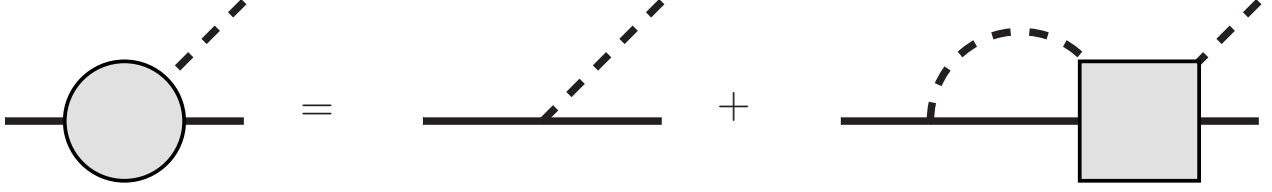


Figure 5.10: Symbolical representation of the dressed meson-baryon amplitude Γ (circle), where the shaded square represents the meson-baryon scattering amplitude T .

way in Fig. 5.10 and reads

$$\Gamma(q', \tilde{p}) = V_{ax}(q') + \int \frac{d^d l}{(2\pi)^d} T(q', l; \tilde{p}) iS(\not{p} - l) \Delta(l) V_{ax}(l) , \quad (5.9)$$

where \tilde{p} denotes the total four-momentum of this process which can take values of the proton momentum or the overall four-momentum of the photoproduction process. The scattering amplitude T consists of 20 different Dirac structures as presented in section 2.3 and gives rise to 6 different structures of the amplitude Γ , i.e.

$$\begin{aligned} \Gamma(q', \tilde{p}) = & \Gamma_1(\tilde{p}) \cdot \not{p} \gamma^5 + \Gamma_2(\tilde{p}) \cdot \gamma^5 + \Gamma_3(\tilde{p}) \cdot q' \not{p} \gamma^5 \\ & + \Gamma_4(\tilde{p}) \cdot q' \gamma^5 + \Gamma_5(\tilde{p}) \cdot \gamma^5 (q' \cdot \tilde{p}) + \Gamma_6(\tilde{p}) \cdot \not{p} \gamma^5 (q' \cdot \tilde{p}) . \end{aligned} \quad (5.10)$$

The coefficients $\Gamma_i(\tilde{p})$ are elementary functions of \tilde{p}^2 , masses, scalar loop integrals, I_M and $I_{MB}(\tilde{p}^2)$, collected in App A, coefficients T_i of the scattering amplitude as well as of the axial coupling constants D and F from Eq. (1.13).

The numerical values of the latter constants should be taken with a grain of salt. Within our approximation the axial coupling enters the photoproduction amplitudes dressed by the meson-baryon loops, for instance the kaon-loops. These effects are known to be quite sizable and thus one has to choose at which level, i.e. on tree level or that of the dressed vertex Γ , one wishes to obtain an agreement with the physical (measured) quantities. It turns out that although the value of Γ depends strongly on the choice of axial couplings, the photoproduction amplitudes calculated with both sets of axial couplings agree with each other within the uncertainty band. For this reason we stick to the commonly used values of $D = 0.8$ and $F = 0.5$.

It remains now to specify how to couple the photon to the hadronic skeleton described above. For consistency reasons we shall consider the photon induced contact terms up to the second chiral order utilizing the first and second order chiral Lagrangian, Eq. (1.13) and Eq. (2.4). Previously we have set all the external currents to zero except the scalar one, whereas here we consider a vector current $v_\mu = -eQ A_\mu$ with the electromagnetic vector potential A_μ and charge matrix $Q = \text{diag}(2/3, -1/3, -1/3)$. A vector current modifies the covariant derivative as well as the chiral vielbein

$$\begin{aligned} [D_\mu, B] = & \partial_\mu B + \frac{1}{2} [([u^\dagger, \partial_\mu u] - i(u^\dagger v_\mu u + u v_\mu u^\dagger)), B] , \\ u_\mu = & iu^\dagger (\partial_\mu U - i[v_\mu, U]) u^\dagger . \end{aligned}$$

A non-vanishing vector potential also features in $\mathcal{L}_{\phi B}^{(2)}$ via the field-strength tensor

$$f_+^{\mu\nu} = u(\partial^\mu v^\nu - \partial^\nu v^\mu)u^\dagger + u^\dagger(\partial^\mu v^\nu - \partial^\nu v^\mu)u .$$

It appears in Eq. (1.13) accompanied by the two LECs b_{12} and b_{13} , which cannot be determined from the scattering process, but are related to the magnetic moments of proton and neutron. As mentioned before we do not wish to perform a fit for the photoproduction observables, therefore we stick to the values determined in Ref. [148] for these two new LECs. Furthermore, the pure mesonic chiral Lagrangian of second chiral order, see Eq. (1.11), gives rise to the photon vertex $W_{\gamma\phi\rightarrow\phi}$. This and the remaining vertices are collected in App. E.

Having specified all building blocks of the graphs collected in Fig. 5.9 we now calculate the photoproduction amplitude $\mathcal{M}^\mu = \sum_{i=A}^H S_i^\mu$, where the amplitudes S_i correspond to a respective class of graphs defined in Fig. 5.9. We wish to emphasize that there are 5 classes which by themselves obey two-body unitarity in the subspace of meson-baryon channels, namely

$$\mathcal{M}^\mu(q', k; p) - \mathcal{M}^\mu(q'k; p)^\dagger = 2i \int \frac{d^d l}{(2\pi)^d} T(q', l; p) \text{Im}(G) \mathcal{M}^\mu(l, k; p) ,$$

where $G = S(\not{p} - \not{l})\Delta(l)$. Each of the unitarity classes is defined via a prescription that an application of the scattering matrix T from right yields an element of the same class. These classes are given by $\mathcal{M}_A^\mu, \mathcal{M}_B^\mu + \mathcal{M}_E^\mu, \mathcal{M}_C^\mu + \mathcal{M}_D^\mu, \mathcal{M}_F^\mu, \mathcal{M}_G^\mu + \mathcal{M}_H^\mu$, where the subscript denotes the topology class as denoted in the Fig 5.9. Gauge invariance is fulfilled for the amplitudes proportional to b_{12} and b_{13} automatically. On the other hand for the remaining terms it is only fulfilled if all graphs presented in Fig. 5.9 are taken into account, i.e. the photon is coupled to every possible part of the hadronic skeleton.

5.3.2 Results

In this section we present the prediction of our model for both sets of scattering amplitudes fixed in the hadronic sector in the last section. There, in both strategies, we have been concentrating on the description of the s-wave, thus we shall stick to the prediction of the quantities connected to this particular partial wave. Such a quantity is the electric multipole E_{0+} , which can be expressed in terms of the Chew, Goldberger, Low and Nambu (CGLN) amplitudes as presented in App. F.

After having fixed the hadronic part of this amplitude, the photoproduction amplitude contains only 4 new parameters, namely D, F, b_{12} and b_{13} . The first two are fixed to the commonly used values of $D = 0.8$ and $F = 0.5$. The 'magnetic' LECs b_{12} and b_{13} shall be taken from Ref. [148], where they have been adjusted to fit the experimental data on magnetic moments. Within the uncertainty due to the choice of m_0 there, these LECs are given by (in units of GeV^{-1})

$$b_{13} = 0.32 \pm 0.06 \quad \text{and} \quad b_{12} = 0.095 \pm 0.015.$$

In order to give an impression of the uncertainty we proceed as follows. First for a fixed energy W_{cms} and for each hadronic solution which lies in the uncertainty band of the hadronic solution as presented in the last section we calculate the photoproduction multipoles as functions of

the 4 new LECs. Then for fixed D and F and a large set of randomly distributed values for b_{12} and b_{13} within the uncertainty range on these two LECs we obtain a prediction on the photoproduction multipoles at the chosen energy. Repeating this procedure for different energy values we obtain a family of curves $E_{0+}(W_{\text{cms}})$. The envelope of all these curves is assumed to reflect the uncertainty of the model properly.

Solution I: As a central prediction of this chapter we present the outcome of the multipole E_{0+} for pion photoproduction in the isospin 1/2 channel in Fig. 5.11. We restrict ourselves to energies below the second nucleonic resonance as its position seems to be shifted as discussed in the last section. Without any fitting we observe an astonishing agreement of our prediction with the outcome of the fit from MAID2007 (updated unitary isobar model) [149] and the one by the SAID group [150]. Of course it is clear that, if none but πN channels are open, Watson's theorem guarantees that the phase of E_{0+} comes out right, once the phase of πN scattering has been fixed to the physical value. This theorem, however, does not fix the magnitude of the real and imaginary part of the photoproduction amplitude, neither it is clear how to apply it above the ηN threshold.

The value of E_{0+} at the threshold has been debated for a long time, see [25] for a nice review on that topic. We obtain the following value

$$E_{0+}^{\pi}(S_{11}) = (+10.4 \pm 1.3) \times 10^{-3}/M_{\pi^+} ,$$

which has to be compared with $E_{0+}(S_{11}) = (+12.5 \pm 0.3) \times 10^{-3}/M_{\pi^+}$ from experimental results [153–155]. Seemingly our prediction is slightly below the experimental result. Throughout this work we have not discussed the isospin 3/2 channel and refrain from giving a numerical value of E_{0+} . For completeness, let us note that in all solutions we observe that the absolute value of the $E_{0+}(S_{31})$ is underestimated significantly. We trace that discrepancy to the missing Born graphs which are known to be important in this channel.

We can go further and make a prediction on the multipole amplitude for eta photoproduction. At the ηN threshold we extract the following value

$$E_{0+}^{\eta} = \left((3.9 \pm 2.5) + i(10.7 \pm 2.7) \right) \times 10^{-3}/M_{\pi^+} .$$

The energy-dependence of $E_{0+}(W_{\text{cms}})$ is presented in Fig. 5.12, where it is compared with fits by the ETAMAID [151] and Bonn-Gatchina [152] groups. Seemingly there is a large qualitative agreement between our prediction and the phenomenological analysis by the ETAMAID and Bonn-Gatchina group. On a quantitative level we observe that the real part of the E_{0+} is suppressed compared to the outcome of the phenomenological analysis. We wish to remind the reader that the 'magnetic' LECs are taken from a tree level calculation only. In some additional fits we have observed that the results of ETAMAID and Bonn-Gatchina group can be reproduced nicely in our approach using these LECs as free parameters. This, however, is not the original purpose of this work, namely the parameter free prediction of the photoproduction after fixing the hadronic scattering.

Solution II: Starting from the second hadronic solution we obtain a prediction for pion photoproduction in the S_{11} channel as presented in Fig. 5.13. Although all parameters of the model are fixed in the hadronic solution or taken from the literature as described above one observes

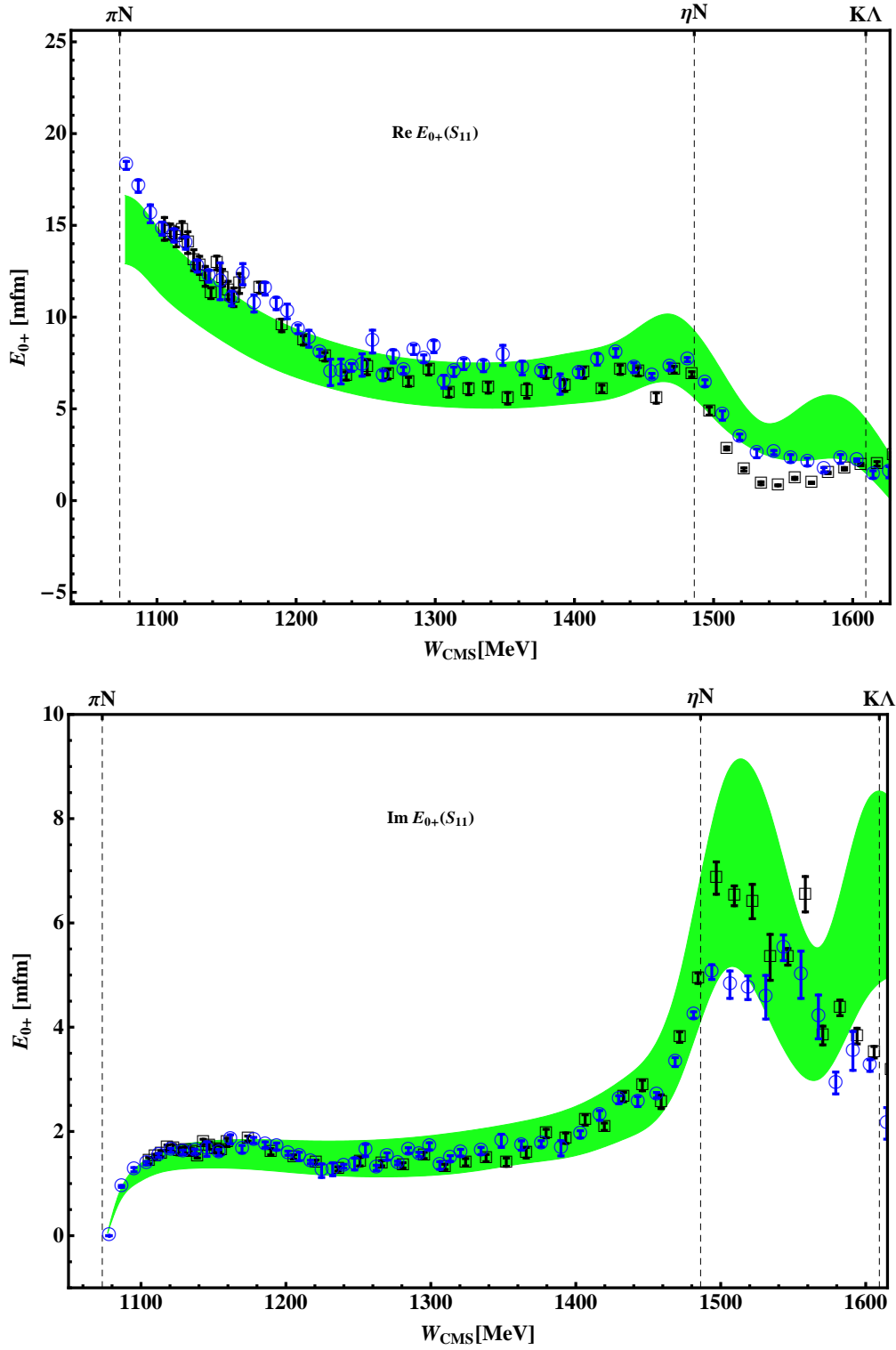


Figure 5.11: Prediction for the multipole E_{0+} for pion photoproduction corresponding to the hadronic solution I. For comparison, fits of the MAID (circles) [149] and SAID (squares) [150] models are represented by blue and black symbols, respectively.

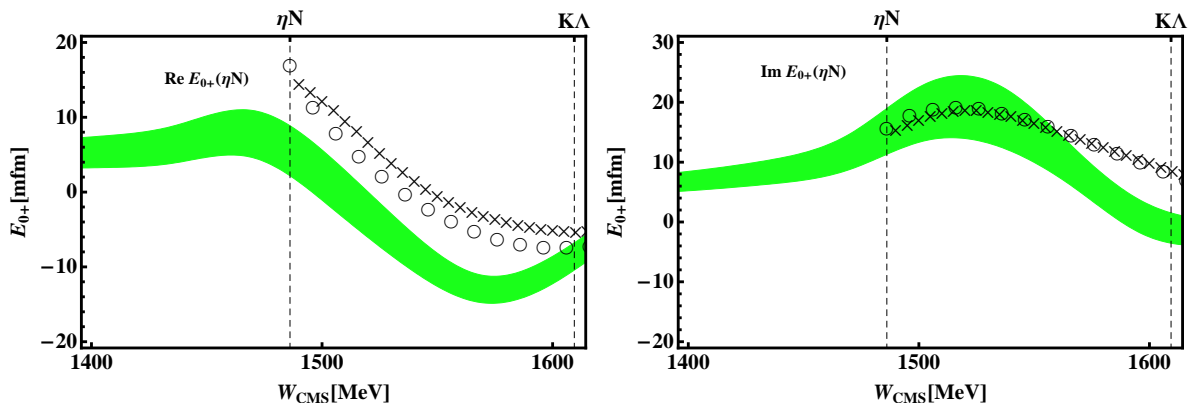


Figure 5.12: E_{0+} for eta photoproduction as predicted based on hadronic solution I. For comparison, we also present the results of the ETAMAID (circles) [151] and Bonn-Gatchina (crosses) [152] analyses.

a fair qualitative agreement of our prediction with the outcome of the SAID and MAID2007 analysis in a very large energy region. At the threshold we extract the following values for the lowest multipole

$$E_{0+}^{\pi}(S_{11}) = (+13.1 \pm 0.7) \times 10^{-3}/M_{\pi^+} ,$$

which agrees nicely with the extraction from the experimental results in Ref. [153–155]. For higher energies, i.e. around 1200 MeV and 1550 MeV, we observe a discrepancy of E_{0+} compared to the fits by SAID and MAID groups. Additionally the uncertainty band appears quite underestimated in this solution. We wish to remind the reader that the main difference of both solutions are the three regularization scales. In the first solution those are used as free fit parameters whereas in the second they are fixed. The particular choice of these values is motivated as described in the previous section, however, one should in principle investigate the influence of this choice on the hadronic solution as well as on the photoproduction amplitudes. To do so one would have to refit the hadronic scattering for any other choice of the parameters in the solution II. Due to an enormous amount of computational time required for each fit, we refrain from including that uncertainty. One should keep in mind that a more realistic uncertainty band might be larger than the one presented here.

To be complete we wish to comment now on the higher energy region, i.e. above the $K\Lambda$ threshold, where the outcome of our prediction starts to deviate from the results of the SAID and MAID groups. In fact this observation is identical to the one made in the analysis of the photoproduction amplitudes in Ref. [138], where no good overall fit could be achieved for the E_{0+} in the low and resonance energy region simultaneously. Although no fit to the photoproduction data was done in the present work, four new parameters are entering the calculation. The axial coupling as well as the 'magnetic' LECs b_{12} and b_{13} are taken from estimations which rely on a strict perturbative calculation. Our non-perturbative framework is on the other hand suited to extend the range of applicability of the effective field theory. Thus it is a priori not clear whether it is sufficient to use these new LECs in the whole energy range. To underline this we fit our model to the SAID pion photoproduction data with axial coupling

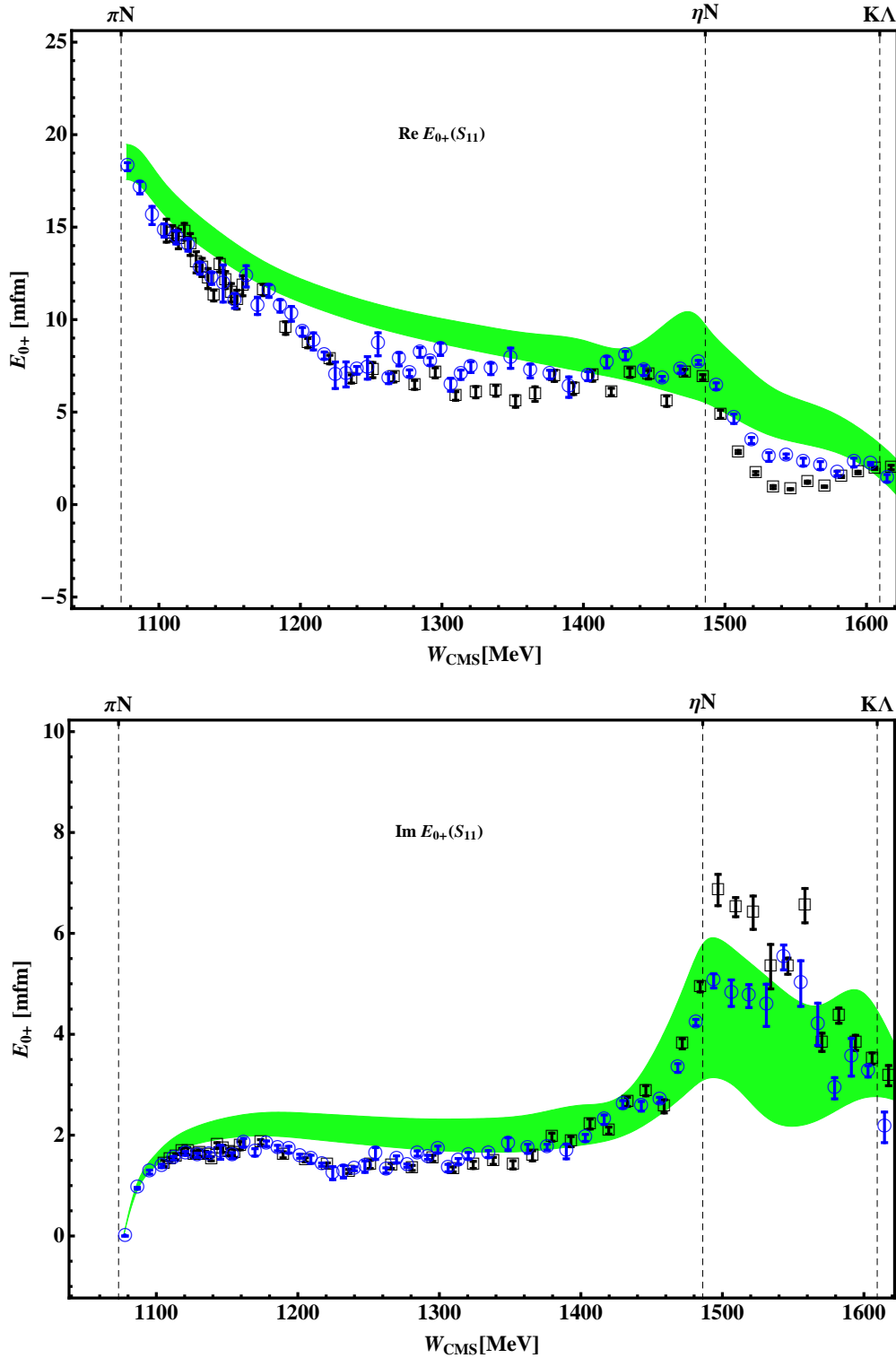


Figure 5.13: Prediction for the multipole E_{0+} for the pion photoproduction corresponding to the hadronic solution II. For comparison, fits of the MAID (circles) [149] and SAID (squares) [150] models are represented by blue and black points with errorbars, respectively.

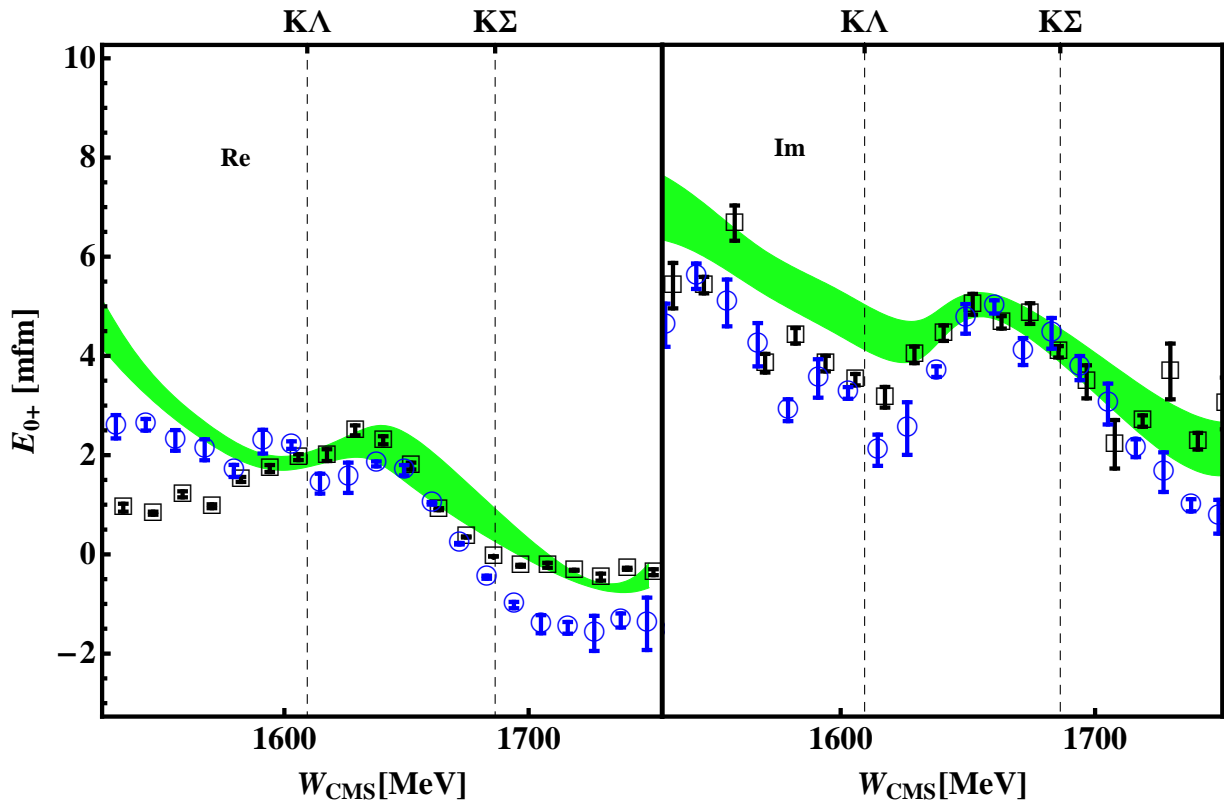


Figure 5.14: A typical fit of our model to the SAID [150] (blue) and MAID [149] (black) analysis for the pion photoproduction as described in the text.

and 'magnetic' LECs treated as free parameters. The best fit is presented in Fig. 5.14, where we observe a nice agreement above the $K\Lambda$ threshold with the phenomenological models from SAID and MAID.

For the eta photoproduction the prediction of the second solution is presented in Fig. 5.15. At the ηN threshold we obtain the following value

$$E_{0+}^{\eta} = \left((-1.2 \pm 2.2) + i(6.9 \pm 2.3) \right) \times 10^{-3} / M_{\pi^+} ,$$

which undershoots the numerical value obtained in the previous solution for the real part slightly and agrees for the imaginary part within the uncertainty range. The functional behavior of E_{0+} is suppressed compared to the previous solution and even more in comparison to the ETAMAID and Bonn-Gatchina fits. As already discussed in the previous solution we can trace this discrepancy to the 'magnetic' LECs, which are taken from the tree level calculation [148]. These LECs do not change the functional form of the photoproduction amplitude but seem to enhance or suppress the structures present in the photoproduction amplitude. Those structures on the other hand seem to reflect one-to-one the structures arising from the dynamics of the hadronic scattering process. Thus the correct description of meson photoproduction is necessarily to be connected to a proper description of the underlying hadronic scattering reactions.

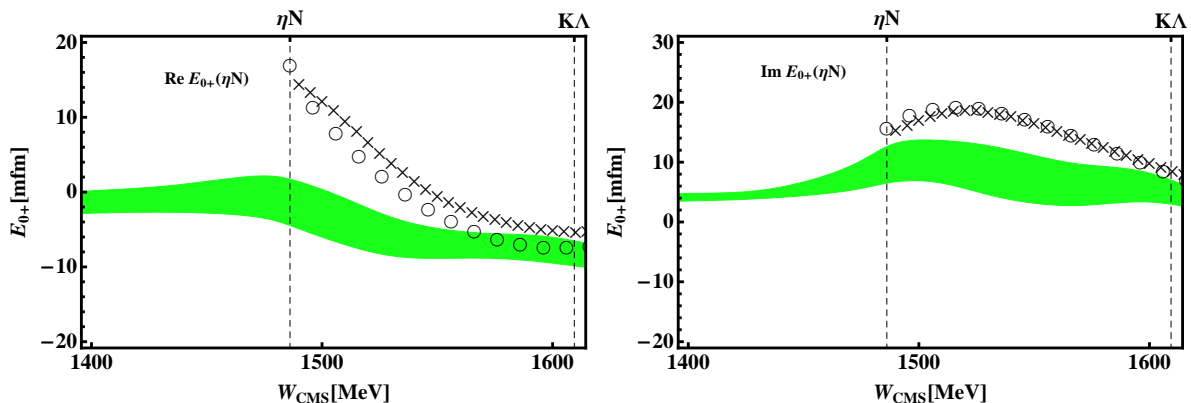


Figure 5.15: E_{0+} for eta photoproduction as predicted starting from the hadronic solution II. For comparison we also present the outcome of the ETAMAID (circles) [151] and Bonn-Gatchina (crosses) [152] analysis.

5.4 Summary and outlook

As the first step, we have considered the meson-baryon scattering processes that are relevant for pion photoproduction. We consider six coupled channels, utilizing the chiral effective Lagrangian at NLO. In the kernel of the underlying Bethe-Salpeter equation, we include all local terms allowed by the symmetries. To pin down the parameters of the approach (low-energy and subtraction constants), we perform two fit strategies. In strategy (I), we use as input the data on elastic πN scattering in the S_{11} and S_{31} partial waves for energies in the range $(m_p + M_\pi) < W_{\text{cms}} < 1.56$ GeV. In strategy (II), three subtraction constants are fixed and the S_{11} partial wave is fitted up to $W_{\text{cms}} < 1.70$ GeV, but the S_{31} only in the near-threshold region, $W_{\text{cms}} < 1.20$ GeV. The data on $\pi^- p \rightarrow \eta n$ from Ref. [134] are included in both fit strategies.

In both fit strategies, the S_{11} partial wave and the data on $\pi^- p \rightarrow \eta n$ are well described. The $N^*(1535)$ and the $N^*(1650)$ are both dynamically generated, the precise pole positions depend on the fit strategy, cf. Eqs. (5.3,5.6). We also give predictions for the scattering lengths $a_{\eta N \rightarrow \eta N}$ and $a_{\pi^- p \rightarrow \eta n}$. Having scrutinized the hadronic sector, we have extended our approach to s-wave pion photoproduction. The only new parameters can be determined from the nucleon magnetic moments and thus parameter-free predictions emerge. We find a good description of the s-wave multipole E_{0+} for pion photoproduction in the S_{11} -wave and also for eta photoproduction.

Having summarized the most important results of our study, it is important to briefly discuss possible improvements of the method. First, the crossed channel dynamics has to be included properly. This will allow e.g. to get a better description of the near-threshold region in pion-nucleon scattering. Unfortunately, the exact implementation of both crossing symmetry and unitarity has not been possible so far in approaches based on Feynman diagrams, in contrast to other approaches as e.g. the one based on Roy-Steiner equations [72] where these constraints are met by construction. For an attempt to approximately restore crossing symmetry in an ansatz comparable to the one employed here, see e.g. Ref. [156]. Further, in some channels, explicit resonance degrees of freedom will have to be incorporated as not all resonances are

generated dynamically. For a method to do that, see e.g. Ref. [78]. Finally, a larger data base including also kaon-nucleon scattering and kaon photoproduction should be considered simultaneously with the processes studied here.

Chapter 6

Outlook

At the end of each chapter we have summarized the results presented there. Hence we refrain from repeating the summaries of each chapter, but wish to take the opportunity to present possible ways in which this work can be developed further.

The analysis in chapters 3 and 4 has shown that our model, described and developed in the first two chapters, can address the hadronic scattering, both for the πN as well as $\bar{K} N$ systems, correctly in a fairly large energy region. Nevertheless, our framework is suited for separable potentials only and lacks two important contributions from the s - and especially u -channel baryon exchange graphs as explained in detail in section 2.1. Hence, from the theoretical point of view, a proper treatment of these contributions in our non-perturbative framework should be the next major step towards a more comprehensive description of the hadronic scattering. Also in view of photoproduction this will presumably allow for a simultaneous description of both lowest multipoles $E_{0+}(S_{11})$ and $E_{0+}(S_{31})$, where the latter could not be described properly in our framework. In the context of Bethe-Salpeter equations, there is presumably only one way to undertake this improvement, namely to perform an appropriate expansion of the Born graphs in some small variable which has to be chosen very carefully. In a (small) region around the expansion point this may allow to account for the dynamics of these graphs properly. Without such an expansion, one probably has to modify the resummation routine. At present, we can only speculate how this modification might look like - some interesting steps have been done utilizing the so-called Feynman-Schwinger representation, see Ref. [93].

Meson-baryon scattering: The field of lattice QCD is evolving very rapidly and in the near future more information on the resonance spectrum might become available. At sufficiently low quark mass such resonances decay on the lattice and the phase shift can be extracted from the energy levels and their dependence on the size of the lattice via Lüscher's formalism [157]. Going to higher energies more channels can be open, the effects of which must be parametrized by some model such as e.g. the coupled-channel Bethe-Salpeter approach, presented in this thesis. Having the solution of this approach on hand one can use the scheme proposed in Ref. [158] to predict the outcome of a lattice simulation or extract the infinite volume limit.

Pion photoproduction: One quite ambitious project which can and should be attacked in the next future is the inclusion of the data on pion- and photon-induced kaon production into

the set of observables in addition to the pion production data. The main modification to be done in the hadronic part is that one cannot stick to the s-wave analysis only, as one has to fix the (differential) cross sections in the $\pi^-p \rightarrow K^0\Lambda$, $\pi^-p \rightarrow K^0\Sigma^0$, $\pi^-p \rightarrow K^+\Sigma^-$ and $\pi^+p \rightarrow K^+\Sigma^+$ channels at quite high energies. Hence, to meet the theoretical standards one has first to fix at least the description of the p-waves which will certainly play a significant role at such high energies. At present, a full inclusion of the p-waves is lacking, that would feature the very prominent resonances $\Delta(1232)P_{33}$ and $\text{Roper}(1440)P_{11}$ which cannot be generated in our approach. In our opinion, the proper inclusion of these resonances and better description of the p-waves is the next issue to be solved before a simultaneous analysis of pion-nucleon scattering and kaon pion-induced production data can be done.

Antikaon-nucleon scattering: The $\bar{K}N$ scattering amplitude was believed to be fixed in the subthreshold region by the very precise data on energy shift and width of the kaonic hydrogen from the SIDDHARTA experiment at DAΦNE as well as by the older measurements on total cross sections for the processes $\bar{K}N \rightarrow \bar{K}N$ and $\bar{K}N \rightarrow \pi\Sigma$. We have shown that we can reproduce the same data very precisely, predicting, however, a different subthreshold behaviour of the scattering amplitudes than usually expected. Also the prediction of our model on the invariant mass distribution of the $\pi\Sigma$ system is not in contradiction with the rather old experimental data. Recently, preliminary results on the process $\gamma p \rightarrow (K^+)\pi\Sigma$ were reported by the CLAS collaboration at Jefferson Lab, see Ref. [159]. Not only that the theoretical analysis of these data requires a full machinery of unitarized ChPT it also has to be built in a larger framework of photoproduction. As a matter of fact, the gauge invariant framework for meson photoproduction presented in this thesis will be (modulo some modifications) a perfect tool for analysis of the upcoming $\pi\Sigma$ photoproduction data.

Appendix A

Loop integrals

Here we collect all loop integrals required for the calculation of the scattering as well as the photoproduction amplitudes. Note that for reasons given in the main part all purely baryonic integrals are set to zero from the beginning. Utilizing dimensional regularization in the \overline{MS} scheme the renormalized one-meson integral is given by

$$I_M(M) := \int_{\overline{MS}} \frac{d^d l}{(2\pi)^d} \frac{i}{l^2 - M^2 + i\epsilon} \stackrel{d=4}{=} \frac{2M^2}{16\pi^2} \log\left(\frac{M}{\mu}\right),$$

where μ is the regularization scale and M denotes the meson mass. We use in the following the common abbreviation $\lambda(a, b, c) = a^2 + b^2 + c^2 - 2ab - 2ac - 2bc$, such that the meson-baryon (of masses M and m , respectively) integral reads

$$I_{MB}(s, m, M) := \int_{\overline{MS}} \frac{d^d l}{(2\pi)^d} \frac{1}{l^2 - M^2 + i\epsilon} \frac{i}{(l-p)^2 - m^2 + i\epsilon} \\ \stackrel{d=4}{=} \frac{1}{16\pi^2} \left[-1 + 2 \log\left(\frac{m}{\mu}\right) + \frac{M^2 - m^2 + s}{s} \log\left(\frac{M}{m}\right) - 2 \frac{\sqrt{\lambda(s, m^2, M^2)}}{s} \operatorname{arctanh}\left(\frac{\sqrt{\lambda(s, m^2, M^2)}}{(m+M)^2 - s}\right) \right].$$

The photoproduction amplitude involves further loop integrals. The triangle graph of class ‘‘D’’ in the Fig. 5.9 gives rise to a meson-meson-baryon as well as via the Passarino-Veltman reduction to a meson-meson loop integral at $s = k^2$, which read

$$I_{MM}(k^2, M) := \int_{\overline{MS}} \frac{d^d l}{(2\pi)^d} \frac{1}{l^2 - M^2 + i\epsilon} \frac{i}{(l-k)^2 - M^2 + i\epsilon} \\ \stackrel{d=4}{=} \frac{1}{16\pi^2} \left[-2 + 2 \log\left(\frac{M}{\mu}\right) - 2 \frac{\sqrt{\lambda(s, M^2, M^2)}}{s} \operatorname{arctanh}\left(\frac{\sqrt{\lambda(s, M^2, M^2)}}{4M^2 - s}\right) \right], \\ I_{MMB}(s, k^2, m, M) := \int_{\overline{MS}} \frac{d^d l}{(2\pi)^d} \frac{1}{l^2 - M^2 + i\epsilon} \frac{1}{(l-k)^2 - M^2 + i\epsilon} \frac{i}{(l-k-p_1)^2 - m^2 + i\epsilon},$$

where $p_1 = p - k$ is the four-momentum of the incoming proton. We wish to emphasize that the photon coupled to a meson propagator does not induce a transition of this meson. Differently, coupled to a baryon propagator it can induce the $\Sigma^0 \leftrightarrow \Lambda$ transition. Thus a meson-baryon-baryon loop integral required for the calculation of Feynman diagrams of class ‘‘E’’ reads in general

$$I_{M\overline{B}B}(s, k^2, M, m_1, m_2) := \int \frac{d^d l}{(2\pi)^d} \frac{1}{l^2 - M^2 + i\epsilon} \frac{i}{(l - p_1)^2 - m_1^2 + i\epsilon} \frac{i}{(l - k - p_1)^2 - m_2^2 + i\epsilon} .$$

Both last integrals cannot be written in terms of elementary functions. We evaluate both integrals utilizing Cutkosky rules to calculate the imaginary part of the meson-baryon-baryon integral. A non-subtracted dispersion relation then gives the real part of the loop integral as follows,

$$\begin{aligned} \text{Im}(I_{M\overline{B}B}(s, k^2, M, m_1, m_2)) &= \frac{1}{32\pi k_{\text{cms}} \sqrt{s}} \log \left(\frac{m_1^2 - m_2^2 + k^2 - 2k_0 q_0 - 2q_{\text{cms}} k_{\text{cms}}}{m_1^2 - m_2^2 + k^2 - 2k_0 q_0 + 2q_{\text{cms}} k_{\text{cms}}} \right) , \\ \text{Re}(I_{M\overline{B}B}(s, k^2, M, m_1, m_2)) &= \frac{1}{\pi} \int_{(m_2+M)^2}^{\infty} ds' \frac{\text{Im}(I_{M\overline{B}B}(s', k^2, M, m_1, m_2))}{s' - s} , \end{aligned}$$

where $k_{\text{cms}} = \sqrt{\lambda(s, p_1^2, k^2)}/(2\sqrt{s})$, $q_{\text{cms}} = \sqrt{\lambda(s, m_1^2, M^2)}/(2\sqrt{s})$ and $k_0 = \sqrt{k_{\text{cms}}^2 + k^2}$, $q_0 = \sqrt{q_{\text{cms}}^2 + M^2}$. The same holds for $I_{M\overline{M}B}$, where in the last formulas one has to replace: $m_1 \rightarrow M$ and $m_2 \rightarrow m$.

Appendix B

Reduction of the loop integrals

The solution of the Bethe-Salpeter equation is deduced in chapter 2. As described there, it relies on the separation of the scattering amplitude into invariant Dirac-momentum structures, collected there in the vector \aleph , which is allowed as long as the interaction potential is separable. After this separation, one is left with various tensor loop integrals, which can be reduced to a sum of scalar loop integrals only via the so-called Passarino-Veltman reduction procedure. In this section we collect all necessary reduction formulas required in the main text of this thesis.

Throughout this section we neglect the $i\epsilon$ prescription for brevity and start with the one-meson-one-baryon tensor loop integral of the following form

$$I_{MB}^\mu := i \int \frac{d^d l}{(2\pi)^d} \frac{l^\mu}{(l^2 - M^2)((l - p)^2 - m^2)} = p^\mu I_{MB}^{(1)}(p^2, m, M) ,$$

where the last equality is due to Lorentz invariance. The unknown function $I_{MB}^{(1)}(p^2, m, M)$ can be deduced contracting the above equation with p_μ which yields

$$I_{MB}^{(1)}(p^2, m, M) = \frac{1}{2p^2} \left(I_B(m) - I_M(M) + I_{MB}(p^2, m, M)(p^2 + M^2 - m^2) \right) .$$

Here the loop integration is expressed in terms of scalar loop integrals I_B , I_M and I_{MB} , which are given in App. A. Please note that we do not address the issue of regularization in this section. Thus neither d is set equal to 4, nor the purely baryonic loop integrals are neglected. The latter are defined in the same way as those containing mesons, replacing the masses adequately. The second tensor loop integral, required for the solution of the BSE, is the following

$$\begin{aligned} I_{MB}^{\mu\nu} &:= i \int \frac{d^d l}{(2\pi)^d} \frac{l^\mu l^\nu}{(l^2 - M^2)((l - p)^2 - m^2)} \\ &= p^\mu p^\nu I_{MB}^{(2)}(p^2, m, M) + g^{\mu\nu} I_{MB}^{(3)}(p^2, m, M) . \end{aligned}$$

Contracting both sides of this equation with $g_{\mu\nu}$ and $p_\mu p_\nu$, one obtains a system of two equations which has the following solution

$$I_{MB}^{(2)}(p^2, m, M) = \frac{d}{4(d-1)p^4} \left(I_M(M)(m^2 - M^2 - p^2) + I_B(m)(d(M^2 - m^2) + (3d-4)p^2) \right)$$

$$\begin{aligned}
& + I_{MB}(p^2, m, M)(d(m^2 - M^2)^2 + dp^4 - 2(dm^2 - dM^2 + 2M^2)p^2) \Big) , \\
I_{MB}^{(3)}(p^2, m, M) = & \frac{1}{4(d-1)p^2} \left(I_B(m)(m^2 - M^2 + p^2) + I_M(M)(-m^2 + M^2 + p^2) \right. \\
& \left. - I_{MB}(p^2, m, M)((m^2 - M^2)^2 + p^4 - 2(m^2 + M^2)p^2) \right) .
\end{aligned}$$

Finally, dealing with the NLO contact terms in the driving term of the Bethe-Salpeter equation we have to carry out the tensor loop integrals of the following form

$$I_{MB}^{\mu\nu\sigma} := i \int \frac{d^d l}{(2\pi)^d} \frac{l^\mu l^\nu l^\sigma}{(l^2 - M^2)((l-p)^2 - m^2)} ,$$

which can only possess four tensor structures build from the four-momentum p and metric tensor, i.e. $p^\mu p^\nu p^\sigma$, $p^\mu g^{\nu\sigma}$, $p^\nu g^{\sigma\mu}$ and $p^\sigma g^{\mu\nu}$. However, only symmetric combinations in $\mu \leftrightarrow \nu \leftrightarrow \sigma$ can appear and consequently

$$I_{MB}^{\mu\nu\sigma} = (p^\mu g^{\nu\sigma} + p^\nu g^{\sigma\mu} + p^\sigma g^{\mu\nu}) I_{MB}^{(4)}(p^2, m, M) + p^\mu p^\nu p^\sigma I_{MB}^{(5)}(p^2, m, M) ,$$

which again can be expressed in terms of the usual scalar loop integrals contracting both sides with the above tensor structures as follows

$$\begin{aligned}
I_{MB}^{(4)}(p^2, m, M) = & \frac{1}{8(d-1)dp^4} \left(I_B(m)(4(d-1)p^2 m^2 - d(m^2 - M^2)^2 + dp^4) \right. \\
& + I_M(M)(d(m^2 - M^2)^2 + p^2(4M^2 - 2d(m^2 + M^2) + dp^2)) \\
& \left. + dI_{MB}(p^2, m, M)((m-M)^2 - p^2)(m^2 - M^2 - p^2)((m+M)^2 - p^2) \right) , \\
I_{MB}^{(5)}(p^2, m, M) = & \frac{1}{8(1-d)dp^6} \left(-I_B(m)(d(d+2)(m^2 - M^2)^2 + d(7d-10)p^4) \right. \\
& - 4(d-1)((d+2)m^2 - dM^2)p^2 + I_M(M)(d(d+2)(m^2 - M^2)^2 \\
& + p^2(-2d(d+2)m^2 + 2((d-2)d+4)M^2 + d(d+2)p^2)) \\
& + dI_{MB}(p^2, m, M)(m^2 - M^2 - p^2)((d+2)(m^2 - M^2)^2 \\
& \left. + p^2(-2(d+2)m^2 + 2(d-4)M^2 + (d+2)p^2)) \right) .
\end{aligned}$$

The photoproduction amplitude contains also the loop integrals with three intermediate particles, see graphs ‘‘D’’ and ‘‘E’’ in Fig. 5.9. All required scalar loop integrals of this form¹, i.e. I_{MBB} and I_{MMB} , are collected in App. A and the tensor structures can be reduced utilizing Passarino-Veltman procedure. In the simplest case we are confronted with the following integral

$$I_{MBB}^\mu := i \int \frac{d^d l}{(2\pi)^d} \frac{l^\mu}{(l^2 - M^2)((l-p)^2 - m_1^2)((l-p_1)^2 - m_2^2)} ,$$

where p_1 and k is the four-momentum of the incoming proton and photon, respectively. There are two possibilities to build a tensor of rank one, namely $I_{MBB}^\mu = p^\mu I_{MBB}^{(1)} + p_1^\mu I_{MBB}^{(2)}$. The coefficients of these tensor structures can be deduced as explained above, which yields

$$I_{MBB}^{(1)} = \frac{2}{A} \left(I_{MBB}((p_1 \cdot k)(p^2 - M^2) + m_2^2(p \cdot p_1) - m_1 p_1^2) \right)$$

¹We suppress the arguments of these loop integrals for brevity, cf. $I_{MBB} = I_{MBB}(p^2, k^2, M, m_1, m_2)$.

$$\begin{aligned}
& + I_{MB}(p^2, M^2, m_1^2)(p \cdot p_1) + I_{MB}(p_1^2, M^2, m_2^2)p_1^2 + I_{BB}(k^2, m_1^2, m_2^2)(k \cdot p_1) \Big) , \\
I_{M_{BB}}^{(2)} = & \frac{2}{A} \Big(I_{M_{BB}}((p \cdot k)(p^2 - M^2) + m_2^2 p^2 - m_1^2(p \cdot p_1)) \\
& + I_{MB}(p^2, M^2, m_1^2)p^2 - I_{BB}(k^2, m_1^2, m_2^2)(p \cdot k) - I_{MB}(p_1^2, M^2, m_2^2)(p \cdot p_1) \Big) .
\end{aligned}$$

Here we have used $A = 4((k \cdot p_1)^2 - k^2 p_1^2)$ as well as $k + p_1 = p$ but without putting the external particles on shell.

The next structure contains two integration momenta in the numerator of the loop integral

$$I_{M_{BB}}^{\mu\nu} := i \int \frac{d^d l}{(2\pi)^d} \frac{l^\mu l^\nu}{(l^2 - M^2)((l - p)^2 - m_1^2)((l - p_1)^2 - m_2^2)} ,$$

which again can be expressed in terms of (scalar) Passarino-Veltman loop functions, which accompany Lorentz invariant tensor structures, as follows

$$I_{M_{BB}}^{\mu\nu} = g^{\mu\nu} I_{M_{BB}}^{(3)} + p^\mu p^\nu I_{M_{BB}}^{(4)} + (p^\mu p_1^\nu + p_1^\mu p^\nu) I_{M_{BB}}^{(5)} + p_1^\mu p_1^\nu I_{M_{BB}}^{(6)} .$$

Note that only four functions can occur since $I_{M_{BB}}^{\mu\nu}$ is symmetric under index permutation $\mu \leftrightarrow \nu$. Each one of them, i.e. $\{I_{M_{BB}}^{(i)} | i \in [3, 6]\}$, can be written in terms of the usual scalar loop integrals as follows

$$\begin{aligned}
I_{M_{BB}}^{(i)} = & F_1^{(i)} I_M(M) + F_2^{(i)} I_B(m_1) + F_3^{(i)} I_B(m_2) + F_4^{(i)} I_{BB}(k^2, m_1^2, m_2^2) \\
& + F_5^{(i)} I_{MB}(p^2, M^2, m_1^2) + F_6^{(i)} I_{MB}(p_1^2, M^2, m_2^2) + F_7^{(i)} I_{M_{BB}} ,
\end{aligned}$$

where the coefficients $F_j^{(i)}$ read

$$\begin{aligned}
F_1^{(3)} &= 0 , \quad F_2^{(3)} = 0 , \quad F_3^{(3)} = 0 , \\
F_4^{(3)} &= \frac{1}{(d-2)A} \left((m_1^2 - m_2^2)(k \cdot p_1) + k^2(M^2 - m_2^2 - (k \cdot p_1) - p_1^2) \right) , \\
F_5^{(3)} &= \frac{1}{(d-2)A} \left(2(k \cdot p_1)^2 - (M^2 + m_1^2 - p_1^2)(k \cdot p_1) + k^2(-M^2 + (k \cdot p_1)) - m_1^2 p_1^2 + m_2^2 p^2 \right) , \\
F_6^{(3)} &= \frac{1}{(d-2)A} \left((k \cdot p_1)(M^2 - m_2^2 - p_1^2) + (m_1^2 - m_2^2 - k^2)p_1^2 \right) , \\
F_7^{(3)} &= \frac{1}{(d-2)A} \left(p_1^2(m_1^2 - m_2^2)^2 - 2(k \cdot p_1)(-M^2 + m_2^2 + p_1^2)(m_1^2 - m_2^2) + 4m_2^2(k \cdot p_1)^2 \right. \\
& \quad \left. + k^4 p_1^2 + k^2((M^2 - m_2^2)^2 + p_1^4 - 2(M^2 + m_1^2)p_1^2 + 2(k \cdot p_1)(-M^2 + m_2^2 + p_1^2)) \right) , \\
F_1^{(4)} &= \frac{(p \cdot p_1)}{A p^2} , \quad F_2^{(4)} = \frac{(p \cdot p_1)(k \cdot p_1)}{A k^2 p^2} - \frac{1}{4k^2 p^2} , \quad F_3^{(4)} = -\frac{(k \cdot p_1)}{A k^2} , \\
F_4^{(4)} &= \frac{4}{(d-2)A^2 k^2} \left((2-d)(m_1^2 - m_2^2)(k \cdot p_1)^3 - k^2(k \cdot p_1)^2(2-d)((k \cdot p_1) + M^2 - m_2^2 - p_1^2) \right. \\
& \quad \left. + k^2 p_1^2(k \cdot p_1)(2d-3)(m_1^2 - m_2^2) - k^4 p_1^2(-M^2 + m_2^2 + (2d-3)(k \cdot p_1) + p_1^2) \right) ,
\end{aligned}$$

$$\begin{aligned}
F_5^{(4)} &= \frac{4}{(d-2)A^2 p^2} \\
&\left(2(2-d)(k \cdot p_1)^4 + ((2-d)(3M^2 - m_1^2 - 2m_2^2) - (d-6)p_1^2)(k \cdot p_1)^3 + p_1^2((6-4d)M^2 \right. \\
&\quad - dm_1^2 + 5dm_2^2 - 6m_2^2 + 2dp_1^2)(k \cdot p_1)^2 - (d-1)(M^2 + 3m_1^2 - 4m_2^2 - p_1^2)p_1^4(k \cdot p_1) \\
&\quad - (d-1)(m_1^2 - m_2^2)p_1^6 + k^4 p_1^2(-M^2 + m_2^2 + (2d-3)(k \cdot p_1) + 2(d-2)p_1^2) \\
&\quad + k^2((2-d)(k \cdot p_1)^3 + (4(d-1)p_1^2 - (d-2)(M^2 - m_2^2))(k \cdot p_1)^2) + k^2 p_1^2(k \cdot p_1)(-3M^2 \\
&\quad - 2dm_1^2 + 3m_1^2 + 2dm_2^2 + (7d-12)p_1^2) + k^2 p_1^4((d-3)M^2 - 2dm_1^2 + 3m_1^2 \\
&\quad \left. + dm_2^2 + 2(d-2)p_1^2) \right), \\
F_6^{(4)} &= \frac{4(d-1)p_1^2}{(d-2)A^2} \left((m_1^2 - m_2^2 - k^2)p_1^2 + (k \cdot p_1)(M^2 - m_2^2 - p_1^2) \right), \\
F_7^{(4)} &= \frac{4}{(d-2)A^2} \\
&\left(((d-2)(M^2 - m_2^2)^2 + (d-2)p_1^4 + (2dm_2^2 - 2(d-2)M^2)p_1^2)(k \cdot p_1)^2 \right. \\
&\quad - 2(d-1)(m_1^2 - m_2^2 - k^2)(-M^2 + m_2^2 + p_1^2)p_1^2(k \cdot p_1) + p_1^2 k^2((M^2 - m_2^2)^2 \\
&\quad \left. - 2(M^2 + (d-1)m_1^2 - (d-2)m_2^2)) + (d-1)k^4 p_1^4 + p_1^4(d-1)(m_1^2 - m_2^2)^2 + p_1^6 k^2 \right), \\
F_1^{(5)} &= -\frac{1}{A}, \quad F_2^{(5)} = -\frac{(k \cdot p_1)}{Ak^2}, \quad F_3^{(5)} = \frac{k^2 + (k \cdot p_1)}{Ak^2}, \\
F_4^{(5)} &= \frac{4}{(d-2)A^2 k^2} \\
&\left((d-2)p_1^2 k^6 + ((k \cdot p_1)^2 + (dp_1^2 - (d-1)(M^2 - m_2^2))(k \cdot p_1) - p_1^2(M^2 + (d-2)m_1^2 \right. \\
&\quad - (d-1)m_2^2 - p_1^2))k^4 + (k \cdot p_1)((d-2)(k \cdot p_1)^2 - ((d-2)M^2 + m_1^2 - dm_2^2 + m_2^2 \\
&\quad \left. - (d-2)p_1^2)(k \cdot p_1) - (2d-3)(m_1^2 - m_2^2)p_1^2 k^2 + (d-2)(m_1^2 - m_2^2)(k \cdot p_1)^3 \right), \\
F_5^{(5)} &= \frac{4}{(d-2)A^2} \\
&\left(-2(k \cdot p_1)^3 + ((2d-3)M^2 + m_1^2 - 2(d-1)m_2^2 + (1-2d)p_1^2)(k \cdot p_1)^2 + (d-1)(M^2 + 2m_1^2 \right. \\
&\quad - 3m_2^2 - p_1^2)p_1^2(k \cdot p_1) + (d-1)(m_1^2 - m_2^2)p_1^4 - (d-2)k^4 p_1^2 + k^2((d-1)(M^2 - m_2^2) \\
&\quad \left. + (5-3d)p_1^2)(k \cdot p_1) + p_1^2(M^2 + (d-2)m_1^2 - (d-1)m_2^2 - (d-2)p_1^2) - (k \cdot p_1)^2 \right), \\
F_6^{(5)} &= -\frac{4}{(d-2)A^2} \left((M^2 - m_2^2 + (3-2d)p_1^2)(k \cdot p_1)^2 + (d-1)(M^2 + m_1^2 - 2m_2^2 - k^2 - p_1^2)p_1^2(k \cdot p_1) \right. \\
&\quad \left. - p_1^2(k^2(p_1^2 - (d-2)(M^2 - m_2^2)) - (d-1)(m_1^2 - m_2^2)p_1^2) \right), \\
F_7^{(5)} &= \frac{4}{(2-d)A^2} \\
&\left(2((2-d)M^2 + dm_2^2 + (d-2)p_1^2)(k \cdot p_1)^3 + ((M^2 - m_2^2)((d-2)M^2 + dm_1^2 - 2(d-1)m_2^2) \right. \\
&\quad \left. + p_1^2(2(2-d)M^2 + (4-3d)m_1^2 + (5d-4)m_2^2 + (d-2)p_1^2))(k \cdot p_1)^2 \right)
\end{aligned}$$

$$\begin{aligned}
& + (d-1)(m_1^2 - m_2^2)(2M^2 + m_1^2 - 3m_2^2 - 2p_1^2)p_1^2(k \cdot p_1) + (d-1)(m_1^2 - m_2^2)^2p_1^4 \\
& + k^4p_1^2((2-d)(M^2 - m_2^2) + (d-1)(k \cdot p_1) + p_1^2) + k^2((d(m_2^2 - M^2) + (3d-4)p_1^2)(k \cdot p_1)^2 \\
& + ((d-1)(M^2 - m_2^2)^2 + (d+1)p_1^4 + 2(m_1^2 - 3m_2^2 - d(M^2 + m_1^2 - 2m_2^2))p_1^2)(k \cdot p_1) \\
& + p_1^2((M^2 - m_2^2)(M^2 + (d-2)m_1^2 - (d-1)m_2^2) - p_1^2(2M^2 + dm_1^2 - (d-2)m_2^2 - p_1^2))) ,
\end{aligned}$$

$$F_1^{(6)} = \frac{(k \cdot p_1) + p_1^2}{Ap_1^2} , \quad F_2^{(6)} = \frac{k^2 + (k \cdot p_1)}{Ak^2} , \quad F_3^{(6)} = -\frac{1}{A} \left(\frac{2 + (k \cdot p_1)}{p_1^2} + \frac{(k \cdot p_1)}{k^2} \right) ,$$

$$\begin{aligned}
F_4^{(6)} &= \frac{4}{(d-2)A^2k^2} \\
&\left(((d-1)(M^2 - m_2^2 - (k \cdot p_1)) + (d-3)p_1^2)k^6 + k^4(p_1^2M^2 + (6-4d)(k \cdot p_1)^2 \right. \\
&+ ((d-1)(2M^2 + m_1^2 - 3m_2^2) - 3p_1^2)(k \cdot p_1) + (2(d-2)m_1^2 + (3-2d)m_2^2 - p_1^2)p_1^2) \\
&+ (k \cdot p_1)(-3(d-2)(k \cdot p_1)^2 + ((d-2)M^2 + 2m_1^2 - dm_2^2 - (d-2)p_1^2)(k \cdot p_1) \\
&\left. + (2d-3)(m_1^2 - m_2^2)p_1^2)k^2 - (d-2)(m_1^2 - m_2^2)(k \cdot p_1)^3 \right) ,
\end{aligned}$$

$$\begin{aligned}
F_5^{(6)} &= \frac{4}{(d-2)A^2} \left((d-1)(k^2 + 2(k \cdot p_1) + p_1^2)(-(M^2 + m_1^2 - 2m_2^2 - 2(k \cdot p_1))(k \cdot p_1) \right. \\
&\left. + k^2(-M^2 + m_2^2 + (k \cdot p_1)) + (-m_1^2 + m_2^2 + (k \cdot p_1))p_1^2) \right) ,
\end{aligned}$$

$$\begin{aligned}
F_6^{(6)} &= \frac{4}{(d-2)A^2p_1^2} \\
&\left((2-d)(M^2 - m_2^2 + 3p_1^2)(k \cdot p_1)^3 + p_1^2(k \cdot p_1)^2(2M^2 + (d-2)m_1^2 - dm_2^2 - (d-2)k^2 \right. \\
&+ (6-4d)p_1^2) + p_1^2(k^2((2d-3)(M^2 - m_2^2) - 3p_1^2) + (d-1)(M^2 + 2m_1^2 - 3m_2^2 - p_1^2)p_1^2)(k \cdot p_1) \\
&\left. + p_1^4(-k^4 + (2(d-2)M^2 + m_1^2 + (3-2d)m_2^2 + (d-3)p_1^2)k^2 + (d-1)(m_1^2 - m_2^2)p_1^2) \right) ,
\end{aligned}$$

$$\begin{aligned}
F_7^{(6)} &= \frac{4}{(d-2)A^2} \\
&\left(4(d-2)(k \cdot p_1)^4 - 4(-2(d-1)m_2^2 + (d-2)(M^2 + m_1^2) - (d-2)p_1^2)(k \cdot p_1)^3 \right. \\
&+ (dM^4 - 2M^4 + 2dm_1^2M^2 + dm_1^4 - 2m_1^4 + 4(d-1)m_2^4 - 4(d-1)(M^2 + m_1^2)m_2^2 \\
&+ p_1^2(2(2-d)M^2 + (8-6d)m_1^2 + 8(d-1)m_2^2 + (d-2)p_1^2))(k \cdot p_1)^2 \\
&+ 2(d-1)(m_1^2 - m_2^2)(M^2 + m_1^2 - 2m_2^2 - p_1^2)p_1^2(k \cdot p_1) + (d-1)(m_1^2 - m_2^2)^2p_1^4 + k^6p_1^2 \\
&+ k^4((d-1)(M^2 - m_2^2)^2 + (d-2)(k \cdot p_1)^2 + 2p_1^4 - 2(M^2 + m_1^2)p_1^2 \\
&+ 2(k \cdot p_1)(2p_1^2 - (d-1)(M^2 - m_2^2))) + k^2(4(d-2)(k \cdot p_1)^3 + 2((4-3d)M^2 \\
&- (d-2)m_1^2 + 4(d-1)m_2^2 + dp_1^2)(k \cdot p_1)^2 + 2((d-1)(M^2 + m_1^2 - 2m_2^2)(M^2 - m_2^2) \\
&- (-2(d-1)m_2^2 + (d+1)(M^2 + m_1^2) - 2p_1^2)p_1^2)(k \cdot p_1) + p_1^2(M^4 + 2dm_1^2M^2 - 4m_1^2M^2 \\
&\left. + m_1^4 + 2(d-1)m_2^4 - 2(d-1)(M^2 + m_1^2)m_2^2 + p_1^2(p_1^2 - 2(M^2 + m_1^2)))) \right) .
\end{aligned}$$

Clearly, the unphysical poles in the limit $k^2 \rightarrow 0$ appear only due to the structures $F_2^{(i)}$, $F_3^{(i)}$ and $F_4^{(i)}$ which accompany the purely baryonic scalar loop integrals. As a matter of fact this is the starting point of the modification of the regularization procedure described in section 2.2.

The last and most involved tensor loop integral contains three integration momenta in the numerator of the loop integral and is only present if the chiral potential of the next-to-leading order is considered. It reads

$$\begin{aligned}
I_{M\!B\!B}^{\mu\nu\sigma} &:= i \int \frac{d^d l}{(2\pi)^d} \frac{l^\mu l^\nu}{(l^2 - M^2)((l-p)^2 - m_1^2)((l-p_1)^2 - m_2^2)} \\
&= (p^\mu g^{\nu\sigma} + p^\nu g^{\sigma\mu} + p^\sigma g^{\mu\nu}) I_{M\!B\!B}^{(7)} + (p_1^\mu g^{\nu\sigma} + p_1^\nu g^{\sigma\mu} + p_1^\sigma g^{\nu\mu}) I_{M\!B\!B}^{(8)} \\
&\quad + p^\mu p^\nu p^\sigma I_{M\!B\!B}^{(9)} + (p_1^\mu p_1^\nu p_1^\sigma + p^\mu p_1^\nu p^\sigma + p^\mu p^\nu p_1^\sigma) I_{M\!B\!B}^{(10)} \\
&\quad + (p_1^\mu p_1^\nu p^\sigma + p_1^\mu p^\nu p_1^\sigma + p^\mu p_1^\nu p_1^\sigma) I_{M\!B\!B}^{(11)} + p_1^\mu p_1^\nu p_1^\sigma I_{M\!B\!B}^{(12)},
\end{aligned}$$

where the last equality is again due to Lorentz invariance and the symmetry of $I_{M\!B\!B}^{\mu\nu\sigma}$ under the index permutation $\mu \leftrightarrow \nu \leftrightarrow \sigma$.

In the usual sense of the Passarino-Veltman reduction we can determine the coefficients $I_{M\!B\!B}^{(i)}$ contracting each element of the above equation with the invariant structures, such as e.g. $p^\mu g^{\nu\sigma}$. This leads to enormously long algebraic expressions. On the other hand it is possible to express every tensor loop integral of the third rank through the coefficients of the tensor loop integrals of the first and second tensor rank. To do so we contract the last equation only with invariant tensors of the first rank, namely p^μ and p_1^μ . Consequently the rank of both sides of the above equation will be reduced by one, allowing us to establish a connection between the coefficients $\{I_{M\!B\!B}^{(i)} | i \in [7, 12]\}$ and $\{I_{M\!B\!B}^{(i)} | i \in [1, 6]\}$, where the latter have been presented explicitly before. The whole set of these relations reads

$$\begin{aligned}
I_{M\!B\!B}^{(7)} &= \frac{4}{A} \left(p_1^2 \text{E} - p_1 \cdot p \text{I} \right), \\
I_{M\!B\!B}^{(8)} &= \frac{4}{A} \left(p^2 \text{I} - p_1 \cdot p \text{E} \right), \\
I_{M\!B\!B}^{(9)} &= \frac{4}{A} \left(\text{C} - \frac{(p_1 \cdot p)}{p_1^2} \text{G} - \frac{8p_1^2}{A} \text{E} + \frac{8(p_1 \cdot p)}{A} \text{I} \right), \\
I_{M\!B\!B}^{(10)} &= \frac{4}{A} \left(p^2 \text{G} - p_1 \cdot p \text{C} + \frac{8(p_1 \cdot p)p_1^2}{A} \text{E} - \frac{8(p_1 \cdot p)^2}{A} \text{I} \right), \\
I_{M\!B\!B}^{(11)} &= \frac{1}{(p_1 \cdot p)} \left(\text{F} - \frac{4p^4}{A} \text{G} + \frac{4p^2 p_1 \cdot p}{A} \text{C} - \frac{32p^2 p_1^2 (p_1 \cdot p)}{A^2} \text{E} + \frac{32p^2 (p_1 \cdot p)^2}{A^2} \text{I} \right), \\
I_{M\!B\!B}^{(12)} &= \frac{1}{(p_1 \cdot p)} \text{D} - \frac{1}{(p_1 \cdot p)} \left(\text{F} - \frac{4p^4}{A} \text{G} + \frac{4p^2 p_1 \cdot p}{A} \text{C} - \frac{32p^2 p_1^2 (p_1 \cdot p)}{A^2} \text{E} + \frac{32p^2 (p_1 \cdot p)^2}{A^2} \text{I} \right),
\end{aligned}$$

where we have used the following abbreviations

$$\begin{aligned}
\text{C} &= \frac{p^2 - m_1^2 + M^2}{2} I_{M\!B\!B}^{(4)} + \frac{1}{2} I_{B\!B}^{(2)}(k^2, m_1^2, m_2^2) + I_{B\!B}^{(1)}(k^2, m_1^2, m_2^2) + \frac{1}{2} I_{B\!B}(k^2, m_1^2, m_2^2), \\
\text{D} &= \frac{p^2 - m_1^2 + M^2}{2} I_{M\!B\!B}^{(6)} - \frac{1}{2} I_{M\!B}(p_1^2, M^2, m_2^2) + \frac{1}{2} I_{B\!B}^{(2)}(k^2, m_1^2, m_2^2), \\
\text{E} &= \frac{p^2 - m_1^2 + M^2}{2} I_{M\!B\!B}^{(3)} - \frac{1}{3} I_{M\!B}(p_1^2, M^2, m_2^2) + \frac{1}{2} I_{B\!B}^{(3)}(k^2, m_1^2, m_2^2), \\
\text{F} &= \frac{1}{2} I_{M\!B\!B}^{(5)} - \frac{1}{2} I_{B\!B}^{(2)}(k^2, m_1^2, m_2^2) - \frac{1}{2} I_{B\!B}^{(1)}(k^2, m_1^2, m_2^2), \\
\text{G} &= \frac{p^2 - m_2^2 + M^2}{2} I_{M\!B\!B}^{(4)} - \frac{1}{2} I_{M\!B}^{(2)}(p^2, M^2, m_1^2)
\end{aligned}$$

$$\begin{aligned}
& + \frac{1}{2} I_{BB}^{(2)}(k^2, m_1^2, m_2^2) + I_{BB}^{(1)}(k^2, m_1^2, m_2^2) + \frac{1}{2} I_{BB}(k^2, m_1^2, m_2^2) , \\
\text{I} = & \frac{p^2 - m_2^2 + M^2}{2} I_{MBB}^{(3)} - \frac{1}{2} I_{MB}^{(3)}(p^2, M^2, m_1^2) + \frac{1}{2} I_{BB}^{(3)}(k^2, m_1^2, m_2^2) .
\end{aligned}$$

Here the Passarino-Veltman functions $I_{MB}^{(i)}(p_1^2, M^2, m_2^2)$ and $I_{BB}^{(i)}(k^2, m_1^2, m_2^2)$ can be obtained from above formulas replacing the arguments correspondingly.

Appendix C

Channel space structures

For the channel indices $\{b, j; i, a\}$ corresponding to the process $\phi_i B_a \rightarrow \phi_j B_b$, the relevant coupling matrices from the leading, Eq. (1.13), and next-to leading, Eq. (2.4), order chiral Lagrangian read

$$A_{WT}^{b,j;i,a} = -\frac{1}{4F_j F_i} \langle \lambda^{b\dagger} [[\lambda^{j\dagger}, \lambda^i], \lambda^a] \rangle ,$$

$$\begin{aligned} A_{14}^{b,j;i,a} = & -\frac{2}{F_j F_i} \left(b_1 \left(\langle \lambda^{b\dagger} [\lambda^{j\dagger}, [\lambda^i, \lambda^a]] \rangle + \langle \lambda^{b\dagger} [\lambda^i, [\lambda^{j\dagger}, \lambda^a]] \rangle \right) \right. \\ & + b_2 \left(\langle \lambda^{b\dagger} \{ \lambda^{j\dagger}, [\lambda^i, \lambda^a] \} \rangle + \langle \lambda^{b\dagger} \{ \lambda^i, [\lambda^{j\dagger}, \lambda^a] \} \rangle \right) \\ & \left. + b_3 \left(\langle \lambda^{b\dagger} \{ \lambda^{j\dagger}, \{ \lambda^i, \lambda^a \} \} \rangle + \langle \lambda^{b\dagger} \{ \lambda^i, \{ \lambda^{j\dagger}, \lambda^a \} \} \rangle \right) + 2b_4 \langle \lambda^{b\dagger} \lambda^a \rangle \langle \lambda^{j\dagger} \lambda^i \rangle \right) , \end{aligned}$$

$$\begin{aligned} A_{57}^{b,j;i,a} = & -\frac{2}{F_j F_i} \left(b_5 \langle \lambda^{b\dagger} [[\lambda^{j\dagger}, \lambda^i], \lambda^a] \rangle + b_6 \langle \lambda^{b\dagger} \{ [\lambda^{j\dagger}, \lambda^i], \lambda^a \} \rangle \right. \\ & \left. + b_7 \left(\langle \lambda^{b\dagger} \lambda^{j\dagger} \rangle \langle \lambda^i \lambda^a \rangle - \langle \lambda^{b\dagger} \lambda^i \rangle \langle \lambda^a \lambda^{j\dagger} \rangle \right) \right) , \end{aligned}$$

$$\begin{aligned} A_{811}^{b,j;i,a} = & -\frac{1}{F_j F_i} \left(b_8 \left(\langle \lambda^{b\dagger} [\lambda^{j\dagger}, [\lambda^i, \lambda^a]] \rangle + \langle \lambda^{b\dagger} [\lambda^i, [\lambda^{j\dagger}, \lambda^a]] \rangle \right) \right. \\ & + b_9 \left(\langle \lambda^{b\dagger} [\lambda^{j\dagger}, \{ \lambda^i, \lambda^a \}] \rangle + \langle \lambda^{b\dagger} [\lambda^i, \{ \lambda^{j\dagger}, \lambda^a \}] \rangle \right) \\ & \left. + b_{10} \left(\langle \lambda^{b\dagger} \{ \lambda^{j\dagger}, \{ \lambda^i, \lambda^a \} \} \rangle + \langle \lambda^{b\dagger} \{ \lambda^i, \{ \lambda^{j\dagger}, \lambda^a \} \} \rangle \right) + 2b_{11} \langle \lambda^{b\dagger} \lambda^a \rangle \langle \lambda^{j\dagger} \lambda^i \rangle \right) , \end{aligned}$$

$$\begin{aligned} A_M^{b,j;i,a} = & -\frac{1}{2F_j F_i} \left(2b_0 \left(\langle \lambda^{b\dagger} \lambda^a \rangle \langle [\lambda^{j\dagger} \lambda^i] \bar{\mathcal{M}} \rangle \right) \right. \\ & + b_D \left(\langle \lambda^{b\dagger} \{ \{ \lambda^{j\dagger}, \{ \bar{\mathcal{M}}, \lambda^i \} \} \lambda^a \} \rangle + \langle \lambda^{b\dagger} \{ \{ \lambda^i, \{ \bar{\mathcal{M}}, \lambda^{j\dagger} \} \} \lambda^a \} \rangle \right) \\ & \left. + b_F \left(\langle \lambda^{b\dagger} \{ \{ \lambda^{j\dagger}, \{ \bar{\mathcal{M}}, \lambda^i \} \} \lambda^a \} \rangle + \langle \lambda^{b\dagger} \{ \{ \lambda^i, \{ \bar{\mathcal{M}}, \lambda^{j\dagger} \} \} \lambda^a \} \rangle \right) \right) . \end{aligned}$$

Here λ^{\dots} denote the 3×3 channel matrices (e.g. $\phi = \phi^i \lambda^i$ for the physical meson fields) and the F_i are the meson decay constants in the respective channel. Moreover, $\bar{\mathcal{M}}$ is obtained from the quark mass matrix \mathcal{M} via the Gell-Mann-Oakes-Renner relations, and given in terms of the meson masses as follows, $\bar{\mathcal{M}} = \frac{1}{2} \text{diag}(M_{K^+}^2 - M_{K^0}^2 + M_{\pi^0}^2, M_{K^0}^2 - M_{K^+}^2 + M_{\pi^0}^2, M_{K^+}^2 + M_{K^0}^2 - M_{\pi^0}^2)$.

For the channel indices $\{b, j; a\}$ corresponding to the process $B_a \rightarrow \phi_j B_b$ the channel-space matrix is given by

$$A_X^{b,j;a} = -\frac{D}{\sqrt{2}F_j} \langle \lambda^{b\dagger} \{ \lambda^{j\dagger}, \lambda^a \} \rangle - \frac{F}{\sqrt{2}F_j} \langle \lambda^b [\lambda^{j\dagger}, \lambda^a] \rangle ,$$

where D and F are the axial coupling constants.

Appendix D

Partial wave analysis of $\pi N \rightarrow \eta N$ scattering

The pion-induced eta production off the neutron is dominated by the contribution of the nearby nucleon resonances, i.e. the $S_{11}(1535)$ and $D_{13}(1520)$. From the previous study of elastic πN scattering we already know that the first one is described perfectly as a dynamically generated resonance within our approach, whereas the d-wave resonance is not. Thus we wish to clarify, whether an ansatz for the scattering amplitudes, which contains s- and p-waves only, is capable to generate a $\cos^2(\theta)$ -like behavior of the differential cross sections $d\sigma/d\Omega(s, \cos(\theta))$ (θ here denotes the scattering angle in the c.m. frame). As a matter of fact this generation of a $\cos^2(\theta)$ -like structure through the iteration of p-waves does not seem to be appreciated in several experimental works, see e.g. Ref. [134]. There, the presence of a $\cos^2(\theta)$ -behavior in the shape of differential cross section is assumed to be a direct indication for a d-wave dominance. Let us start from the most general form of the T-matrix, which is invariant under Lorentz as well as parity transformations. For the scattering of a meson-baryon system from initial state (i) with the meson momentum (q), and baryon momentum and spin (p, s) to the final state (f) with meson momentum (q'), and baryon momentum and spin (p', s') it reads with the usual conventions used by Höhler [160]

$$M_{fi} = \frac{1}{8\pi\sqrt{s}} \bar{u}_f(p', s') \{ A_{fi}(s, t) + \frac{1}{2}(\not{q} + \not{q}') B_{fi}(s, t) \} u_i(p, s),$$

where $s = P^2 := (p + q)^2 = (p' + q')^2$ and $t = (q - q')^2 = (p - p')^2$ are the Mandelstam variables. The amplitudes A and B can be recombined to the scattering amplitude on the mass shell $T_{ON}(\not{q}', \not{q}; P)$ as follows

$$T_{ON}(\not{q}', \not{q}; P) = T_{ON}^0(s, z) + \not{P} T_{ON}^1(s, z) = A(s, t) + \frac{1}{2}(\not{q} + \not{q}') B(s, t).$$

Here, $z = \cos(\theta)$ is the standard representation of the scattering angle. In fact, z is related to the Mandelstam t via

$$t = M_f^2 + M_i^2 - 2\sqrt{q_i^2 + M_i^2}\sqrt{q_f^2 + M_f^2} + 2q_i q_f z, \quad (\text{D.1})$$

where $q_{i/f}$ is the modulus of the center of mass momentum of the in- and outgoing system, respectively. Suppressing the kinematic variables for the moment the unpolarized differential cross section in the center of mass system reads

$$\left(\frac{d\sigma(i \rightarrow f)}{d\Omega}\right) = \frac{1}{64\pi^2} \frac{q_f}{q_i} \frac{1}{2} \sum_{s,s'} \left| \bar{u}_f(p', s') \{T_{ON}^{0:fi} + \not{P}T_{ON}^{1:fi}\} u_i(p, s) \right|^2.$$

For Dirac spinors normalized such that $\bar{u}_f(p)u_i(p) = 2m\delta_{fi}$, and suppressing for brevity the channel indices, the spin sum can be calculated in terms of T_{ON}^0 and T_{ON}^1 as follows

$$\frac{1}{2} \sum_{s,s'} \left| \bar{u}_f(p', s') \{T_{ON}^0 + \not{P}T_{ON}^1\} u_i(p, s) \right|^2 = c_{00}|T_{ON}^0|^2 + 2c_{01}\text{Re}(T_{ON}^{1*}T_{ON}^0) + c_{11}|T_{ON}^1|^2,$$

where

$$\begin{aligned} c_{00} &= \frac{1}{2s} \left((s + m_i^2 - M_i^2)(s + m_f^2 - M_f^2) + 4s(m_i m_f - zq_f q_i) \right), \\ c_{01} &= m_i(s + m_f^2 - M_f^2) + m_f(s + m_i^2 - M_i^2), \\ c_{11} &= \frac{1}{2} \left((s + m_i^2 - M_i^2)(s + m_f^2 - M_f^2) + 4s(m_i m_f + zq_f q_i) \right). \end{aligned}$$

The above formulae specify all required kinematics and spin structure. The dynamical input is incorporated within the scattering amplitudes, A and B . In the main body of this work these are taken to be solutions of the BSE. In view of the above question, we wish to make an ansatz for the scattering amplitudes. First of all, the standard amplitudes A and B can be expanded in Legendre polynomials $P_l(z)$ as follows

$$\begin{aligned} \frac{A(s, t)}{4\pi} &= \frac{\sqrt{W_{\text{cms}} + m_i}}{\sqrt{E_{\text{cms};i} + m_i}} f_1(s, t) \frac{\sqrt{W_{\text{cms}} + m_f}}{\sqrt{E_{\text{cms};f} + m_f}} - \frac{\sqrt{W_{\text{cms}} - m_i}}{\sqrt{E_{\text{cms};i} - m_i}} f_2(s, t) \frac{\sqrt{W_{\text{cms}} - m_f}}{\sqrt{E_{\text{cms};f} - m_f}}, \\ \frac{B(s, t)}{4\pi} &= \frac{1}{\sqrt{E_{\text{cms};i} + m_i}} f_1(s, t) \frac{1}{\sqrt{E_{\text{cms};f} + m_f}} + \frac{1}{\sqrt{E_{\text{cms};i} - m_i}} f_2(s, t) \frac{1}{\sqrt{E_{\text{cms};f} - m_f}}, \end{aligned}$$

where $W_{\text{cms}} = \sqrt{s}$ and $E_{\text{cms};i/f} = \sqrt{q_{i/f}^2 + m_{i/f}^2}$. After a variable transformation the amplitudes $f_{1,2}$ are related to the commonly used partial wave amplitudes $f_{l\pm}(s)$ as follows [160, 161],

$$\begin{aligned} f_1(s, z) &= \sum_{l=1}^{\infty} (f_{(l-1)+}(s) - f_{(l+1)-}(s)) P'_l(z), \\ f_2(s, z) &= \sum_{l=1}^{\infty} (f_{l-}(s) - f_{l+}(s)) P'_l(z). \end{aligned}$$

For the purpose of this section we do not consider additional constraints for the partial wave amplitudes, e.g. due to analyticity or unitarity. Thus both real and imaginary part of those are used as free parameters, which will be adjusted to reproduce the data on differential cross sections for the process $\pi^- N \rightarrow \eta N$, measured by Prakhov et al., see Ref. [134]. For the truncation of the partial wave expansion we assume three different scenarios:

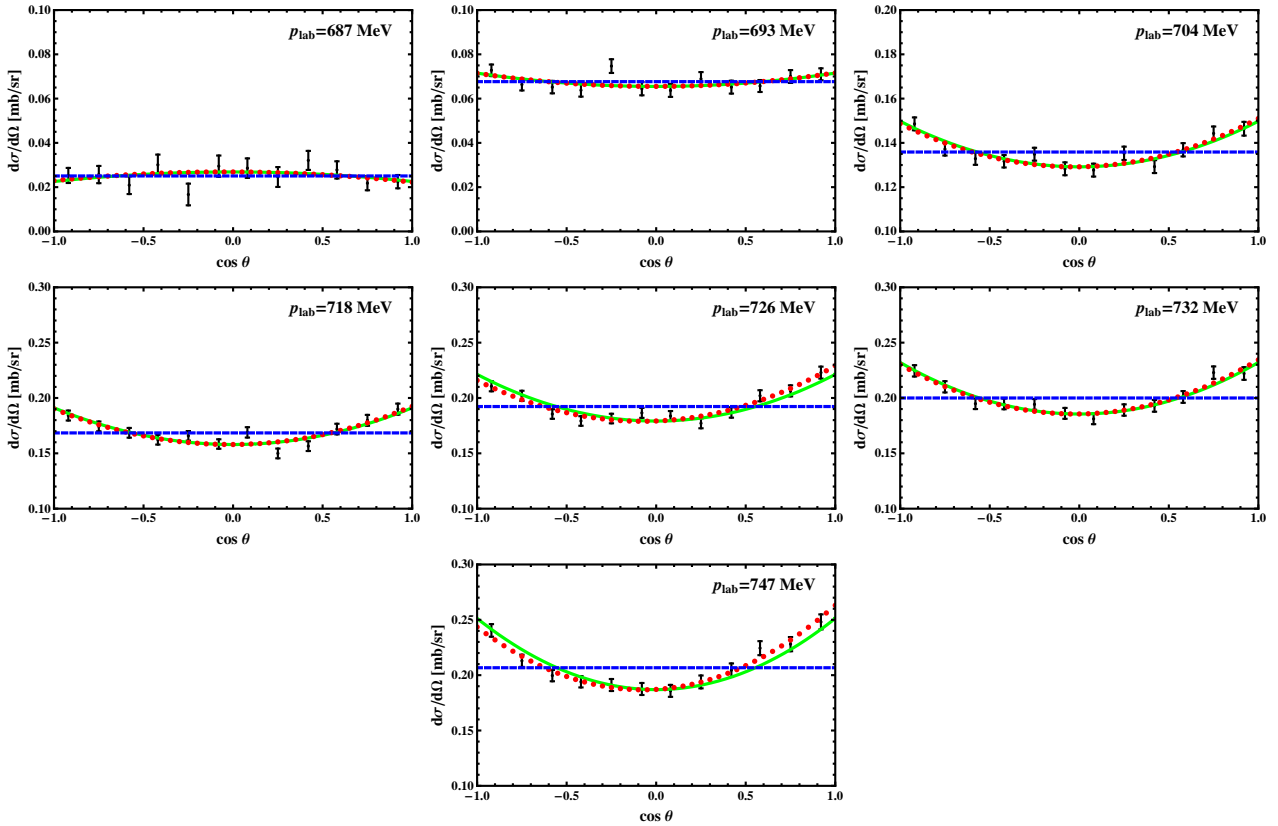


Figure D.1: Best fits of three assumed scenarios to the data of the differential cross sections from Ref. [134] for different pion momenta p_{lab} . The dashed (blue), red (dotted) and green (full) line correspond to the first, second and third scenario, respectively, as described in the text.

1. The scattering amplitude contains only the s-wave dynamically, meant in the sense of the above discussion. Free parameters are $\{\text{Re}(f_{0+}), \text{Im}(f_{0+})\}$.
2. Both, s- and p-waves are included dynamically. This is the case for the solution of the BSE with contact terms from NLO chiral Lagrangian as performed in our approach. Without restricting the parity of the p-waves we end up with the following free parameters for this scenario: $\{\text{Re}(f_{0+}), \text{Im}(f_{0+}), \text{Re}(f_{1-}), \text{Im}(f_{1-}), \text{Re}(f_{1+}), \text{Im}(f_{1+})\}$.
3. The scattering amplitude is determined by s- and d-wave (for instance D_{13}), whereas the p-wave is negligible. This is the case for the process $\pi N \rightarrow \eta N$ from the phenomenological point of view. For phenomenological reasons we assume only the D_{13} wave to be non-negligible. Thus the free parameters are $\{\text{Re}(f_{0+}), \text{Im}(f_{0+}), \text{Re}(f_{2-}), \text{Im}(f_{2-})\}$.

For each incident π^- momenta separately and for each scenario we obtain best fits as presented in Fig. D.1. As expected the first scenario is only capable to fit the data at lowest beam momenta. The s-wave is dominant at low energies, however, at higher energies it lacks the

angular dependence and thus fails to describe the data properly. Going to higher beam momenta both, the second and third scenario describe the data equally well. It turns out that the presence of p-waves of both parities is required to reproduce the z^2 -behavior. Thus albeit our approach based on the unitarization of the NLO chiral potential does not produce d-waves in the sense of the above discussion, it is in principle capable to reproduce the data on differential cross sections well enough.

Appendix E

One-photon vertices

For all vertices the in-(out-)going meson and baryon are denoted by the channel index $i(j)$ and $a(b)$, respectively, whereas the charge of the corresponding particle is denoted by Q . All required photon induced vertices W from the leading order chiral Lagrangian Eq. (1.13) read

$$\begin{aligned} W_{\gamma B \rightarrow B}^\mu{}^{b;a} &= ieQ_a \gamma^\mu, & W_{\gamma \phi \rightarrow \phi}^\mu{}^{j;i} &= ieQ_i(2q_2^\mu - k^\mu), \\ W_{\gamma B \rightarrow \phi B}^\mu{}^{b,j;a} &= ieQ_j A_x^{b,j;a} \gamma^\mu \gamma^5, & W_{\gamma \phi B \rightarrow \phi B}^\mu{}^{b,j;i,a} &= -ie(Q_i + Q_j) A_{WT}^{b,j;i,a} \gamma^\mu, \end{aligned}$$

where q_2 denotes the four-momentum of the produced (outgoing) meson. The vertices from the second order chiral Lagrangian (2.4) possess more involved channel structures, which for instance can be traced back elegantly to the already defined channel matrices in App. C. The interaction vertex for the process $\gamma(k)\phi_i(q_1)B_a(p_1) \rightarrow \phi_j(q_2)B_b(p_2)$ reads

$$\begin{aligned} W_{\gamma \phi B \rightarrow \phi B}^\mu{}^{b,j;i,a} &= iA_{14} \left(Q_j q_1^\mu + Q_i q_2^\mu \right) \\ &+ iA_{57} \left(Q_j [\gamma^\mu, \not{q}_1] + Q_i [\gamma^\mu, \not{q}_2] \right) \\ &+ iA_{811} \left(Q_j \gamma^\mu (q_1, p_1 + q_1) + Q_j \not{q}_1 (q_1^\mu + p_1^\mu) \right. \\ &\quad \left. + Q_i \gamma^\mu (q_2, q_2 + p_2) + Q_i \not{q}_2 (q_2^\mu + p_2^\mu) + Q_j \not{q}_1 q_1^\mu + Q_i \not{q}_2 q_2^\mu \right) \\ &- \frac{i}{2F_i F_j} (\not{k} \gamma^\mu - \gamma^\mu \not{k}) \\ &\quad \left(b_{12} \langle \lambda^{b\dagger} [Q_i [\lambda^i, \lambda^{j\dagger}] - Q_j [\lambda^{j\dagger}, \lambda^i], \lambda^a] \rangle + b_{13} \langle \lambda^{b\dagger} \{ Q_i [\lambda^i, \lambda^{j\dagger}] - Q_j [\lambda^{j\dagger}, \lambda^i], \lambda^a \} \rangle \right). \end{aligned}$$

The latter expression originates from the electromagnetic field-strength tensor $f_+^{\mu\nu}$. Furthermore, the same term gives rise to an additional coupling of the photon to a baryon, which does not vanish for electrically neutral baryons. It also induces a baryon transition $\Sigma^0 \leftrightarrow \Lambda$, the corresponding vertex reads

$$W_{\gamma B \rightarrow B}^\mu{}^{b;a} = 2ie \left(b_{12} \langle \lambda^{b\dagger} [Q, \lambda^a] \rangle + b_{13} \langle \lambda^{b\dagger} \{ Q, \lambda^a \} \rangle \right) (\not{k} \gamma^\mu - \gamma^\mu \not{k}),$$

where $Q = \text{diag}(2/3, -1/3, -1/3)$ is the charge matrix and e is the charge of the electron.

Appendix F

Multipoles

In this section we wish to specify the major technical steps on the way from the photoproduction amplitude as calculated utilizing usual Feynman rules to the multipole amplitudes as well as to the cross sections. In large parts of this section we use the conventions of Ref. [140] and start from the most general Lorentz covariant transition matrix element for the process of meson (ϕ_f) production of the baryon (B_i) via an incoming photon ($\gamma(k)$), i.e. $\gamma(k)B_i(p-k) \rightarrow B_f(p-q)\phi_f(q)$. It reads

$$T_{fi} = i\epsilon_\mu \bar{u}_f \left(\sum_{k=1}^8 \mathcal{B}_k \mathcal{N}_k^\mu \right) u_i, \quad (\text{F.1})$$

where ϵ_μ is the photon polarization vector. The initial and final Dirac spinors u_i and u_f are normalized like $\bar{u}u = 2m$, with m the mass of the corresponding baryon. The coefficients \mathcal{B}_i are functions of the coefficients of the hadronic scattering amplitude $\{\mathcal{T}_i; i = 1, \dots, 20\}$ as defined in section. 2.3, loop integrals from App. A as well as vertices from App. C. Since both baryons are on-shell there are only 8 different structures, i.e.

$$\mathcal{N}_i^\mu \in \{ \gamma_5 \gamma^\mu \not{k}, 2\gamma_5 P^\mu, 2\gamma_5 q^\mu, 2\gamma_5 k^\mu, \gamma_5 \gamma^\mu, \gamma_5 \not{k} P^\mu, \gamma_5 \not{k} k^\mu, \gamma_5 \not{k} q^\mu \},$$

where $P = \frac{1}{2}(2p - q - k)$.

Fixing the axis of quantization to the z-axis, one is able to reduce the Dirac spinors to the two-component spinors χ as follows

$$T_{fi} = 8\pi\sqrt{s} \chi_f^\dagger \sum_{k=1}^8 \mathcal{F}_k \mathcal{G}_k \chi_i. \quad (\text{F.2})$$

amplitudes \mathcal{F}_i , which are defined in the basis given by

$$\mathcal{G}_k \in \{ i(\vec{\sigma} \cdot \vec{\epsilon}), (\vec{\sigma} \cdot \hat{q})(\vec{\sigma} \cdot [\hat{k} \times \vec{\epsilon}]), i(\vec{\sigma} \cdot \hat{k})(\hat{q} \cdot \vec{\epsilon}), i(\vec{\sigma} \cdot \hat{q})(\hat{q} \cdot \vec{\epsilon}), \\ i(\vec{\sigma} \cdot \hat{k})(\hat{k} \cdot \vec{\epsilon}), i(\vec{\sigma} \cdot \hat{q})(\hat{k} \cdot \vec{\epsilon}), i(\vec{\sigma} \cdot \hat{q})(\hat{k} \cdot \vec{\epsilon}), i(\vec{\sigma} \cdot \hat{q})\epsilon_0, i(\vec{\sigma} \cdot \hat{k})\epsilon_0 \}.$$

Here, an arrow denotes a three-dimensional vector and a hat a normalized three-vector. Due to current conservation, two of the eight CGLN amplitudes can be eliminated via

$$\mathcal{F}_1 + (\hat{k} \cdot \hat{q})\mathcal{F}_3 + \mathcal{F}_5 - \frac{k_0}{|k|}\mathcal{F}_8 = 0 \quad \text{and} \quad (\hat{k} \cdot \hat{q})\mathcal{F}_4 + \mathcal{F}_6 - \frac{k_0}{|k|}\mathcal{F}_7 = 0,$$

which serves as a good check of our calculation. Furthermore, two of the remaining six amplitudes are accompanied by scalar components of ϵ only and thus have no influence on photoproduction amplitudes, i.e. process including real photons. Finally the lowest electric multipole E_{0+} can be calculated as follows

$$E_{0+} = \int_{-1}^1 dz \left(\frac{1}{2} P_0 \mathcal{F}_1 - \frac{1}{2} P_1 \mathcal{F}_2 + \frac{1}{6} (P_0 - P_2) \mathcal{F}_4 \right), \quad (\text{F.3})$$

where P_l denote the Legendre polynomials. The latter as well as the CGLN amplitudes are functions of the cosine of the scattering angle in the c.m. system, z . The unpolarized differential cross section for meson photoproduction is given by

$$\begin{aligned} \frac{d\sigma}{d\Omega} = \frac{|q|}{|k|} & \left(|\mathcal{F}_1|^2 + |\mathcal{F}_2|^2 + \frac{1}{2} |\mathcal{F}_3|^2 + \frac{1}{2} |\mathcal{F}_4|^2 + \text{Re}(\mathcal{F}_1 \mathcal{F}_4^*) + \text{Re}(\mathcal{F}_2 \mathcal{F}_3^*) + z \text{Re}(\mathcal{F}_3 \mathcal{F}_4^* - 2\mathcal{F}_1 \mathcal{F}_2^*) \right. \\ & \left. - z^2 \left(\frac{1}{2} |\mathcal{F}_3|^2 + \frac{1}{2} |\mathcal{F}_4|^2 + \text{Re}(\mathcal{F}_1 \mathcal{F}_4^* + \mathcal{F}_2 \mathcal{F}_3^*) \right) - z^3 \text{Re}(\mathcal{F}_3 \mathcal{F}_4^*) \right). \end{aligned} \quad (\text{F.4})$$

Acknowledgments

First of all, I would like to express my sincere gratitude to Prof. Dr. Ulf-G. Meißner for giving me the opportunity to work on this interesting subject of effective field theory, for being open for new ideas, the quickness and the precision of his advices, interest in my work and motivation. I also wish to thank PD Dr. A. Rusetsky for proofreading and assessing this thesis.

I am deeply grateful to my mentor Dr. Peter Christian Bruns, to whom I always looked up, both in physics as well as in his attitude to life, for his permanent assistance during my whole scientific life. In innumerable conversations about physics, philosophy, arts, et cetera, both in the office and over a glass of wine he has become my best friend.

My thank goes also to all members of the theory division for the support, in particular Dr. Simon Kreuzer, Dr. Harald Van Pee, PD Dr. Bernard Ch. Metsch, Sebastian König and Prof. Dr. Carsten Urbach for their help with programming and IT issues and Dr. Michael Döring for proofreading this thesis and useful discussions. I would also like to acknowledge the scientific work done by Dr. Buğra Borasoy, Dr. Robin Nißler and Dr. Peter Christian Bruns which served a good foundation for the studies presented in this thesis.

Finally, I am very thankful to all of my friends and especially to my dear parents, Natalie and Waldemar Mai, for their constant support and motivation. Last but not least, I am very grateful to my girlfriend, Eleni Sismanidou, for her understanding, motivation and love.

I thank the Deutsche Forschungsgemeinschaft (SFB/TR 16, "Subnuclear Structure of Matter") and the Bonn-Cologne Graduate School of Physics and Astronomy for financial support.

Bibliography

- [1] L. Wittgenstein, ” *Tractatus logico-philosophicus: Logisch-philosophische Abhandlung*”, Suhrkamp Verlag; Auflage: 33 (1963).
- [2] P. C. Bruns, M. Mai and U.-G. Meißner, Phys. Lett. B **697** (2011) 254 [arXiv:1012.2233 [nucl-th]].
- [3] M. Mai and U.-G. Meißner, [arXiv:1202.2030 [nucl-th]].
- [4] M. Mai, P. C. Bruns and U.-G. Meißner, [arXiv:1207.4923 [nucl-th]].
- [5] S. R. Coleman and D. J. Gross, Phys. Rev. Lett. **31** (1973) 851.
- [6] C. A. Baker, D. D. Doyle, P. Geltenbort, K. Green, M. G. D. van der Grinten, P. G. Harris, P. Iaydjiev and S. N. Ivanov *et al.*, Phys. Rev. Lett. **97** (2006) 131801 [arXiv:hep-ex/0602020].
- [7] I. Montvay and G. Münster, Cambridge, UK: Univ. Pr. (1994) 491 p. (Cambridge monographs on mathematical physics).
- [8] M. Creutz, [arXiv:1103.3304 [hep-lat]].
- [9] S. Dürr, Z. Fodor, J. Frison, C. Hoelbling, R. Hoffmann, S. D. Katz, S. Krieg and T. Kurth *et al.*, Science **322** (2008) 1224 [arXiv:0906.3599 [hep-lat]].
- [10] S. Weinberg, PoS CD **09** (2009) 001 [arXiv:0908.1964 [hep-th]].
- [11] S. L. Adler, Phys. Rev. **177** (1969) 2426.
- [12] C. Vafa and E. Witten, Nucl. Phys. B **234** (1984) 173.
- [13] S. Coleman, J. Math. Phys. **7**, 787 (1966).
- [14] M. Gell-Mann, Phys. Rev. **125** (1962) 1067.
- [15] M. Gell-Mann, R. J. Oakes and B. Renner, Phys. Rev. **175** (1968) 2195.
- [16] S. Weinberg, Phys. Rev. Lett. **17** (1966) 616.
- [17] S. Weinberg, Physica A **96** (1979) 327.
- [18] V. Bernard and U.-G. Meißner, Ann. Rev. Nucl. Part. Sci. **57** (2007) 33 [arXiv:hep-ph/0611231].

- [19] V. Bernard, Prog. Part. Nucl. Phys. **60** (2008) 82 [arXiv:0706.0312 [hep-ph]].
- [20] S. Scherer, Adv. Nucl. Phys. **27** (2003) 277 [arXiv:hep-ph/0210398].
- [21] U.-G. Meißner, Rept. Prog. Phys. **56** (1993) 903 [arXiv:hep-ph/9302247].
- [22] J. Gasser and H. Leutwyler, Nucl. Phys. B **250** (1985) 465.
- [23] J. Gasser and H. Leutwyler, Annals Phys. **158** (1984) 142.
- [24] B. Kubis, [arXiv:hep-ph/0703274].
- [25] V. Bernard, N. Kaiser and U.-G. Meißner, Int. J. Mod. Phys. E **4** (1995) 193 [arXiv:hep-ph/9501384].
- [26] H. Leutwyler, [arXiv:hep-ph/0008124].
- [27] A. Manohar and H. Georgi, Nucl. Phys. B **234** (1984) 189.
- [28] J. Beringer *et al.* [Particle Data Group], Phys. Rev. D **86**, (2012) 010001.
- [29] J. Goldstone, Nuovo Cim. **19** (1961) 154.
- [30] S. Kamefuchi, L. O’Raifeartaigh and A. Salam, Nucl. Phys. **28** (1961) 529.
- [31] H. Lehmann, K. Symanzik and W. Zimmermann, Nuovo Cim. **1** (1955) 205.
- [32] R. Haag, Phys. Rev. **112** (1958) 669.
- [33] J. Bijnens, G. Colangelo and G. Ecker, JHEP **9902** (1999) 020 [arXiv:hep-ph/9902437].
- [34] G. Ecker, J. Gasser, A. Pich and E. de Rafael, Nucl. Phys. B **321** (1989) 311.
- [35] J. F. Donoghue, C. Ramirez and G. Valencia, Phys. Rev. D **39** (1989) 1947.
- [36] B. Moussallam, JHEP **0008** (2000) 005 [arXiv:hep-ph/0005245].
- [37] R. Kaiser and J. Schweizer, JHEP **0606** (2006) 009 [arXiv:hep-ph/0603153].
- [38] M. Schmid, PhD Thesis, University of Bern (2007).
- [39] J. Gasser, C. Haefeli, M. A. Ivanov and M. Schmid, Phys. Lett. B **652** (2007) 21 [arXiv:0706.0955 [hep-ph]].
- [40] J. Gasser, C. Haefeli, M. A. Ivanov and M. Schmid, [arXiv:0903.0801 [hep-ph]].
- [41] M. Frink, U.-G. Meißner and I. Scheller, Eur. Phys. J. A **24** (2005) 395 [arXiv:hep-lat/0501024].
- [42] M. Mai, P. C. Bruns, B. Kubis and U.-G. Meißner, Phys. Rev. D **80** (2009) 094006 [arXiv:0905.2810 [hep-ph]].
- [43] J. Gasser, M. E. Sainio and A. Švarč, Nucl. Phys. B **307** (1988) 779.

- [44] A. Krause, *Helv. Phys. Acta* **63** (1990) 3.
- [45] S. Weinberg, *Phys. Lett. B* **251** (1990) 288.
- [46] S. R. Beane, P. F. Bedaque, W. C. Haxton, D. R. Phillips and M. J. Savage, In *Shifman, M. (ed.): At the frontier of particle physics, vol. 1* 133-269 [nucl-th/0008064].
- [47] E. Epelbaum, H. -W. Hammer and U.-G. Meißner, *Rev. Mod. Phys.* **81** (2009) 1773 [arXiv:0811.1338 [nucl-th]].
- [48] H. Georgi, Menlo Park, USA: Benjamin/cummings (1984) 165p.
- [49] G. Ecker, *Prog. Part. Nucl. Phys.* **35** (1995) 1 [arXiv:hep-ph/9501357].
- [50] J. Liu *et al.* [UCNA Collaboration], *Phys. Rev. Lett.* **105** (2010) 181803 [arXiv:1007.3790 [nucl-ex]].
- [51] R. L. Jaffe and A. Manohar, *Nucl. Phys. B* **337** (1990) 509.
- [52] B. Borasoy, *Phys. Rev. D* **59** (1999) 054021 [arXiv:hep-ph/9811411].
- [53] U.-G. Meißner, *Int. J. Mod. Phys. E* **1** (1992) 561.
- [54] Y. -R. Liu and S. -L. Zhu, *Phys. Rev. D* **75** (2007) 034003 [arXiv:hep-ph/0607100].
- [55] E. E. Jenkins and A. V. Manohar, *Phys. Lett. B* **255** (1991) 558.
- [56] V. Bernard, N. Kaiser, J. Kambor and U.-G. Meißner, *Nucl. Phys. B* **388** (1992) 315.
- [57] T. Becher and H. Leutwyler, *Eur. Phys. J. C* **9** (1999) 643 [arXiv:hep-ph/9901384].
- [58] P. J. Ellis and H. -B. Tang, *Phys. Rev. C* **57** (1998) 3356 [arXiv:hep-ph/9709354].
- [59] H. -B. Tang, [arXiv:hep-ph/9607436].
- [60] J. Gegelia, G. Japaridze and X. Q. Wang, *J. Phys. G* **29** (2003) 2303 [arXiv:hep-ph/9910260].
- [61] M. F. M. Lutz and E. E. Kolomeitsev, *Nucl. Phys. A* **700** (2002) 193 [arXiv:nucl-th/0105042].
- [62] T. Fuchs, J. Gegelia, G. Japaridze and S. Scherer, *Phys. Rev. D* **68** (2003) 056005 [arXiv:hep-ph/0302117].
- [63] P. J. Ellis and K. Torikoshi, *Phys. Rev. C* **61** (2000) 015205 [arXiv:nucl-th/9904017].
- [64] V. Bernard, N. Kaiser and U.-G. Meißner, *Z. Phys. C* **60** (1993) 111 [arXiv:hep-ph/9303311].
- [65] N. Kaiser, *Phys. Rev. C* **64** (2001) 045204 [Erratum-*ibid.* **C 73** (2006) 069902] [arXiv:nucl-th/0107006].
- [66] T. Becher and H. Leutwyler, *JHEP* **0106** (2001) 017 [arXiv:hep-ph/0103263].

- [67] B. Borasoy and U.-G. Meißner, *Annals Phys.* **254** (1997) 192 [arXiv:hep-ph/9607432].
- [68] A. Torok, S. R. Beane, W. Detmold, T. C. Luu, K. Orginos, A. Parreno, M. J. Savage and A. Walker-Loud, *Phys. Rev. D* **81** (2010) 074506 [arXiv:0907.1913 [hep-lat]].
- [69] S. Weinberg, “*The Quantum Theory of Fields. Vol. 1: Foundations*”, Cambridge Univ. Press (1995).
- [70] G. F. Chew, “*The analytic S matrix: A Basis for Nuclear Democracy*”, New York: W. A. Benjamin, Inc. (1966).
- [71] S. M. Roy, *Phys. Lett. B* **36** (1971) 353.
- [72] C. Ditsche, M. Hoferichter, B. Kubis and U.-G. Meißner, *JHEP* **1206** (2012) 043 [arXiv:1203.4758 [hep-ph]].
- [73] W. Heisenberg, *Z. Phys.* **120** (1943) 513.
- [74] E. E. Salpeter and H. A. Bethe, *Phys. Rev.* **84** (1951) 1232.
- [75] R. Nißler, Ph.D. thesis, University of Bonn (2008), <http://hss.ulb.uni-bonn.de/2008/1316/1316.htm>.
- [76] M. F. M. Lutz and E. E. Kolomeitsev, *Nucl. Phys. A* **730** (2004) 392 [arXiv:nucl-th/0307039].
- [77] J. Nieves and E. Ruiz Arriola, *Phys. Lett. B* **455** (1999) 30 [nucl-th/9807035].
- [78] U.-G. Meißner and J. A. Oller, *Nucl. Phys. A* **673** (2000) 311 [arXiv:nucl-th/9912026].
- [79] J. A. Oller and U.-G. Meißner, *Phys. Lett. B* **500** (2001) 263 [arXiv:hep-ph/0011146].
- [80] N. Kaiser, P. B. Siegel and W. Weise, *Nucl. Phys. A* **594** (1995) 325 [arXiv:nucl-th/9505043].
- [81] N. Kaiser, P. B. Siegel and W. Weise, *Phys. Lett. B* **362** (1995) 23 [arXiv:nucl-th/9507036].
- [82] E. Oset and A. Ramos, *Nucl. Phys. A* **635** (1998) 99 [arXiv:nucl-th/9711022].
- [83] J. A. Oller, E. Oset and A. Ramos, *Prog. Part. Nucl. Phys.* **45** (2000) 157 [arXiv:hep-ph/0002193].
- [84] J. Nieves and E. Ruiz Arriola, *Phys. Rev. D* **64** (2001) 116008 [arXiv:hep-ph/0104307].
- [85] W. Pauli and F. Villars, *Rev. Mod. Phys.* **21** (1949) 434.
- [86] G. 't Hooft and M. J. G. Veltman, *Nucl. Phys. B* **153** (1979) 365.
- [87] J. A. Oller and E. Oset, *Nucl. Phys. A* **620** (1997) 438 [Erratum-ibid. *A* **652** (1999) 407] [arXiv:hep-ph/9702314].
- [88] J. Nieves and E. Ruiz Arriola, *Nucl. Phys. A* **679** (2000) 57 [arXiv:hep-ph/9907469].

- [89] M. E. Peskin, D. V. Schroeder, *An Introduction to Quantum Field Theory* (Westview Press, 1995).
- [90] J. Collins, *Renormalization* (Cambridge University Press, 1984).
- [91] W. A. Bardeen, A. J. Buras, D. W. Duke and T. Muta, *Phys. Rev. D* **18** (1978) 3998.
- [92] P. C. Bruns, Ph. D. Thesis, Univ. Bonn, 2009 (<http://hss.ulb.uni-bonn.de/2009/1831/1831.htm>).
- [93] C. Savkli, J. Tjon and F. Gross, *Phys. Rev. C* **60** (1999) 055210 [Erratum-ibid. *C* **61** (2000) 069901] [arXiv:hep-ph/9906211].
- [94] H. Haberzettl, *Phys. Rev. C* **56** (1997) 2041 [arXiv:nucl-th/9704057].
- [95] Y. Ikeda, T. Hyodo and W. Weise, *Nucl. Phys. A* **881** (2012) 98 [arXiv:1201.6549 [nucl-th]].
- [96] B. Borasoy, R. Nißler and W. Weise, *Eur. Phys. J. A* **25** (2005) 79 [arXiv:hep-ph/0505239].
- [97] H.M. Nieland and J.A. Tjon, *Phys./ Lett./ B* **27** (1968) 309 (<http://igitur-archive.library.uu.nl/phys/2006-1207-200726>).
- [98] A. D. Lahiff and I. R. Afnan, *Phys. Rev. C* **60** (1999) 024608 [arXiv:nucl-th/9903058].
- [99] M. Döring, C. Hanhart, F. Huang, S. Krewald and U.-G. Meißner, *Nucl. Phys. A* **829** (2009) 170 [arXiv:0903.4337 [nucl-th]].
- [100] M. Döring, C. Hanhart, F. Huang, S. Krewald, U.-G. Meißner and D. Rönchen, *Nucl. Phys. A* **851** (2011) 58 [arXiv:1009.3781 [nucl-th]].
- [101] M. Frink and U.-G. Meißner, *JHEP* **0407** (2004) 028 [arXiv:hep-lat/0404018].
- [102] G. Passarino and M. J. G. Veltman, *Nucl. Phys. B* **160** (1979) 151.
- [103] T. Inoue, E. Oset and M. J. Vicente Vacas, *Phys. Rev. C* **65** (2002) 035204 [arXiv:hep-ph/0110333].
- [104] J. A. Oller, *Eur. Phys. J. A* **28** (2006) 63 [arXiv:hep-ph/0603134].
- [105] B. Borasoy, U.-G. Meißner and R. Nißler, *Phys. Rev. C* **74** (2006) 055201 [arXiv:hep-ph/0606108].
- [106] B. Borasoy, P. C. Bruns, U.-G. Meißner and R. Nißler, *Eur. Phys. J. A* **34** (2007) 161 [arXiv:0709.3181 [nucl-th]].
- [107] R. A. Arndt, W. J. Briscoe, I. I. Strakovsky and R. L. Workman, *Phys. Rev. C* **74** (2006) 045205 [arXiv:nucl-th/0605082].
- [108] R. L. Workman, R. A. Arndt, W. J. Briscoe, M. W. Paris and I. I. Strakovsky, [arXiv:1204.2277 [hep-ph]].
- [109] R. Koch, *Nucl. Phys. A* **448** (1986) 707.

- [110] Minuit2 released in **ROOT 5.22/00**
[<http://lcgapp.cern.ch/project/cls/work-packages/mathlibs/minuit>].
- [111] F. James, MINUIT Reference Manual, CERNProgram Library Writeup D506.
- [112] V. Baru, C. Hanhart, M. Hoferichter, B. Kubis, A. Nogga and D. R. Phillips, Phys. Lett. B **694** (2011) 473 [arXiv:1003.4444 [nucl-th]].
- [113] A. M. Gasparyan, J. Haidenbauer, C. Hanhart and J. Speth, Phys. Rev. C **68** (2003) 045207 [arXiv:nucl-th/0307072].
- [114] M. Bazzi, *et al.*, Phys. Lett. B **704** (2011) 113, [arXiv:1105.3090 [nucl-ex]].
- [115] R. H. Dalitz and S. F. Tuan, Annals Phys. **10** (1960) 307.
- [116] Y. Ikeda, T. Hyodo and W. Weise, Phys. Lett. B **706** (2011) 63, [arXiv:1109.3005 [nucl-th]].
- [117] J. Ciborowski, *et al.*, J. Phys. G **8** (1982) 13.
- [118] W. E. Humphrey and R. R. Ross, Phys. Rev. **127** (1962) 1305.
- [119] M. Sakitt, T. B. Day, R. G. Glasser, N. Seeman, J. H. Friedman, W. E. Humphrey and R. R. Ross, Phys. Rev. **139** (1965) B719.
- [120] M. B. Watson, M. Ferro-Luzzi and R. D. Tripp, Phys. Rev. **131** (1963) 2248.
- [121] D. N. Tovee, *et al.*, Nucl. Phys. B **33** (1971) 493.
- [122] R. J. Nowak, *et al.*, Nucl. Phys. B **139** (1978) 61.
- [123] U.-G. Meißner, U. Raha and A. Rusetsky, Eur. Phys. J. C **35** (2004) 349, [arXiv:hep-ph/0402261].
- [124] G. Beer *et al.* [DEAR Collaboration], Phys. Rev. Lett. **94**, (2005) 212302.
- [125] T. M. Ito, *et al.*, Phys. Rev. C **58** (1998) 2366.
- [126] J. K. Kim, Phys. Rev. Lett. **14** (1965) 29.
- [127] A. D. Martin, Nucl. Phys. B **179** (1981) 33.
- [128] R. J. Hemingway, Nucl. Phys. B **253** (1985) 742.
- [129] D. Jido, J. A. Oller, E. Oset, A. Ramos and U.-G. Meißner, Nucl. Phys. A **725** (2003) 181, [arXiv:nucl-th/0303062].
- [130] M. Niiyama, H. Fujimura, D. S. Ahn, J. K. Ahn, S. Ajimura, H. C. Bhang, T. H. Chang and W. C. Chang *et al.*, Phys. Rev. C **78** (2008) 035202 [arXiv:0805.4051 [hep-ex]].
- [131] K. Moriya *et al.* [CLAS Collaboration], Nucl. Phys. A **835** (2010) 325 [arXiv:0911.2705 [nucl-ex]].

- [132] D. Ruic, M. Mai and U.-G. Meißner, Phys. Lett. B **704** (2011) 659 [arXiv:1108.4825 [nucl-th]].
- [133] M. Frink and U.-G. Meißner, Eur. Phys. J. A **29** (2006) 255 [arXiv:hep-ph/0609256].
- [134] S. Prakhov, B. M. K. Nefkens, C. E. Allgower, R. A. Arndt, V. Bekrenev, W. J. Briscoe, M. Clajus and J. R. Comfort *et al.*, Phys. Rev. C **72** (2005) 015203.
- [135] private communication with S. Prakhov.
- [136] M. F. M. Lutz and M. Soyeur, Nucl. Phys. A **773** (2006) 239 [arXiv:nucl-th/0511055].
- [137] R. A. Arndt, W. J. Briscoe, T. W. Morrison, I. I. Strakovsky, R. L. Workman and A. B. Gridnev, Phys. Rev. C **72** (2005) 045202 [arXiv:nucl-th/0507024].
- [138] M. Döring and K. Nakayama, Eur. Phys. J. A **43** (2010) 83 [arXiv:0906.2949 [nucl-th]].
- [139] K. M. Watson, Phys. Rev. **95** (1954) 228.
- [140] F. A. Berends, A. Donnachie and D. L. Weaver, Nucl. Phys. B **4** (1967) 1.
- [141] V. Bernard, N. Kaiser and U.-G. Meißner, Nucl. Phys. B **383** (1992) 442.
- [142] V. Bernard, N. Kaiser and U.-G. Meißner, Z. Phys. C **70** (1996) 483 [arXiv:hep-ph/9411287].
- [143] F. Huang, M. Döring, H. Haberzettl, J. Haidenbauer, C. Hanhart, S. Krewald, U.-G. Meißner and K. Nakayama, Phys. Rev. C **85** (2012) 054003 [arXiv:1110.3833 [nucl-th]].
- [144] A. N. Kvinikhidze and B. Blankleider, Phys. Rev. C **60** (1999) 044003 [arXiv:nucl-th/9901001].
- [145] F. Gross and D. O. Riska, Phys. Rev. C **36** (1987) 1928.
- [146] C. H. M. van Antwerpen and I. R. Afnan, Phys. Rev. C **52** (1995) 554 [arXiv:nucl-th/9407038].
- [147] B. Borasoy, P. C. Bruns, U.-G. Meißner and R. Nißler, Phys. Rev. C **72** (2005) 065201 [arXiv:hep-ph/0508307].
- [148] B. Kubis, U.-G. Meißner, Eur. Phys. J. **C18** (2001) 747, [arXiv:hep-ph/0010283].
- [149] D. Drechsel, S. S. Kamalov and L. Tiator, Eur. Phys. J. A **34** (2007) 69 [arXiv:0710.0306 [nucl-th]].
- [150] R. L. Workman, M. W. Paris, W. J. Briscoe and I. I. Strakovsky, [arXiv:1202.0845 [hep-ph]].
- [151] W. -T. Chiang, S. -N. Yang, L. Tiator and D. Drechsel, Nucl. Phys. A **700** (2002) 429 [arXiv:nucl-th/0110034].
- [152] A. V. Anisovich, E. Klempt, V. A. Nikonov, M. A. Matveev, A. V. Sarantsev and U. Thoma, Eur. Phys. J. A **44** (2010) 203 [arXiv:0911.5277 [hep-ph]].

- [153] R. Beck, F. Kalleicher, B. Schoch, J. Vogt, G. Koch, H. Ströher, V. Metag and J. C. McGeorge *et al.*, *Phys. Rev. Lett.* **65** (1990) 1841.
- [154] J.P. Burg, *Ann. Phys. (Paris)* **10** (1965) 363.
- [155] M.J. Adamovitch *et al.*, *Sov. J. Nucl. Phys.* **2** (1966) 95.
- [156] A. Gasparyan and M. F. M. Lutz, *Nucl. Phys. A* **848** (2010) 126 [arXiv:1003.3426 [hep-ph]].
- [157] M. Luscher, *Commun. Math. Phys.* **105** (1986) 153.
- [158] M. Döring, J. Haidenbauer, U.-G. Meißner and A. Rusetsky, *Eur. Phys. J. A* **47** (2011) 163 [arXiv:1108.0676 [hep-lat]].
- [159] K. Moriya *et al.* [CLAS Collaboration], *AIP Conf. Proc.* **1441** (2012) 296.
- [160] G. Höhler, *Landolt-Boernstein* (Springer-Verlag, Berlin, 1983).
- [161] G. F. Chew, M. L. Goldberger, F. E. Low and Y. Nambu, *Phys. Rev.* **106** (1957) 1337.

Scientific publications:

- 2009** M. Mai, P. C. Bruns, B. Kubis and U.-G. Meißner, “Aspects of meson-baryon scattering in three and two-flavor chiral perturbation theory,” *Phys. Rev. D* **80** (2009) 094006 [arXiv:0905.2810 [hep-ph]].
- 2011** P. C. Bruns, M. Mai and U.-G. Meißner, “Chiral dynamics of the S11(1535) and S11(1650) resonances revisited,” *Phys. Lett. B* **697** (2011) 254 [arXiv:1012.2233 [nucl-th]].
- 2011** D. Ruic, M. Mai and U.-G. Meißner, “ η -photoproduction in a gauge-invariant chiral unitary framework,” *Phys. Lett. B* **704** (2011) 659 [arXiv:1108.4825 [nucl-th]].
- 2012** M. Mai and U.-G. Meißner, “New insights into antikaon-nucleon scattering and the structure of the Lambda(1405),” [arXiv:1202.2030 [nucl-th]].
- 2012** M. Mai, P. C. Bruns and U.-G. Meißner, “Pion photoproduction off the proton in a gauge-invariant chiral unitary framework,” [arXiv:1207.4923 [nucl-th]]. (Accepted for publication in PRD)